Modelling and Analysis of a Production Plant for Low Density Polyethylene

Dissertation

zur Erlangung des akademischen Grades

Doktoringenieurin / Doktoringenieur
(Dr.-Ing.)

von Dipl.-Ing. Martin Häfele

geb. am 1971-04-28 in Tettnang

genehmigt durch die Fakultät für Elektrotechnik und Informationstechnik

der Otto-von-Guericke Universität Magdeburg

Gutachter:
Prof. Dr.-Ing. Achim Kienle
Prof. Subramaniam Pushpavanam

Promotionskolloquium am 2006-12-07

Acknowledgements

This thesis is the result of an employment at both the Institute for System Dynamics and Control (University Stuttgart), where I initially started the studies towards the PhD degree in 1997, and the Max Planck Institute for Dynamics of Complex Technical Systems (Magdeburg), where these studies were continued from 1998 onwards.

I am gratefully thankful to my scientific supervisor Prof. Dr. Achim Kienle for his kindness and readiness to help me during the whole period of preparation of this work, for his suggestions, useful discussions and always very constructive criticism. Moreover I want to thank him for being not only a supervisor but also a friend who was almost impossible to beat in tennis. For his interest in this work I am thankful to Prof. Subramaniam Pushpavanam, who not only helped me with fruitful discussions on non-linear model analysis but who also made me finalize this work by suggesting an one-month scientific stay in Magdeburg in 2006.

Next, I want to thank the cooperation partners, Dr. Frank-Olaf Mähling and Dr. Christian-Ulrich Schmidt (Basell Polyolefine GmbH, Wesseling, Germany) and Dr. Jens Bausa, Dr. Marco Boll and Martin Schwibach (BASF AG, Ludwigshafen, Germany) for providing me with all the data that was required to include the detailed reaction scheme into the dynamic model and for each quick but not too restrictive review of any kind of publication.

Furthermore, my thank goes to the foundation director of the Max Planck Institute for Dynamics of Complex Technical Systems, Prof. Dr.-Ing. Dr. h.c. mult. Ernst Dieter Gilles for giving me the opportunity to work on this interesting topic at the Institute of System Dynamics and Control initially and at the Max Planck Institute thereafter.

Additionally, I want to thank all former colleagues in Stuttgart and Magdeburg for the inspiring and cordial atmosphere. We had a very good relationship amongst each

other not only on a scientific basis, we also had a jolly good time together during our spare time activities, e.g. participating annually in a skiing week, playing basketball almost every Monday evening, watching the FC Magdeburg defeating FC Bayern Munich in the German Soccer Cup or the SC Magdeburg winning against Flensburg in the handball league. Special thanks go to Cornelia Trieb for lending me her ear on many occasions, which still holds. Moreover I thank Barbara Munder, Carolyn Mangold and Silke Eckart for joining Spanish classes, although almost everything has vanished in nothingness again (of course, here I'm just talking of myself!).

Also I want to thank Prof. Dietrich Flockerzi, Andrea Focke, Dr. Michael Mangold, Sergej Svjatnyj, Dr. Roland Waschler and Dr. Klaus-Peter Zeyer for building up car pools heading to various locations in the south of Germany. During these trips we had some very nice discussions on various topics of both scientific as well as everyday life.

For the review of the first versions of this work I want to thank my former colleagues Dr. Ilknur Disli-Uslu and Dr. Michael Mangold and my colleagues from Linde AG, Dr. Ingo Thomas and Dr. Hans-Jörg Zander.

Last but not least, I want to thank my parents, Irene and Elmar Häfele, my sister Sabine, Melanie Eykmann and her parents, Inge and Prof. Dr. Walter Eykmann for their support and encouragement in each and every aspect.

Munich, December 2006 Martin Häfele

Contents

List of Figures

List of Tables

Notation

Arabic Symbols

Symbol	Meaning	SI-Unit
A	area	[m^2]
c_p	heat capacity	[W/(m^2 K)]
Δh_{reac}	heat of reaction	[J]
E	radiation energy	[J]
F	force	[N]
Gr	Grashof number	
H	enthalpy	[J]
$\dot{H}$	enthalpy flux	[J/s]
i	component index	
I	total number of components	
j	reaction number index	
J	total number of reactions	
k	reaction constant	[kmol/s]
M	molar mass	[kg/kmol]
m	mass	[kg]
$\dot{m}$	mass flux	[kg/s]
$\dot{m}_A$	mass flux through area A	[kg/(s m^2)]
N_C	number of components	
Nu	Nusselt number	
p	pressure	[N/m^2]

Continued on next page

Symbol	Meaning	SI-Unit
P_n	number average	
PD	polydispersity	
Pr	Prandtl number	
$\dot{Q}$	energy flux	[J/s]
r	extent of reaction	[mol/(kg s)]
	radius	[m]
R	overall heat transfer coefficient	[K m/W]
Re	Reynolds number	
t	time	[s]
T	temperature	[K]
U	inner energy	[J]
	perimeter	[m]
v	velocity	[m/s]
V	volume	[m^3]
w	weight fraction	[-]
$\mathbf{W}$	sensitivity matrix	
z	spatial coordinate	[m]

Greek Symbols

Symbol	Meaning	SI-Unit
α	heat transfer coefficient	[W/(m^2 K)]
Δ	difference	
ε	emissivity	
γ	weight factor in objective function	
	skewness of the distribution	
λ	heat transport coefficient	[W/(m K)]
μ_k	k-th statistical moment	
ν	stoichiometric index	
π	pi	

Continued on next page

Symbol	Meaning	SI-Unit
Φ	objective function	[-]
σ	Stefan-Boltzmann constant	[W/(m^2 K^4)]
	variance	
ϱ	density	[kg/m^3]
Θ	dimensionless temperature	[-]
τ	dimensionless time	[-]
	grid node concentration	
ζ	pressure drop coefficient	

Abbreviations

Symbol	Meaning
BC	boundary condition
DAE	differential and algebraic equation
DB	double bond
HDPE	high-density polyethylene
IC	initial condition
IUPAC	International Union of Pure and Applied Chemistry
LCB	long chain branching
LDPE	low-density polyethylene
LLDPE	linear low-density polyethylene
MFI	melt flow index
PDAE	partial differential and algebraic equation
PE	polyethylene
SCB	short chain branching

Components

Symbol	Meaning
I	initiator

Continued on next page

Symbol	Meaning
M	monomer
P	dead polymer
R	radical, living polymer
X	modifier

Subscripts

Symbol	Meaning
0	initial condition
amb	ambience
A	flux, applied through cross section with area A
air	air
β	β-scission
bb	back biting
C	coolant
ex	external wall
hp	high pressure flash
i	index of chain length
	at the inner reactor wall
in	at inlet conditions
$inner$	at the inner reactor wall (emphasized)
$init$	between two initiator injections
iso	insulation
j	index of reactions
liq	liquid phase
ll	laminar layer
lp	low pressure flash
m	logarithmic mean
M	monomer
v	index for initiators

Continued on next page

Symbol	Meaning
o	at the outer reactor wall
$outer$	at the outer reactor wall (emphasized)
p	propagation
rad	radial
$reac$	reaction
rem	reminder of the tube
res	residence time
R	friction
	reactor
RX	modifier radical
sec	secondary living polymer
st	steel
sl	slime layer
tc	termination due to combination
td	termination due to disproportion
th	thermal
tr	transfer
vap	vapor phase
W	wall
X	modifier

Superscripts

Symbol	Meaning
P	dead polymer
R	primary living polymer
R, sec	secondary living polymer

German Abstract

Im Vordergrund der vorliegenden Arbeit steht die Herleitung eines geeigneten dynamischen Modells für die nichtlineare Analyse des Produktionsprozesses von Hochdruck-Polyethylen (low density polyethylene = LDPE). Das mathematische Modell wird anschliessend verwendet, um Prozessführungsstrategien zu untersuchen. Dabei stehen die Optimierung von Spezifikations- und Lastwechseln sowie die Stabilisierung der Arbeitspunkte gegenüber unvorhergesehenen Störungen im Fokus. Derartige Störungen können schlimmstenfalls durch thermische Zersetzung sogar zum Durchgehen des Reaktors führen.

Das dynamische Modell der Hochdruck-Polymerisation von LDPE wird ausgehend von dem Verfahrensdiagramm (Abb. 2.1) hergeleitet. Dabei wird neben einem detaillierten Reaktionsschema auch eine Energiebilanz für die dicke innere Reaktorwand des Rohrreaktors berücksichtigt. Um das Gleichungssystem mit dem am Institut für Systemdynamik und Regelungstechnik (Universität Stuttgart) entworfenen und am Max-Planck-Institut für komplexe technische Systeme weiterentwickelten Prozesssimulator DIVA lösen zu können, wird das örtlich verteilte Modell wird mit Hilfe des in Mathematica implementierten symbolischen Vorverarbeitungswerkzeuges SyPProT in ein Modell überführt, welches nur noch aus Differential- oder algebraischen Gleichungen besteht. Dabei wird eine finite Differenzen-Methode verwendet, welcher entweder ein ortsfestes oder ein bewegliches Gitter zu Grunde liegt.

Das erste Modul des Rohrreaktors wird anhand von Daten des Kooperationspartners validiert. Zur Validierung wird ein ortsfestes, sehr hoch auflösendes Gitter verwendet. Die Übereinstimmung zwischen den Daten und den Profilen aus einer stationären Simulation ist sehr gut. Allerdings ist ein Gesamtmodell mit einem derart hoch auflösenden Gitter nicht auf einem gewöhnlichen Standard-PC numerisch lösbar. Daher werden Simulationsresultate des hoch auflösenden Gitters mit denen verglichen,

welche weniger Gitterpunkte verwenden. Dabei steigt der Diskretisierungsfehler mit der Verringerung der Anzahl der Gitterpunkte. Durch die Verwendung eines adaptiven anstelle eines ortsfesten Gitters kann allerdings bei deutlich weniger Stützstellen ein vergleichbares Ergebnis erzielt werden. Daher wird in allen folgenden Simulationen die adaptive Diskretisierungsmethode verwendet.

Wie schon im vorhergehenden Abschnitt erwähnt, berücksichtigt das detaillierte Modell die axiale und radiale Wärmeleitung in der Rohrwand. Damit wäre es allerdings notwendig, die Rohrwand auch in radialer Richtung zu diskretisieren. Um das Modell dadurch nicht zusätzlich erheblich zu vergrößern, wird die innere Reaktorwand in zwei Schichten gleicher Dicke geteilt. Die Temperatur in der Mitte wird als eine gemittelte Wandtemperatur betrachtet und die radiale Wärmeleitung kann im Wärmeübergangskoeffizienten berücksichtigt werden. Die Dicke der Wand beeinflusst die stationären Simulationsergebnisse nur geringfügig, wohingegen sich die Zeitkonstanten um einen Faktor in der Größenordnung einer Dekade verändern.

Obwohl die Simulationsdauer für einzelne Szenarien beträchtlich ist, erweist sich das detaillierte Modell ohne Materialrückführung robust gegenüber allen aufgeprägten sprungförmigen Störungen. Ein Schließen der Rückführungen führt jedoch dazu, dass das Gesamtsystem instabil werden kann. Dieses Verhalten soll durch eine nichtlineare Modellanalyse untersucht werden, aber das detaillierte Modell kann auf Grund seiner Größe mit den dafür in DIVA zur Verfügung stehenden Methoden nicht gelöst werden. Daher wird ein vereinfachtes Modell für diese Betrachtungen herangezogen. Dieses Modell enthält zahlreiche Annahmen, welche die Anzahl der Gleichungen reduzieren, z.B. entfällt durch eine konstante Kühltemperatur die Energiebilanz für das Kühlmedium, außerdem entfallen vier partielle Differentialgleichungen für Initiatoren bzw. deren Radikale, etc.. Trotz der z.T. erheblichen Vereinfachungen gibt das reduzierte dynamische Modell qualitativ das Verhalten des detaillierten wieder. Lediglich im Reaktoraustritt kommt es zu größeren Abweichungen, welche durch die Annahme eines konstanten Wärmedurchgangskoeffizienten erklärbar sind.

Die nichtlineare Analyse des vereinfachten Modelles kann die Resultate anderer Forschungsgruppen übereinstimmend wiedergeben. Durch eine Parameterfortsetzung kann neben Betriebsbereichen mit bis zu fünf stationären Betriebspunkten auch eine Hopf-Bifurkation gefunden werden. Jedoch überschreitet dieser Betriebspunkt den realen Betriebsbereich der Anlage. Nichtsdestoweniger kann der Hopfpunkt im Rah-

men von weitergehenden Untersuchungen als Ausgangspunkt für eine Zweiparameterfortsetzung herangezogen werden.

Für eine dynamische Optimierung ist die Sensitivitätsanalyse ein wichtiger erster Schritt. Diese wird mit dem detaillierten Modell durchgeführt, um die wesentlichen Einflußgrößen auf den Prozess zu ermitteln. Dazu werden drei Zielfunktionen definiert, hinsichtlich derer der Einfluss der Parameter untersucht wird. Resultat dieser Untersuchung ist, dass zwar für eine nichtlineare Analyse Momente höherer Ordnung vernachlässigt werden dürfen, dies jedoch für eine Optimierung nicht sinnvoll erscheint. Denn die physikalischen Eigenschaften des Polymers hängen von der Kettenlängenverteilung ab und wesentliche Kenngrößen dieser Verteilung lassen sich auf der Basis von Momenten ableiten.

Es bleibt festzuhalten, dass selbst mit derzeitigen Standard-PCs die dynamische Simulation eines rigorosen Modells der LDPE Produktion im Rohrreaktorverfahren ein sehr anspruchsvolles numerisches Problem darstellt. Vielleicht könnte die Wahl eines anderen Simulators das Problem der großen Rechenzeiten lösen, jedoch müssen dann evtl. Abstriche hinsichtlich Optimierung und nichtlinearer Analyse gemacht werden. Nichtsdestotrotz kann das in dieser Arbeit abgeleitete detaillierte Modell sehr gut als Ausgangsbasis verwendet werden, um daraus für die jeweilige Applikation geeignete einfachere Modelle zu gewinnen, z.B. für dynamische Optimierungen oder modellprädiktive Regelungsaufgaben.

Chapter 1

Introduction

A journey of a thousand miles begins with a single step.
– Confucius

The primary objective of this work is the development of a suitable dynamic model for the analysis of a polyethylene production plant. The mathematical model is used for a successive study of process control strategies. Most important tasks in this regard are optimization of grade or load changes and stabilization of steady state behavior due to unforeseen disturbances. In worst case, such disturbances may render the reactor unstable, i.e. might lead to thermal runaway. So, in this chapter, an overview of the development of polyethylene production and a summary of the most important polyethylene properties is given (Sec. 1.1 and 1.2).

Thereafter, a literature survey is presented followed by a short introduction into the simulation environment that is used in this work (Sec. 1.4). A brief scope closes this chapter (Sec. 1.5).

1.1 Polyethylene Production – Past to Present

A very detailed history of development of the different types of polyethylene can be found e.g. in Plastics and Rubber Institute (1983a,b); Seymour and Cheng (1986); Whiteley et al. (1998).

Polyethylene is a polymer that is produced from the monomer ethene. The name of the polymer is derived from the non-IUPAC (**I**nternational **U**nion of **P**ure and **A**pplied

Chemistry) monomer name ethylene (≡ ethene).

The discovery of polyethylene (PE) was the result of experiments carried out to evaluate the effort of applying high pressures on chemical reactions. In 1933, ethylene gas was compressed to 1400 bar. As a result, a white solid was formed in the vessel and that solid turned out to be **L**ow-**D**ensity **P**oly**E**thylene (LDPE). Later it was shown that the presence of traces of oxygen caused the polymerization and that larger amounts of oxygen would lead to heavy explosions. A pilot plant with a small reactor produced small amounts of LDPE with at that time interesting product properties.

The first commercial plant started its production in 1939. In World War II, LDPE was used as a flexible, low density coating and insulating material for electrical cables. E.g. as an underwater cable coating or more important from a strategic military point of view as a critical insulating material for such applications as radar insulation. Because of its light weight, radar equipment was easier to carry on a plane, which allowed the out-numbered Allied aircrafts to detect German bombers. By the end of the war, England's production of PE was 20 times higher than before the war.

In the beginning of the industrial production of low-density polyethylene, polymerization was started only by using free radical initiators leading to partially crystalline polymers. The degree of the crystalline structure was determined by measuring the density. The process was carried out at high pressure and high temperatures. At higher temperatures one has to deal with side reactions which lead to a branched polymer and thus the densities were lower than what could be expected of a completely amorphous and crystalline polyethylene.

Later developments led to a process involving catalysts. Such a process could be carried out at lower pressure and lower temperatures and hence the densities were

Process	Autoclave	Tubular
Capacity ($10^3 t/a$)	117	200
Capital cost (10^6 €)	70	96
Production cost	565	544
Depreciation	71	59
Total costs	636	603

Table 1.1: Investment and running costs comparison of the autoclave and tubular reactor process (€/t, Whiteley et al. (1998)).

higher (**H**igh-**D**ensity-**P**oly**E**thylene). High-density polyethylene has a density that ranges from 0.94 to 0.97 $\frac{kg}{m^3}$. Its molecules have an extremely long carbon backbone with no side groups. As a result, these molecules align into more compact arrangements, accounting for the higher density of HDPE. High-density polyethylene is stiffer, stronger, and less translucent than low-density polyethylene.

The original process for the LDPE production was based on an autoclave reactor. There, the hot reactants mix with the cold incoming ethylene and keep the process stable. Later on, the process involving the tubular reactor was developed. This process produced LDPE with a consistent molecular weight. Still, both production processes are commercially used, and although they are operated at very high pressures, some of these reactors have been in service for many years. Not only LDPE, but also LLDPE (**L**inear LDPE) can be produced in the high-pressure process.

The physical properties of LDPE produced in autoclave reactors differ significantly from those of the tubular reactor process. Autoclave LDPE products are considered to be the products of choice for extrusion coating applications. On the other hand, LDPE resins produced using tubular reactors are more suitable for extruded foam applications. Hence, depending on the application, the reactor type has to be chosen (Auger and Nguyen, 2001). If the application allows both types, then one advantage of autoclave reactors is that they have lower investment costs, based on the cost of the reactor system. On the other hand, variable costs for tubular reactors are slightly lower (Tab. 1.1).

	N. America	Europe	Japan	Rest	Total
LDPE	3891	7701	1444	4210	17246
LLDPE	4422	1948	1059	3728	11157
HDPE	6198	4881	1024	4715	16891
Total	14511	14530	3527	12653	45221

Table 1.2: Low-density, linear low-density and high-density polyethylene production capacities in $10^3 t$ per year in 1995 (Whiteley et al., 1998)

Since it can be produced within a very broad range of both different grades and different manufacturing processes, polyethylene has now become one of *the* major plastic worldwide. Summing up the most important types of polyethylene, in particu-

lar low-density, linear low-density and high-density polyethylene, the annual production rate is $\approx 45\ 10^6 t$ in 1995, see Table 1.2. Such a high production rate also implies, that any failure in the production process is very costly. Failure includes also up- or downstream processing.

In Germany, the vast majority of steam crackers is located in the Rhine valley in the Köln/Wesseling/Gelsenkirchen area. But also Münchsmünster and Burghausen are very important production sites. Because of their island position (far in the south, far-off from the major consumers except of Wacker-Chemie), it is planned to built an ethylene pipeline from there to the production sites of BASF in Ludwigshafen (see Ethylen-Pipeline Süd GbR (2006)). This pipeline should bring more process reliability and flexibility to both, the ethylene production sites and the ethylene processing sites, because the produced ethylene has to be processed further on immediately. Hence a failure in the ethylene production would always result in a failure of the whole production site and vice versa.

1.2 Physical Properties

Usually polyethylenes are characterized by their density or by the **M**elt **F**low **I**ndex (MFI). The MFI test was initially developed for LDPE as a measure for the melt characteristic under conditions related to its processing. Low-density polyethylene has a density ranging from 0.91 to 0.93 $\frac{kg}{m^3}$. The molecules of LDPE have a carbon backbone with side groups of four to six carbon atoms attached randomly along the main backbone. LDPE has a high number of long- and short-chain branches which results in a lower tensile strength and increased ductility. It is a whitish solid that is flexible.

LDPE combines electrical insulation properties with toughness, flexibility, lightness and inertness. Inertness means here that it is resistant to acids, alcohols, bases and esters. Moreover it is easily weldable.

Some of the most important physical properties are given in Tab. 1.3. The correlation of important properties to process variables is depicted in Fig. 1.1. As one can see from there, the operation conditions are of major importance for the properties of the final product. The plot in the top left position shows that from a conversion point of view, the higher temperature and pressure in the process, the higher the conversion.

Property	Value
Melting point	$100 \div 120\ ^{\circ}C$
Utilization temperature	$-50.0 \div [50.0 \ldots 80.0]\ ^{\circ}C$
Glass transition temperature	$\approx -40\ ^{\circ}C$
Density	$0.91 \div 0.93\ \frac{kg}{m^3}$
Tensile Strength	$5 \div 25\ MPa$
Viscosity	$17\ kPa \cdot s$
Thermal conductivity (at $23^{\circ}C$)	$0.33\ \frac{W}{Km}$
Specific heat	1900-2300 $\frac{J}{kgK}$
Transparency	translucent
Chemical resistance	against acids, solvents and alkalis

Table 1.3: Some physical properties of low-density polyethylene.

But if one also looks at the other three diagrams, then it is clear that operating this process is always a balancing act between conversion and properties and also between properties amongst each other.

The predominant uses of both LDPE and LLDPE is for films, e.g. for packaging in food industry because of its translucency and inertness. But these films are not all for packaging purposes, e.g. by welding one end bags are produced directly from the film. Apart from these packaging applications also of heavy duty sacks are made out of LDPE or LLDPE. Moreover it can be used e.g. for sealing membranes in civil engineering constructions or for shrink-wrap, squeezable food bottles or as insulation material for wires and cables.

1.3 Literature Survey

As indicated by Tab. 1.2, LDPE is one of the most often produced polymers in the world. Hence also the amount of publications dealing with the kinetics and physical properties as well as the production of low-density polyethylene is enormous. A good overview on the polymerization of olefins in general is given in Kiparissides et al. (1993); Ray (1983) and Whiteley et al. (1998). There the most important reaction steps, the different types of PE as well as the main production processes are introduced. Ray (1972) focuses on the mathematical modeling of polymerization reactors in general. This review lists different techniques for the calculation of molec-

ular weight distributions. One of these techniques is the introduction of statistical moments, and a summary lists properties of distributions, which can be expressed in terms of those moments, e.g. number average chain length or the variance of the number average chain length distribution σ^2. Congalidis and Richards (1998); Schuler (1981) and Kiparissides (1996) focus on the control of polymerization processes. A general solution to both control and optimization is an accurate mathematical model of the process, an appropriate set of control/optimization parameters, a suitable objective and an efficient numerical method for the solution of the specific problem. In particular, the definition of the objective function is not always easy in the sense that some controlled variables may react in opposite directions to variations of a control/optimization parameter. Moreover, the resulting problems are challenging to solve numerically.

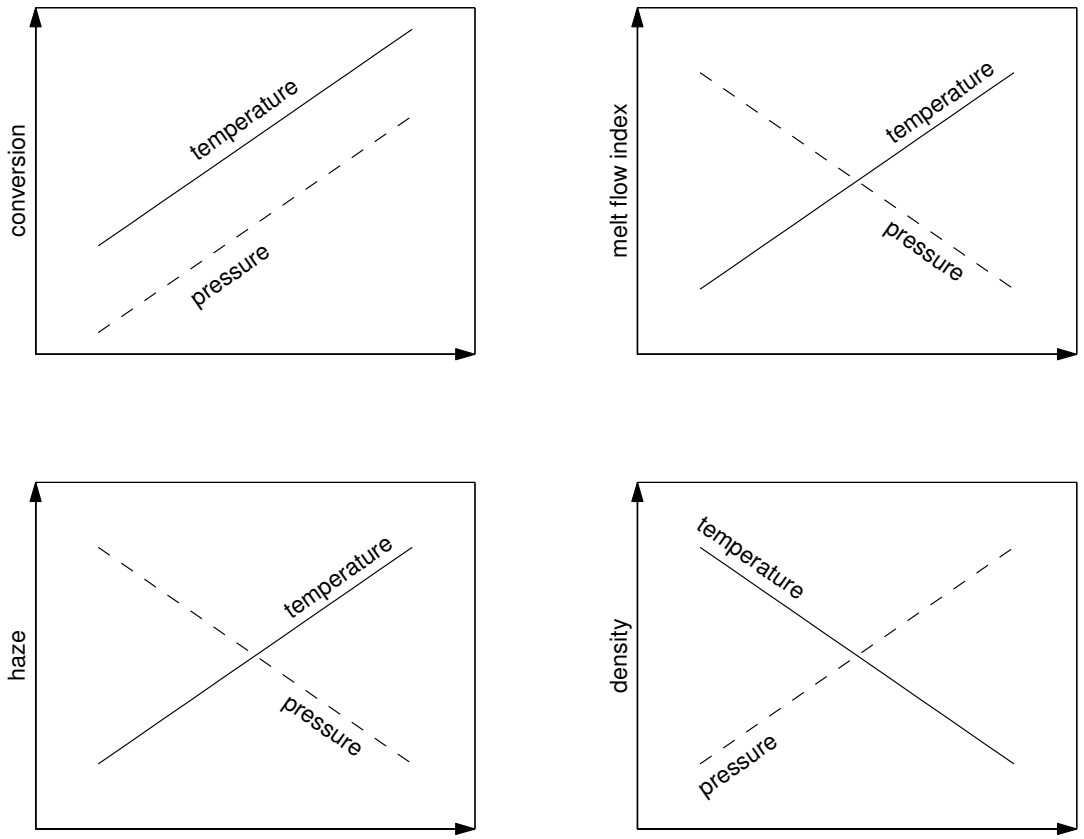

Figure 1.1: Relationship of physical properties to process variables, such as temperature or pressure (Meyers, 2004)

Publications of Luft (1979, 2000) give a good overview on the production of high-density polyethylene in both lab-scale and industrial processes. In particular, due to the rise in energy costs, a rise in operating pressure is now obsolete, even though this influences product properties for some applications positively. However, in the high pressure process, there is an enormous effort to save energy costs. This also implies well designed separators, since the degree of separation is higher, the lower the flash pressure is taken. Hence, also the solubility of monomer in the polymer melt has been studied intensively, e.g. Bokis et al. (2002); Koak et al. (1999); Liu and Hu (1998); Orbey et al. (1998). But for this work, a two parametric equation is fitted to measured data. Not only the phase equilibrium, but also all reaction rates have been subject of research projects. Luft et al. (1978) investigated the decomposition rates of different initiators for high pressure polymerizations. They reported a pressure dependency of those rates which they expressed in terms of activation volumes in the reaction rate.

Beuermann and Buback (1997) primarily addressed the propagation and termination rate coefficients of homo-polymerizations. Their special emphasis has been on a conversion dependent termination rate of low-density polyethylene at pressures up to 3000 bar and temperatures up to 300$^{\circ}C$. They also reported that limitations of previous simulation studies mainly resulted from limited availability and reliability of kinetic data even for homo-polymerizations. Other literature, e.g. by Luft et al. (1982) reported that initiator types have no effect on long- or short-chain branching, whereas higher temperatures promote the formation of both branching types. Moreover also the reactor geometry influences the long-chain branching, since this changes the temperature distribution in the reactor.

Buback et al. (2000) reported a termination rate that is dependent on the chain length and additionally Busch (2001a) used a reaction rate for the transfer reaction to polymer which is dependent on the chain length. Thereby a better estimate for propagation reaction could be derived. In these studies and also in Busch (2001b), simulations using *Predici®* supported the experiments.

According to Hutchinson and Fuller (1998), β-scission and long-chain branching are the reaction steps, that are very important for the physical properties of the produced polymer. Additionally, these reactions prevent gel formation even though on the one hand the rate coefficients of these reactions are small compared to propagation and on the other hand only 2.4% of all secondary radicals undergo intramolecular

β-scission.

Lorenzini et al. (1992a,b) fitted the kinetic parameters of a very detailed reaction scheme in an autoclave reactor. They reported, that the application of a quasi steady state assumption is problematic for free radicals in the tubular reactor process, because of rapid temperature changes occurring along the axis.

Various publications use different modeling methods for the simulation of polymerization reactors. In particular, Tsai and Fox (1996) used computational fluid dynamics for three-dimensional simulations of the polymerization of low density polyethylene in a tubular reactor at the nominal operating point. Although their kinetics is rather simple, also they reported, that depending on the kinetics the quasi steady state assumption sometimes fails. For some cases, they found an error larger than 100 % for monomer conversion, if this assumption is used. Moreover also reactor geometry and operating parameters have large influence on monomer conversion. Read et al. (1997) confirmed this result and concluded, that there is a need for an optimization of operating parameters. Also Zhou et al. (2001) used CFD simulations for the solution of a two-dimensional tubular and a three-dimensional autoclave reactor. Additionally their models provided information on the physical properties of the polymer, such as polydispersity or mean of the molecular weight distribution.

Zacca et al. (1997) applied population balances to the model of an autoclave reactor and examined effects of the residence time distribution. According to their findings, this plays a significant role in the formation of the physical properties of the homo-polymer. A brief overview on the different modeling and simulation strategies can be found in Bartke and Reichert (1999).

Publications, dealing with steady state models of the tubular reactor process are numerous. Here only a few examples are listed. Zabisky et al. (1992) derived a steady state model, using a very sophisticated reaction scheme with additional initiation using oxygen. Yet, none of the rate coefficients was depending or either chain length or conversion. A similar reaction scheme was used (by the same authors) in Chan et al. (1993) for an autoclave reactor. Kiparissides et al. (1996) derived a steady state model for on-line parameter estimation, such that the model captures the actual reactor operation. Lacunza et al. (1998) investigated on the influence of the overall heat transfer coefficient. They reported, that correct estimates of the heat transfer coefficient are a major issue for predicting the plant behavior using rigorous mathematical models.

In Mähling et al. (1999) results of the reference of the rigorous model in this work are published. There the simulations are coupled to *Predici®*, in order to derive the molecular weight distribution.

The first dynamic mathematical model is reported in Gilles and Schuchmann (1966) using a simple reaction scheme (only the main reactions for free radical polymerizations) and constant parameters such as overall heat transfer coefficients, density etc. As a first publication in a series, Brandolin et al. (1996) derived a rather detailed steady state model. However, also this model shows no reaction rate depending on chain length or conversion. Moreover the overall heat transfer coefficient is constant. Later on, the complex steady state model has been converted into a rather simple dynamic model, still using constant parameters, e.g. for heat transfer. The simple model has then been used for simulation and optimization results in several publications (Asteasuain et al., 2000, 2001; Cervantes et al., 2000).

Additionally, Ray (1981) investigated the dynamic behavior of polymerization reactors. Runaway, multiple steady states and autonomous oscillations are reported there for CSTRs and autoclave reactors. According to Villa et al. (1998) and Ray and Villa (1999), the nonlinear behavior depends on the type of polymer and its kinetics, the type of reactor, the heat removal system and the phase behavior. However, these results have only been investigated on autoclave or continuous-stirred tank reactors.

Hence, despite of various sources in literature, only few dynamic models are available in literature so far, which additionally lack some important features, that are reported to have significant influence (e.g. a variable overall heat transfer coefficient). One reason might be, that in former days, the plants have been built as single-product plants. However, nowadays, due to technical progress, polymers can be produced in different grades in the same plant just by changing the operating conditions. So these plants are not only operated in steady state regimes, they undergo frequent dynamic transitions between these steady states. In fact, in modern tubular reactor processes, up to 15 different grades may be produced. In order to simulate and optimize grade changes, a rigorous dynamic model has to be developed.

The level of detail is needed to have a physical insight to the very complex process, that not only incorporates many components but is also operated at extreme conditions, such as high pressure or high temperature, which is quite close to glass temperature. Since dynamical aspects are the main focus of this work, the influence

of the tube wall cannot be neglected. Because almost all models available in literature are of steady state type, this effect has never been studied so far, although there might occur some interesting unexpected behavior, as this reaction is highly exothermic. Eigenberger (1974) reported such behavior for highly exothermic reactions. It has been stated, that the effect of the heat accumulation causes excess temperatures to occur for lowering the feed temperature or raising the feed flow rate. In fixed-bed reactors Mangold et al. (1998, 2000b) observed similar effects. Since in these publications gas phase reactions have been studied, the effects become much more visible.

Of course, the level of detail required for such purposes like optimization, also causes difficulties. Deriving the mathematical model equations from first principles, one ends up with a considerable number of partial differential and algebraic equations (PDAEs). The simulator DIVA, which is briefly introduced in the Sec. 1.4, is only capable to solve differential and algebraic equation (DAE) systems. Hence the system of PDAEs has to be transformed into a set of DAEs, which is done by a Method of Lines approach utilizing a moving grid (Köhler, 2002; Köhler et al., 2001; Wouwer et al., 2001). Moving grid means, that the grid points are not fixed to some location, but the position of the grid points may change with respect to a monitored function. This enables one to reduce the number of grid points, while the resolution in regions of large gradients is still reasonable.

1.4 Simulation Environment DIVA and SyPProT

In this section, the simulation environment which is used throughout this work is introduced. As one can observe from Fig. 1.2, this environment integrates the four main tools, the process simulator DIVA (Holl et al., 1988; Kröner et al., 1990), the preprocessing tool for differential and algebraic equations Code Generator (Räumschüssel et al., 1994), the symbolic pre-processing tool for integro partial differential and algebraic equations SyPProT (Köhler, 2002) and the process modeling tool ProMoT (Tränkle, 2000; Waschler et al., 2006), which presently supports a DAE description of the mathematical model implementation.

The process simulator DIVA integrates different numerical methods for the simulation, analysis and optimization of large nonlinear differential algebraic equation systems. Therefore it utilizes very efficient state-of-the-art sparse numerical algo-

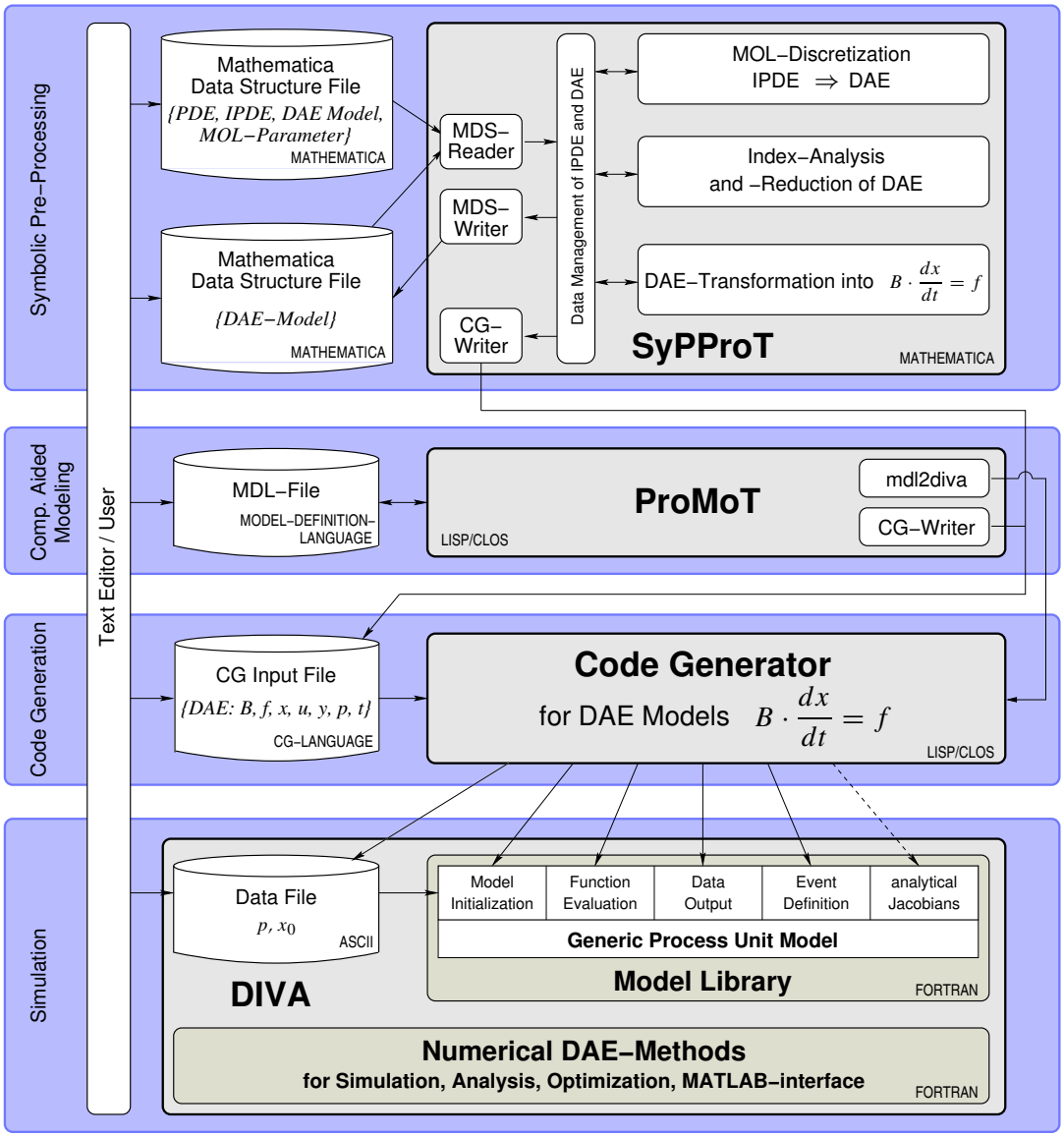

Figure 1.2: Architecture of the simulation environment comprising the process simulator DIVA, the FORTRAN source code generation tool Code Generator, symbolic pre-processing tool SyPProT and process modeling tool ProMoT (modified form from Köhler (2002))

rithms, e.g. for time integration the extrapolation method LIMEX (Ehrig et al., 1999), which has been implemented into DIVA in its latest version as one part of this work, or the sparse implementation of the BDF algorithm DDASAC (Caracotsios and Stewart, 1985). Both, the numerical algorithms and the model descriptions in the model library

are implemented in FORTRAN. The mathematical models of individual process units are represented in the form of linear-implicit differential and algebraic equations with a differential index ≤ 1

$$\mathbf{B}(\mathbf{x}, \mathbf{p}, \mathbf{u}, t)\dot{\mathbf{x}} = \mathbf{f}(\mathbf{x}, \mathbf{p}, \mathbf{u}, t) \tag{1.1}$$

with the initial conditions

$$\mathbf{x}(t = t_0) = \mathbf{x}_0. \tag{1.2}$$

In general, $\mathbf{B} \in I\!R^{N_x \times N_x}$ is a not necessarily regular left-hand side matrix, and $\mathbf{f} \in I\!R_x^N$ is the right-hand side function vector. $\mathbf{x} \in I\!R^{N_x}$ is the vector of the state variables with initial values $\mathbf{x_0}$, where N_x is the total number of states. $\mathbf{p} \in I\!R^{N_p}$ and $\mathbf{u} \in I\!R^{N_u}$ are parameter and input variables.

Since the coding of individual process units in FORTRAN is very inconvenient, the Code Generator allows a symbolic description of the mathematical model equations and automatically converts them into efficient FORTRAN code. Still the model *must* be represented as DAE system. Nevertheless, the Code Generator is both the interface to DIVA for users and the interface for more advanced tools, such as SyPProT and ProMoT.

ProMoT is a modeling tool for object-oriented and equation-based modeling of arbitrary equation systems. It contains modeling entities that represent the structure of unit models, in particular its model equations and interface definition. By aggregation and inheritance knowledge bases may be designed, whose modeling entities (the process units) have standard interfaces, are well documented and hence suitable for direct reuse and refinement. ProMoT either generates a Code Generator input file, or directly accesses the Code Generator. However, ProMoT also does not support distributed models.

This gap is closed by the package SyPProT . This package symbolically transforms a given system of integro partial differential and algebraic equations into a discretized set of ordinary differential and algebraic equations. The latter is then converted into a format the Code Generator supports. So far, ProMoT and SyPProT are not connected to each other, even though both would benefit from the advantages of

the other. Here, because of the nature of the rigorous model equations, the symbolic pre-processing tool SyPProT is used for the implementation of the model.

1.5 Outline of this Work

Each chapter starts with a more detailed introduction on its scope. Hence, here only a brief overview of this work is given. At first, in Chap. 2, the production process is introduced, and the detailed dynamical model for all involved process units will be derived and presented. The partial differential equation system of the rigorous mathematical model is transformed into a system of differential and algebraic equations using an Adaptive Method of Lines. Moreover, a second, simpler model is presented and discussed in this chapter. The simple model is used for the nonlinear analysis of the system. Simulation results are presented in Chap. 3, which is divided into three parts. The first two parts present steady-state (Sec. 3.1) and dynamic (Sec. 3.2) simulation results of the detailed model. The third part (Sec. 3.3) shows the nonlinear analysis using the simple model. Chap. 4 gives an outlook on dynamic optimization of the process, therefore a sensitivity analysis is used to identify both, suitable objectives and important optimization parameters. Finally, a summary will be given in Chap. 6 and the interested reader may look in detail at all model equations (App. B) and some additional remarks on the Adaptive Method of Lines in App. C.

Chapter 2

Modeling

No human investigation can be called real science if it cannot be demonstrated mathematically.
– Leonardo da Vinci

In this chapter, one of the main parts of this work is introduced, the derivation of the rigorous dynamic mathematical model. At first, a detailed overview of the production process involving a tubular reactor is given (see process flowsheet in Fig. 2.1). Then, in Sec. 2.2, the reaction scheme and the detailed distributed model of the tubular reactor are introduced. To include the heat capacity of the thick reactor wall, without increasing the model size drastically, a simple discretization scheme is proposed to account also for the radial heat transfer. The partial differential and algebraic equations are transformed into a system of ordinary differential and algebraic equations using a Method of Lines approach. Both, simulations of only the tubular reactor with an equidistant and an adaptive grid are compared to each other and the moving grid is chosen for the remainder of this work since it offers a reasonable compromise between model size and accuracy. In Sec. 2.3, the mathematical models of the peripheral units, such as compressors, flash units or recycle lines are shown. These units are described by ordinary differential and algebraic equations. For the nonlinear analysis, in addition to the rigorous dynamic model, a simpler dynamic model of the tubular reactor is presented, which includes also a simplified reaction scheme.

2.1 Process Description

LDPE can be produced in either an autoclave or a tubular reactor. As mentioned in Chap. 1, both types are commercially in use. In this work, only the tubular reactor production process is considered. A rough flowsheet of the process is shown in Fig. 2.1.

The feed to the plant is fresh monomer (ethylene) together with the modifier that controls the molecular weight. The feed is mixed with the low pressure recycle stream and pre-compressed in a primary compressor to an intermediate pressure of approx. $250-300\ bar$. The outlet of the primary compressor is mixed with the high pressure recycle and compressed in the hyper compressor to a final pressure of approx. $2000-3000\ bar$. The hyper compressor consists of two stages. After the second stage the ethylene is further heated up for the reaction to take place. The high pressure is required since ethylene is gaseous above its critical temperature of $9^{\circ}C$. At pressures above 2000 bar and temperatures higher than $160^{\circ}C$, the polymer is able to dissolve in the unreacted ethene.

The outlet of the hyper compressor is fed to the main unit of the low-density production process, the tubular reactor. Right at the inlet of the tubular reactor, a mixture of three different initiators is injected into the feed stream. These initiators decompose selectively with respect to temperature and start the chain growth reaction. The reaction is highly exothermic and heat is removed by coolant cycles that are operated co- or counter-current wise. The coolant is kept at two different temperature levels. Usually for removing the heat in the two cooling zones right after an initiator injection point warmer coolant is taken. The next two zones are operated at a lower level, to be able to add fresh initiator at the successive injection point. Since the temperature at the successive injection points is already at a higher level, only initiators decomposing at intermediate and high temperatures are added there.

The length of a tubular reactor for LDPE production is $> 1000\ m$. Inspite of this length, the conversion acchieved in the reactor is only about $25-35\ \%$. Hence, unreacted monomer and modifier have to be separated from the product in two flash units. The unreacted monomer and the modifier are recycled in two recycle lines, which are operated at different pressure levels. There they are cooled down and fed again to the process at the compressors with corresponding inlet pressure level. The

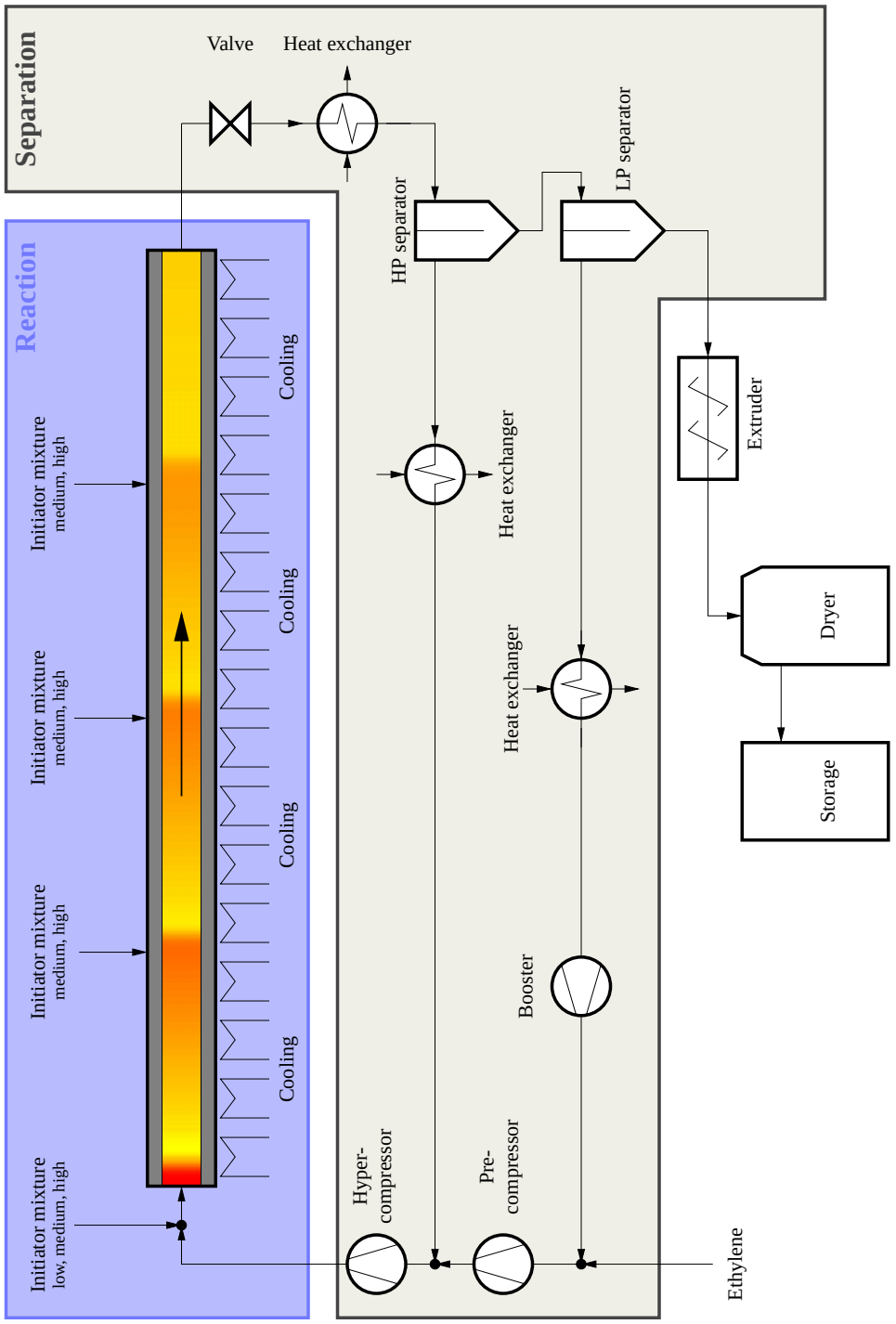

Figure 2.1: Flowsheet of the tubular production process of low-density polyethylene

polyethylene melt, which still contains minor quantities of ethylene is completely withdrawn from the plant, and processed downstream further on. The downstream processing involves an extruder for degassing and for inclusion of additives to meet the final customer requirements. Common additives are dyeing agents, UV-stabilizer (e.g. carbon black), anti-static additives or fire protectors.

As one can see from Fig. 2.1, the plant can be considered as reactor-separator system. Reaction takes place of course in the tubular reactor, whereas the separator units are located downstream to recover unreacted monomer from the product. The unreacted material is recycled in the two recycle lines. For purposes of clarity the reactor section in Fig. 2.1 is shown in a blue box, whereas the separator units are enclosed in a gray box.

In this chapter the model of the plant is derived from first principles using conservation laws for momentum, mass and energy. All units except the downstream processing units, i.e. the extruders for the incorporation of additives and degassing will be part of the detailed mathematical model. Starting with the model of the tubular reactor in Sec. 2.2, the model equations of the more peripheral units (compressors (see Sec. 2.3.2) and the flash units (see Sec. 2.3.3)) will be presented. In Sec. 2.4 a

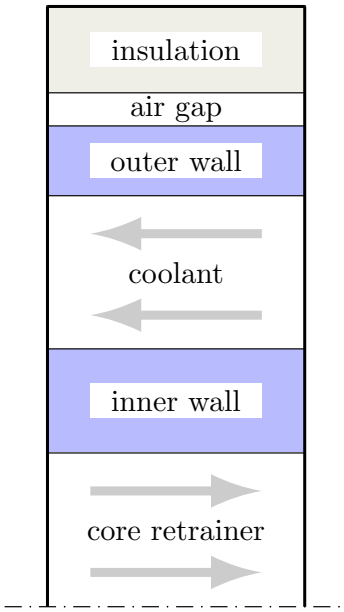

Figure 2.2: Cross section of the tubular reactor

simplified model of the process will be introduced which will enable us to analyze the nonlinear behavior of this reactor-separator system in detail.

2.2 Detailed Model of the Tubular Reactor

A sketch of a cross-section of the tubular reactor is depicted in Fig. 2.2. As one can observe, the reactor itself consists of three nested tubes, the inner wall, the outer wall and the insulation. Moreover, between outer wall and insulation there is an air gap for additional insulation. In the detailed model, which will be derived in this section, the coolant will flow in the counter-current direction, but in the real process, it is possible to operate each coolant cycle differently. Although the sketch in Fig. 2.2 is not provided with a scale, the relations of the different thicknesses are drawn correctly. In particular, the thickness of the inner wall is approximately of the same order as the inner diameter and large compared to the thickness of the outer wall and the insulation.

In the tubular reactor the single-phase ethylene-polyethylene mixture allows the reaction to take place as a free radical initiated polymerization. A detailed explanation of the reaction mechanism is given in the following subsection. Then the model equations are derived and the simplifications are introduced and discussed. Moreover, the model will be validated and different discretization schemes are compared. Based on this comparison, an appropriate scheme is selected and used throughout the remainder of this work for all simulations that use the rigorous model of the tubular reactor.

2.2.1 Reaction Mechanism

Both, in a tubular or an autoclave reactor, LDPE is produced by a free radical polymerization. For free radical polymerizations, the reaction scheme can be divided into two parts, the main reactions (Sec. 2.2.1.1), which are characteristic for all free radical polymerizations and the side reactions (Sec. 2.2.1.2). Side reactions usually account for the structure (linear or branched chains, longer or shorter branches) and hence for the physical properties of the polymer.

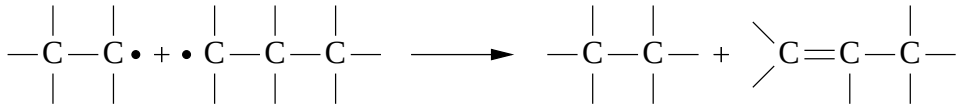

Figure 2.3: Symbolic scheme of a termination by disproportion (2.7)

2.2.1.1 Main Reactions

The main reactions, which are common to all free radical polymerizations, comprise initiation, propagation and termination. Therefore free radical donators, such as oxygen or peroxides are used to initiate the polymerization. In this work, the reaction is started with a mixture of different initiators. Each of them decomposes into radicals at a distinct temperature level. E.g. at the inlet of the tubular reactor, a mixture of three different initiators is used. One decomposes at moderate temperatures, another one at intermediate and the third one only at very high temperatures. Buback (1980) reported a thermal initiation of ethylene, also leading to radicals. The rate of thermal initiation usually is much lower than the one corresponding to the other initiation reactions. The next main step is the chain growth reaction. In the presence of radicals, new monomer molecules are added to the reactive end of the radical, forming longer radicals, so-called "living polymer". When the concentration of radicals is high enough, in the third step, the chain growth reaction terminates resulting in "dead polymer". Two different mechanisms lead to the termination, combination and disproportion. A schematic sketch of the termination by disproportion reaction is depicted in Fig. 2.3. Since Reac. (2.7) results in two dead polymer chains, one end of the one chain is unsaturated, meaning that there occur double bonds.

The following reaction scheme summarizes the main reactions,

$$I_v \xrightarrow{k_{I_v}} 2\, R_{I_v} \qquad \text{initiator decomposition,} \tag{2.1}$$

$$R_{I_v} + M \xrightarrow{k_{p,I_v}} R_1 \qquad \text{initiation,} \tag{2.2}$$

$$R_X + M \xrightarrow{k_{p,X}} R_1 \qquad \text{initiation,} \tag{2.3}$$

$$3\, M \xrightarrow{k_{th}} 2\, R_1 + M \qquad \text{thermal initiation,} \tag{2.4}$$

$$R_i + M \xrightarrow{k_p} R_{i+1} \qquad \text{propagation,} \tag{2.5}$$

$$R_i + R_j \xrightarrow{k_{t,c}} P_{i+j} \qquad \text{termination by combination and} \qquad (2.6)$$

$$R_i + R_j \xrightarrow{k_{t,d}} P_i + P_j + DB \qquad \text{termination by disproportion.} \qquad (2.7)$$

In this notation, the index ν is used for the distinction of the different initiators I ($\nu = 1, 2, 3$). A higher index means a lower decomposition temperature of the initiator, i.e. initiator 1 decomposes at high, initiator 3 at low temperatures. Moreover, R_{I_ν} denote the corresponding initiator radicals. M is the monomer (ethene or ethylene). R_i in general is living polymer and P_i dead polymer of chain length i. Note that from a chain growth point of view there is no distinction between the radicals coming from an initiation by initiators (2.2), by modifier X (2.3) or by thermal initiation (2.4), since the main difference between the generated living polymer chain of chain length one is the terminating molecule. In order to account for the formation of double bonds by the termination reaction (2.7), the additional "species" DB is introduced. This species represents the concentration of molecules containing double bonds. All $k_\bullet$ denote the rates of the different reactions.

2.2.1.2 Side Reactions

In addition to the main reaction steps (2.1)–(2.7), which occur in all free radical polymerization processes, several side reactions are also present. These reactions lead to long- or short-chain branching and to an additional formation of double bonds. Both, long- and short-chain branching are crucial factors which influence the physical properties of low-density polyethylene. In fact, Hutchinson and Fuller (1998) reported that long-chain branching and β-scission have an important influence on the molecular weight distribution of the produced polymer. The reaction schemes for those reactions are

$$R_i + M \xrightarrow{k_{tr,M}} P_i + R_1 + DB \qquad \text{chain transfer to monomer} \qquad (2.8)$$

$$R_i + P_j \xrightarrow{j \cdot k_{tr,P}} P_i + R_{sec,j} \qquad \text{chain transfer to polymer} \qquad (2.9)$$

$$R_i + X \xrightarrow{k_{tr,X}} P_i + R_X \qquad \text{chain transfer to modifier} \qquad (2.10)$$

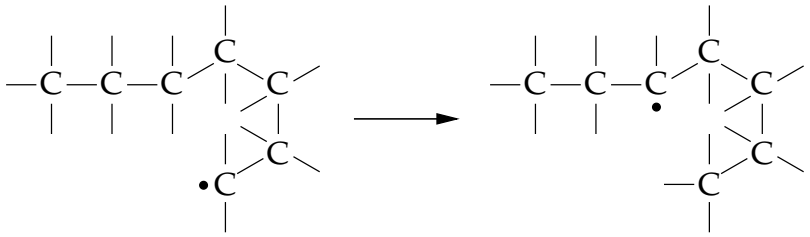

Figure 2.4: Reaction scheme for the back-biting reaction (2.12), that leads to short-chain branches (here with a butyl branch).

$$R_{sec,i} + M \xrightarrow{k_{p,sec}} R_{i+1} + LCB \qquad \text{propagation of sec. radicals} \qquad (2.11)$$

$$R_i \xrightarrow{k_{bb}} R_i + SCB \qquad \text{back biting} \qquad (2.12)$$

$$R_{sec,i} \xrightarrow{k_\beta} P_{i-k} + R_k + DB \qquad \beta\text{-scission} \qquad (2.13)$$

Reactions leading to long- and short-chain branching are (2.11) and (2.12). The back biting reaction is depicted in more detail in Fig. 2.4. It is an intramolecular transfer reaction, where the radical is transferred from the end to an intermediate position within the chain. This intramolecular transfer only happens within the first six to ten carbon atoms, hence it is the origin of short-chain branches SCB. Fig. 2.4 shows the formation of a butyl branch, but it is also possible that hexyl or amyl branches are established.

Long-chain branching is a result of the chain transfer reaction to polymer (Busch and van Boxtel (1998), Reac. (2.9)). There dead and living polymer are produced, where the reactive atom is not located at the end of the chain, but at an intermediate position (at least further away than ten carbon atoms from the end). Such a living

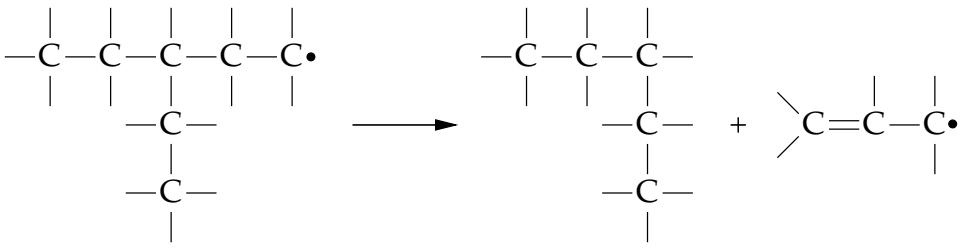

Figure 2.5: Reaction scheme for the β-scission (2.13) leading to an unsaturated end.

radical is denoted by the subscript sec for secondary living polymer. Secondary living polymer is then consumed by either a propagation reaction (2.5) leading to long-chain branching, or by the β-scission reaction (2.13). The propagation step of the secondary radicals is straightforward. New monomer adds to the branched molecule leading to longer branches. Hence the additional enumerator LCB increases. The β-scission reaction is more sophisticated and hence depicted in detail in Fig. 2.5. In the β-scission reaction, a carbon-carbon bond is split up, forming two shorter polymer chains. One dead polymer chain of length $i-k$ and a primary living polymer chain of chain length k with an unsaturated end. Such breakage might occur at any point k within the chain of the secondary living radical $R_{sec,i}$.

Additionally to the main termination reactions and β-scission, dead polymer is produced by the chain transfer reactions (2.8)–(2.10). The difference between step growth in (2.5) and the transfer reaction in (2.8) is that in the latter case a dead polymer with unsaturated end is produced. The probability that the first reaction takes place though is much higher.

Most of the reaction rates, i.e. those of Eqns. (2.1), (2.2), (2.8)–(2.10) and (2.13), are of Arrhenius type,

$$k_\bullet = k_{0,\bullet} \exp\left(\frac{-dE_\bullet - (p-p_0)\,dV_\bullet}{\mathbb{R}T}\right). \tag{2.14}$$

The other reaction rates, i.e. propagation (2.5) and termination (2.6) and (2.7) consist of two terms, one that follows the Arrhenius equation and another term that is a nonlinear correlation of dynamic viscosities and weight fraction of polymer. Both, the detailed precise rate expressions of those reactions as well as all kinetic parameters used in the reaction rates of the detailed dynamic model are intellectual property of Basell and cannot be published by the author. But one can use the data and correlations given by Kiparissides et al. (1993) instead, which yield similar results. In fact, the data given by Kiparissides et al. (1993) is used in the reaction kinetics of the simple dynamic model, derived in Sec. 2.4.

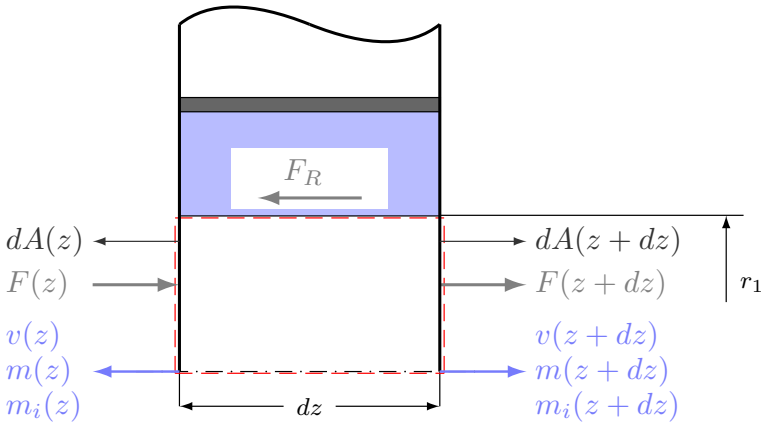

Figure 2.6: Sketch for the momentum balance of the reactor inner tube.

2.2.2 Model Equations

In this section, the mathematical model of the main unit in the LDPE production process, the tubular reactor, is introduced. The rigorous dynamic model is derived from first principles using conservation laws for momentum, mass and energy. Momentum and energy balance equations calculate the pressure drop and the temperature profiles over the reactor.

2.2.2.1 Global Mass Balance Equation

Buback (1980) reported that the ethylene-polyethylene mixture is homogeneous at industrial operating conditions in a tubular reactor of the process considered here. Hence, one phase liquid plug-flow without axial mixing and with heat transfer to either reactor wall or to the coolant jacket can be assumed. Whiteley et al. (1998) stated that plug-flow is achieved by a suitable ratio of pipe diameter and flow rate, which results in sufficient turbulence and good mixing.

The global mass balance equation yields

$$\frac{\partial \varrho(z,t)}{\partial t} + \frac{\partial \varrho(z,t) v(z,t)}{\partial z} = 0. \tag{2.15}$$

Using the quasi steady state assumption ($\frac{\partial \varrho(z,t)}{\partial t} = 0$) results in the continuity equation

$$\dot{m} = const. \tag{2.16}$$

$$v(z,t) = \frac{\dot{m}}{\varrho(z,t)A}, \tag{2.17}$$

with A as the the cross-section of the tubular reactor.

2.2.2.2 Momentum Balance Equation

Generally speaking, the momentum balance equations states, that the change of momentum of a infinitely small element is due to forces acting on that element. In other words:

$$\begin{aligned}\frac{dm_Z v}{dt} &= \sum_i F_i + \dot{m}v(z) - \dot{m}v(z+dz) \\ &= F(z) + F(z+dz) + F_R(z) - dz\frac{\partial \dot{m}v(z)}{\partial z} \\ &= -\int_A p(A,z)\, dA(z) \\ &\quad -\int_A p(A,z+dz)\, dA(z+dz) - \frac{\partial F_z(z)}{\partial z}dz - dz\frac{\partial \dot{m}v(z)}{\partial z}\end{aligned} \tag{2.18}$$

where $F(\bullet)$ is the force due to the pressure and F_R is the force due to friction.

Again, quasi steady state is assumed. Moreover, the cross-section A is constant and the pressure $p(\bullet)$ shall be equally distributed over A. Then the previous equation transforms into

$$0 = -\frac{\partial p}{\partial z} - \frac{1}{A}\frac{\partial F_z}{\partial z} - \frac{\partial \varrho v \cdot v}{\partial z} = -\frac{\partial p}{\partial z} - \frac{\partial p_z}{\partial z} - \frac{\partial \varrho v \cdot v}{\partial z}. \tag{2.19}$$

For technical applications, it is a very common assumption, that the pressure drop is proportional to the square of the velocity,

$$\Delta p_z \sim \varrho\frac{v^2}{2} \quad \rightarrow \quad \Delta p_z = \varphi_z \frac{1}{2}\frac{\dot{m}^2}{\varrho A^2} = \varphi_z \cdot \frac{\dot{m}_A^2}{2\varrho}.$$

Moreover, φ_z should relate to the dimension of the tube, and hence $\varphi_z = \zeta \cdot \frac{\Delta z}{2r_1}$. This finally results in

$$\lim_{\Delta z \to 0} \frac{\Delta p_z}{\Delta z} = \frac{\partial p_z}{\partial z} = \frac{1}{4} \zeta \frac{\dot{m}_A^2}{\varrho r_1},$$

where ζ is a pressure drop factor, r_1 the inner radius and $\dot{m}_A$ the flux with regard to the cross section. Using these results, the momentum balance equation simplifies to

$$\varrho v \frac{\partial v}{\partial z} = -\frac{\partial p}{\partial z} - \frac{1}{4} \zeta \frac{\dot{m}_A^2}{\varrho r_1}. \tag{2.20}$$

However, it is a valid assumption that acceleration forces are negligible compared to friction forces in this application. Then, the momentum balance equation finally yields

$$\frac{\partial p(z)}{\partial z} = -\frac{1}{4} \zeta \frac{\dot{m}_A^2}{\varrho(z) r_1} \tag{2.21}$$

$$BC : p(0,t) = p_{in}(t) \tag{2.22}$$

While in the reactor, the pressure drop is significant (up to 800 bar) and has an influence on all physical properties, the pressure drop is neglected for the coolant.

2.2.2.3 Component Mass Balance Equations

In this section only the general form of the equations is derived. A complete listing of the component balance equations of all species (three initiators, their radicals, modifier, modifier radical and monomer) can be found in App. B.

Using Fig. 2.6, the general form of the component mass balance for species i reads as follows

$$\frac{dm_{Z,i}(z,t)}{dt} = \dot{m}_i(z,t) - \dot{m}_i(z+dz,t) + A\,dz\,M_i \sum_{j=1}^{J} \nu_{ij} r_j(z,t), \tag{2.23}$$

where M_i is the molar mass of component i. The application of a Taylor series expansion with respect to the spatial coordinate for $m_{Z,i}(z+dz,t)$, using $m_{Z,i}(z,t) = m_Z(z,t)\ w_i(z,t) = \varrho(z,t)\ A\ dz\ w_i(z,t)$ and the utilization of the general form of an

overall mass balance (2.15) transform that expression into

$$\frac{\partial w_i(z,t)}{\partial t} + v(z,t)\frac{\partial w_i(z,t)}{\partial z} = \frac{M_i}{\varrho}\sum_{j=1}^{J} \nu_{ij} r_j(z,t) \tag{2.24}$$

$$IC : w_i(z,0) = w_{i,0}(z) \tag{2.25}$$

$$BC : w_i(0,t) = w_{i,in}(t) \tag{2.26}$$

Here (2.25) and (2.26) represent the initial condition and the boundary condition respectively.

The weight fraction of polymer $w_P(z,t)$ is calculated using the summation condition

$$w_P(z,t) = 1 - \Big(w_M + w_X + w_{RX} + \sum_{\nu=1}^{N_I}(w_{I,\nu} + w_{RI,\nu})\Big), \tag{2.27}$$

with $N_I = 3$.

2.2.2.4 Energy Balance Equations

In total, three different energy balance equations are required for the model of the tubular reactor. One describes the temperature profile in the reactor, one the profile in the wall and one is needed for the coolant, which is operated counter-current wise. The reactor consists of two nested tubes, the main tube where reactant and product resides, the intermediate tube, where coolant flows co- or counter current wise and the outer tube with the insulation. The heat insulation is made up of two layers, the first one is just a small air gap, the second one consists of insulation material.

First the energy balance for the inner tube, separating coolant from the reaction mixture will be derived, then the distributed model equations for the reactor and the coolant are shown.

Inner Wall. In this section the energy balance for the wall is derived. At first, a two-dimensional model for the temperature in the reactor wall is derived. Then this equation, which is distributed in two parameters (z, r) is transformed into a semi-

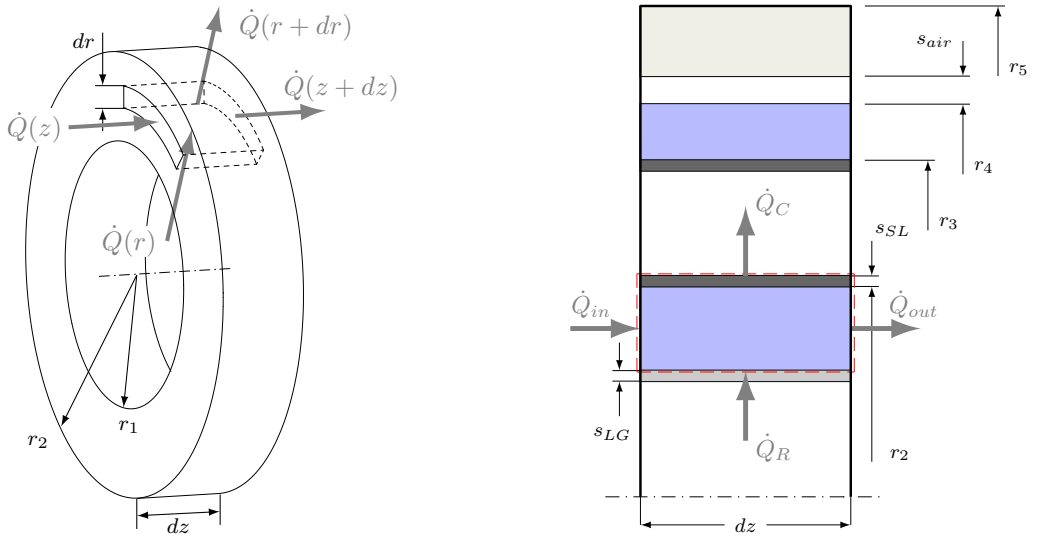

(a) 2-dim (b) 1-dim

Figure 2.7: Cut out of the tubular reactor with heat fluxes for the energy balance equation of the wall

lumped equation, distributed only in the axial dimension. Both partial differential model equations are compared and shortcomings of the semi-lumped model are discussed. Then a suitable modification is proposed for the semi-lumped model in order to improve the validity of the model.

At first, the two dimensional model equation is derived. Using Fig. 2.7(a) one starts with

$$\frac{dU_W}{dt} = \dot{Q}(z) - \dot{Q}(z+dz) + \dot{Q}(r) - \dot{Q}(r+dr). \tag{2.28}$$

Herein, $\dot{Q}(r+dr)$ can be expressed using the Fourier law with a Taylor series expansion by

$$-2\pi\lambda_W dz(r+dr)\frac{\partial \hat{T}_W(r+dr)}{\partial r} = -2\pi\lambda_W dz \left[r\frac{\partial \hat{T}_W(r)}{\partial r} + dr\frac{\partial \hat{T}_W(r)}{\partial r} + rdr\frac{\partial^2 \hat{T}_W(r)}{\partial r^2}\right].$$

This result and the definition $\frac{dU_W}{dt} = \varrho_W A_W c_{p,W}\frac{\partial \hat{T}_W}{\partial t}$, which follows from the caloric equation of state, can be used in Eq. (2.28) to derive the general form of the two-

dimensional temperature distribution in the reactor wall as

$$2\pi c_{p,W}(\hat{T}_W)\varrho_W r\,dr\,dz\frac{d\hat{T}_W}{dt} = 2\pi\lambda_W r\,drdz\frac{\partial^2\hat{T}_W}{\partial z^2} + 2\pi\lambda_W drdz\Big[\frac{\partial\hat{T}_W}{\partial r} + \frac{\partial^2\hat{T}_W}{\partial r^2}\Big],$$

which finally can be transformed to

$$c_{p,W}(\hat{T}_W)\varrho_W\frac{d\hat{T}_W}{dt} = \lambda_W\frac{\partial^2\hat{T}_W}{\partial z^2} + \lambda_W\frac{\partial^2\hat{T}_W}{\partial r^2} + \frac{\lambda_W}{r}\frac{\partial\hat{T}_W}{\partial r}. \tag{2.29}$$

Note that in (2.29) the wall density ϱ_W and the heat conductivity λ_W are constant, in particular the values for steel are $\varrho_W = 7800\frac{kg}{m^3}$ and $\lambda_W = 42\frac{W}{Km}$. The heat capacity is a linear function of the wall temperature.

Radial boundary conditions for Eq. (2.29) are

$$-2\pi\lambda_W r_1\left.\frac{\partial\hat{T}_W}{\partial r}\right|_{r=r_1} = \dot{Q}_R(T, \hat{T}_W|_{r=r_1}) \tag{2.30}$$

and

$$-2\pi\lambda_W r_2\left.\frac{\partial\hat{T}_W}{\partial r}\right|_{r=r_2} = \dot{Q}_C(T, \hat{T}_W|_{r=r_2}) \tag{2.31}$$

for $r = r_1$ and $r = r_2$ respectively. Heat fluxes $\dot{Q}_R$ and $\dot{Q}_C$ transferred at the boundaries can be calculated by

$$\dot{Q}_R = k_{inner}(T - \hat{T}_W|_{r=r_1}) \tag{2.32}$$

$$\dot{Q}_C = k_{outer}(\hat{T}_W|_{r=r_2} - T_C). \tag{2.33}$$

Herein, T is the reactor temperature, T_C the temperature of the coolant. Moreover, k_{inner} and k_{outer} are the overall heat transfer coefficients from reactor to the wall and from the coolant to the wall respectively. These coefficients can be calculated by

$$k_{inner} = \frac{1}{R_i + R_{ll,i}}, \tag{2.34}$$

$$k_{outer} = \frac{1}{R_{sl,i} + R_{C,i}}. \tag{2.35}$$

R_i and $R_{C,i}$ account for heat transfer by convection, $R_{ll,i}$ is the conductive heat transport through a laminar layer and $R_{sl,i}$ is the conductive heat transport through a slime layer. They are evaluated by the following expressions (Stephan et al., 2006)

$$R_i = \frac{1}{\alpha_i U_i} \qquad \alpha_i = \frac{Nu_i \lambda_i}{2(r_1 - s_{ll})}$$

$$U_i = 2\pi (r_1 - s_{ll})$$

$$R_{ll,i} = \frac{s_{ll,i}}{\lambda_{ll,i} U_{m,ll,i}} \qquad U_{m,ll,i} = \frac{2\pi (r_1 - (r_1 - s_{ll}))}{\ln \frac{r_1}{r_1 - s_{ll}}}$$

$$R_{sl,i} = \frac{s_{sl,i}}{\lambda_{sl,i} U_{m,sl,i}} \qquad U_{m,sl,i} = \frac{2\pi s_{sl}}{\ln \frac{r_2 + s_{sl}}{r_2}}$$

$$R_{C,i} = \frac{1}{\alpha_{C,i} U_{C,i}} \qquad \alpha_{C,i} = \frac{\lambda_{C,i} Nu_C}{2(r_3 - r_2 - 2s_{sl})}$$

$$U_{C,i} = 2\pi (r_2 + s_{sl})$$

Axial boundary conditions for Eq. (2.29) are

$$-\pi \lambda_W (r_2^2 - r_1^2) \frac{\partial \hat{T}_W}{\partial z} = \dot{Q}|_{z_k^-} \tag{2.36}$$

and

$$-\pi \lambda_W (r_2^2 - r_1^2) \frac{\partial \hat{T}_W}{\partial z} = \dot{Q}|_{z_k^+}. \tag{2.37}$$

For the internal boundaries, $\dot{Q}|_{z_k^+} = \dot{Q}|_{z_{k+1}^-}$ with the module index $k = 2, \ldots, 15$. For $k = 1$ and $k = 16$, the outermost heat fluxes ($\dot{Q}_{z_1^-}$ and $\dot{Q}_{z_{16}^+}$ respectively) are calculated from

$$\dot{Q}|_{z_k^\bullet} = k_{wall} \pi (r_2^2 - r_1^2)(\hat{T}_W|_{z_k^\bullet} - T_{amb}). \tag{2.38}$$

The heat transfer coefficient k_{wall} accounts for heat transfer by convection, by conduction and by radiation, hence

$$k_{wall} = \frac{1}{R_{b,iso} + R_{b,amb}}, \tag{2.39}$$

where

$$R_{b,iso} = \frac{s_{air}}{\lambda_{air}}$$
$$R_{b,amb} = \frac{1}{\frac{\lambda_{air} Nu_{air}}{2(r_2 - r_1)} + \varepsilon\sigma \frac{T_{iso}^4 - T_{amb}^4}{T_{iso} - T_{amb}}}.$$

Using a mathematical model for the energy balance of the reactor wall which is distributed both in axial and radial direction, would drastically increase the size of the overall model. Of course, DIVA is capable of solving such large systems, depending on the available hardware. However, due to memory limitations, at that time it has not been possible to solve such a detailed system on a standard PC. So, in order to receive a reasonable size of the dynamic mathematical model, a semi-lumped version of Eq. (2.29) is needed. Therefore, a radial average operator is introduced and defined by

$$T_W = \frac{2\pi}{A_W} \int_{r_1}^{r_2} r \hat{T}_W dr = \frac{2}{r_2^2 - r_1^2} \int_{r_1}^{r_2} r \hat{T}_W dr. \tag{2.40}$$

Application of Eq. (2.40) to Eq. (2.29) results in

$$\begin{aligned} c_{p,W} \varrho_W \frac{\partial T_W}{\partial t} &= \lambda_W \frac{\partial^2 T_W}{\partial z^2} + \frac{2\pi\lambda_W}{A_W} \int_{r_1}^{r_2} r \frac{\partial^2 \hat{T}_W}{\partial r^2} dr + \frac{2\pi\lambda_W}{A_W} \int_{r_1}^{r_2} \frac{\partial \hat{T}_W}{\partial r} dr \\ &= \lambda_W \frac{\partial^2 T_W}{\partial z^2} + \frac{2\pi\lambda_W}{A_W} \left\{ \left[r \frac{\partial \hat{T}_W}{\partial r} \right]_{r_1}^{r_2} - \int_{r_1}^{r_2} \frac{\partial \hat{T}_W}{\partial r} dr + \int_{r_1}^{r_2} \frac{\partial \hat{T}_W}{\partial r} dr \right\} \\ &= \lambda_W \frac{\partial^2 T_W}{\partial z^2} + \frac{1}{A_W} \left\{ -\dot{Q}_C + \dot{Q}_R \right\}. \end{aligned} \tag{2.41}$$

The lumped version of the boundary conditions (Eqns. (2.32) and (2.33)) is

$$\dot{Q}_R = k_{inner}(T - T_W),$$
$$\dot{Q}_C = k_{outer}(T_W - T_C),$$

with the same heat transfer coefficients defined in Eqns. (2.34) and (2.35).

Hence, the lumped version of the energy balance reads

$$\varrho_W c_{p,W} \frac{\partial T_W}{\partial t} - \lambda_W \frac{\partial^2 T_W(z)}{\partial z^2} = \frac{k_{inner}}{\pi (r_2^2 - r_1^2)} (T - T_W) - \frac{k_{outer}}{\pi (r_2^2 - r_1^2)} (T_W - T_C) \tag{2.42}$$

which can also be derived directly using an energy balance equation for a one dimensional model as depicted in Fig. 2.7(b).

By comparison of (2.29) and (2.42) with k_{inner} and k_{outer} defined in (2.34) and (2.35), one realizes that in the equation distributed in only one parameter, the radial heat transfer is not properly accounted for. Since this heat transfer coefficient and the thickness of the wall are quite large, it is not acceptable to drop that term. In order to include it, the following procedure is proposed. The idea is to make a very simple and rough discretization in radial direction. Therefore, the wall is separated artificially into two layers. Doing this, implies the assumption that the temperature in between the two layers remains constant over the whole diameter. Next, the coefficients for the radial heat transfer have to be included into (2.42). So the suggestion is to change in Eq. (2.42) only the global heat transfer from the inner side to the wall (k_{inner}) and from the outer side to the wall (k_{outer}). The modified heat transfer coefficients then read

$$k_{inner} = \frac{1}{R_i + R_{ll,i} + R_{rad,i}} \tag{2.43}$$

$$R_{rad,i} = \frac{\frac{1}{2}(r_2 - r_1)}{\lambda_W U_{m,rad,i}} \qquad U_{m,rad,i} = \frac{\frac{\pi}{2}(r_2 - r_1)}{\ln \frac{r_2 + r_1}{2r_1}} \tag{2.44}$$

and in analogy

$$k_{outer} = \frac{1}{R_{sl,i} + R_{C,i} + R_{rad,o}} \tag{2.45}$$

$$R_{rad,o} = \frac{\frac{1}{2}(r_2 - r_1)}{\lambda_W U_{m,rad,o}} \qquad U_{m,rad,o} = \frac{\frac{\pi}{2}(r_2 - r_1)}{\ln \frac{2r_2}{r_2 + r_1}}. \tag{2.46}$$

The other heat transfer resistors (R_i, $R_{ll,i}$, $R_{sl,i}$ and $R_{C,i}$) can still be calculated by the

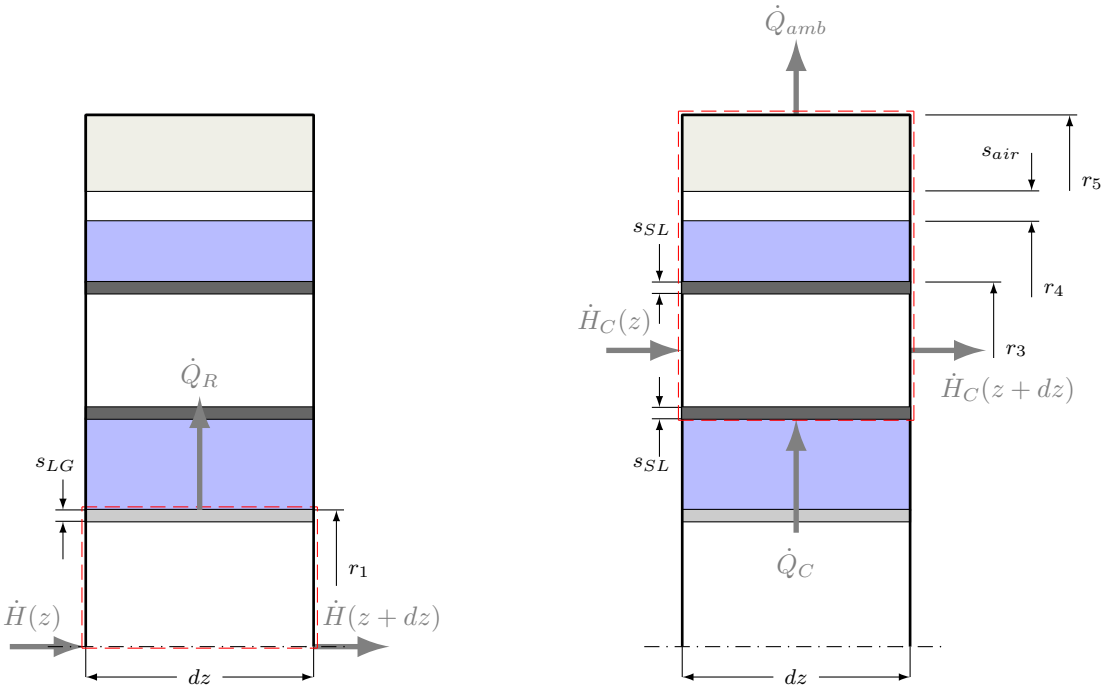

(a) Reactor (b) Coolant

Figure 2.8: Cut out of the tubular reactor with heat fluxes for the energy balance equations (if a separate energy balance for the reactor wall is included)

previously introduced expressions. So, now it is possible to use the simple one dimensional energy balance (2.42) without neglecting the heat transport in radial direction through the wall.

Reactor. It is assumed that the temperature in one cross section is constant, so that there is no additional radial temperature distribution. The energy balance for the reactor and the coolant are similar to derive, so that here only the reactor is shown to some extent of detail.

If the reactor wall is modelled separately, one can write for the energy balance equation of the reactor using the dashed box in Fig. 2.8(a) as boundary

$$\frac{dU_R}{dt} = \dot{H}(z) - \dot{H}(z+dz) - p\frac{dV_R}{dt} - \dot{Q}_R, \tag{2.47}$$

where $\dot{H}(\bullet)$ is the enthalpy of the flux entering and leaving the small element respec-

tively. $\dot{Q}_R$ takes the heat exchange to the thick inner reactor wall into account. U_R denotes the inner energy of the boxed element. In this equation, the kinetic energy $\frac{1}{2}\dot{m}v^2$ and the potential energy $m\,g\,h$ are neglected, it is assumed that gravity has no significant influence on the chemical process in the tubular reactor.

Hence, using a Taylor series expansion for $\dot{H}(z+dz)$ and with $U_R = H_R - pV_R$ this equation can be written as

$$\frac{dH_R}{dt} = -\frac{\partial \dot{H}(z)}{\partial z}dz + V_R\frac{dp}{dt} - \dot{Q}_R.$$

Introducing $H_R = m_R\,h = \varrho A\,dz\,h$, $\dot{H} = \dot{m}\,h = \varrho A v\,h$ and (2.15) one ends up with

$$\varrho A dz\left(\frac{dh}{dt} + v\frac{\partial h}{\partial z}\right) = V_R\frac{dp}{dt} - \dot{Q}_R.$$

The molar enthalpy h is a function of the intensive variables p and T as well as the composition of the mixture. So the total derivative of h

$$dh = \underbrace{\left.\frac{\partial h}{\partial T}\right|_{p,w_i}}_{c_p} dT + \underbrace{\left.\frac{\partial h}{\partial p}\right|_{T,w_i}}_{\approx 0} dp + \sum_{i=1}^{I}\underbrace{\left.\frac{\partial h}{\partial w_i}\right|_{p,T}}_{\bar{h}_i} dw_i.$$

Here, the dependency with respect to the pressure p can be neglected, since it is required for gases and steams only, if pressure or temperature are close to a phase boundary or pressure is close to the critical pressure or exceeds it. Since neither of this holds for the LDPE production, the balance equations transforms to

$$\varrho A\,dz\left[c_p\left(\frac{\partial T}{\partial t} + v\frac{\partial T}{\partial z}\right) + \sum_{j=1}^{J}\bar{h}_j\left(\frac{\partial w_j}{\partial t} + v\frac{\partial w_j}{\partial z}\right)\right] = A\,dz\frac{dp}{dt} - \dot{Q}_R.$$

The sum can be rewritten using (2.24), so for the left-hand side, one ends up with

$$\varrho A\,dz\left[c_p\left(\frac{\partial T}{\partial t} + v\frac{\partial T}{\partial z}\right) + \frac{1}{\varrho}\sum_{j=1}^{J}(\Delta h_{reac})_j r_j\right] = A\,dz\frac{dp}{dt} - \dot{Q}_R.$$

For the heat of reaction, only the following reactions are assumed to have a significant

influence,

- initiation (see reaction scheme (2.1) and (2.4)),
- propagation (see (2.5)) and
- termination (see (2.6) and (2.7))

Moreover, the heat of reaction is assumed to be the same for these reactions, in other words $(\Delta h_{reac}^{init}) \equiv (\Delta h_{reac}^{prop}) \equiv (\Delta h_{reac}^{term})$. Additionally, the pressure dynamics is very fast, so one can safely suppose that a quasi-stationary approach for the pressure dynamic holds.

$\dot{Q}_R$ comprises the heat transfer caused by convection and the thermal transfer through a thin laminar layer. Both effects are combined in the inner heat transfer resistor k_{inner}. Hence

$$\dot{Q}_R = k_{inner}(T - T^*)\,dz.$$

Here, depending on the inclusion of the energy balance for the reactor wall, T^* denotes either the average temperature of the inner reactor wall T_W or the coolant temperature T_C. Moreover, the overall heat transfer coefficient k_{inner} is

- either to be taken from Eq. (2.43) (if the additional energy balance equation for the wall is included into the dynamic model), or
- defined by the following equation, if the large capacitance of the inner reactor wall is neglected for the transient behavior,

$$k_{inner} = \frac{1}{R_i + R_{ll,i} + R_{st,i} + R_{sl,i} + R_{C,i}} \tag{2.48}$$

with

$$R_{st,i} = \frac{r_2 - r_1}{\lambda_{st,i}}. \tag{2.49}$$

Finally, one ends up with

$$\varrho c_p \left(\frac{\partial T}{\partial t} + v \frac{\partial T}{\partial z} \right) = \frac{1}{\varrho} \sum_{j=1}^{J} (\Delta h_{reac})_j r_j - \frac{k_{inner}}{A} (T - T^*) \tag{2.50}$$

$$IC : T(z,0) = T_0(z) \tag{2.51}$$

$$BC : T(0,t) = T_{in}(t) \tag{2.52}$$

Note again, that depending on the application, k_{inner} is defined by either (2.43) with $T^* = T_W$ or by (2.48) with $T^* = T_C$. Moreover, all parameters depend on temperature and pressure, some are also dependent on the composition of the reactor mixture.

Coolant. For the coolant some simplifying assumptions hold as well. Again, it is assumed to have plug flow without any radial temperature distribution. The kinetic and potential energy can be neglected. Additionally, pressure and mass flux are kept constant and no reaction takes place. It is important to note that the flux direction is counter-current wise. Hence the energy balance equation for the dashed box in Fig. 2.8(b) reads

$$\varrho_C c_{pC} \left(\frac{\partial T_C}{\partial t} - v_C \frac{\partial T_C}{\partial z} \right) = \frac{k_{outer}}{A_C} (T_* - T_C) - \frac{k_{amb}}{A_C} (T_C - T_{amb}) \tag{2.53}$$

$$IC : T_C(z,0) = T_{C,0}(z) \tag{2.54}$$

$$BC : T_C(L,t) = T_{C,in}(t) \tag{2.55}$$

Here, k_{outer} and k_{amb} are the overall heat transfer coefficients accounting for the heat transfer to reactor or wall and to the ambience. Depending on the inclusion of the energy balance equation for the inner reactor wall, k_{outer} is either defined by Eq. (2.45) with $T_* = T_W$ or by $k_{outer} = k_{inner}$ with k_{inner} from Eq. (2.48) and with $T_* = T$. The heat transfer coefficient to the ambience k_{amb} can be evaluated by the following expression

$$k_{amb} = \frac{1}{R_{C,o} + R_{sl,o} + R_{st,o} + R_{air} + R_{iso} + R_{amb}}. \tag{2.56}$$

The overall heat transfer coefficient k_{amb} hence includes the following effects

- heat transfer by convection ($R_{C,o}$ from coolant to outside and R_{amb} from insulation to outside)

- heat transfer by conduction ($R_{sl,o}$ through the outer slime layer, $R_{st,o}$ through the outer wall, R_{air} through the air gap and R_{iso} through the insulation)

- heat transfer by radiation (in particular, E_s, which is one summand in of R_{amb})

The resistances are calculated by

$$
\begin{aligned}
R_{C,o} &= \frac{1}{\alpha_{C,o} U_o} & \alpha_{C,o} &= \frac{\lambda_C \, Nu_C}{2(r_3 - r_2 - 2\,s_{sl})} \\
& & U_{C,o} &= 2\pi\,(r_3 - s_{sl}) \\
R_{sl,o} &= \frac{s_{sl}}{\lambda_{sl} U_{m,sl}} & U_{m,sl} &= \frac{2\pi\, s_{sl}}{\ln \frac{r_3}{r_3 - s_{sl}}} \\
R_{st,o} &= \frac{s_{st,o}}{\lambda_{st,o} U_{m,st,o}} & U_{m,st,o} &= \frac{2\pi\,(r_4 - r_3)}{\ln \frac{r_4}{r_3}} \\
R_{air} &= \frac{s_{air}}{\lambda_{air} U_{m,air}} & U_{m,air} &= \frac{2\pi\,(r_4 + s_{air} - r_4)}{\ln \frac{r_4 + s_{air}}{r_4}} \\
R_{iso} &= \frac{s_{iso}}{\lambda_{iso} U_{m,iso}} & U_{m,iso} &= \frac{2\pi\,(r_5 - (r_4 + s_{air}))}{\ln \frac{r_5}{r_4 + s_{air}}} \\
R_{amb} &= \frac{1}{\alpha_{air} U_{amb} + E_s} & \alpha_{air} &= \frac{\lambda_{air} Nu_{air}}{2 r_5} \\
& & U_{amb} &= 2\pi\, r_5 \\
& & E_s &= 2\pi\, r_5\, \varepsilon\, \sigma\, \frac{T_{iso}^4 - T_{amb}^4}{T_{iso} - T_{amb}}.
\end{aligned}
$$

The overall heat transfer coefficient R_{amb} includes both free convection and radiation. For the free convection, $Nu_{air} = Nu(Gr_{air}, Pr_{air})$. The Grashof number is calculated using $Gr_{air} = 8\left(\frac{\varrho_{air}}{\eta_{air}}\right)^2 \frac{\beta_{air}}{g} r_5^3 (T_{iso} - T_{amb})$. In all equations $T_{iso} = 50^\circ C$. The Prandtl number is evaluated by $Pr_{air} = \frac{\eta_{air} c_{P,air}}{\lambda_{air}}$. The Nusselt number is computed using Eq. (25) in Sec. Gb7 of VDI-Wärmeatlas (1991). The heat transfer by radiation is calculated using the Stefan-Boltzman constant $\sigma = 5.6704\ 10^{-8} \frac{W}{m^2 K^4}$ and the emissivity $\varepsilon = 0.93$, i.e. it is assumed, that emissivity does not depend on the wavelength.

2.2.2.5 Moment Equations

Generally speaking, moments are widely used in the modelling of polymerization systems where chain length, branching or double bonds play an important role. Mainly they are utilized in order to reduce the size of those models, since it is not necessary to balance every single molecule. Using moments enables one to specify characteristic properties of e.g. the chain length distribution, such as average chain length or width of the distribution. But usually the information on the distribution itself is lost and can only be recalculated using infinitely many moments.

Strictly speaking, if we think of $w_{P,i}$, $w_{R,i}$ and $w_{R,sec,i}$ in terms of distributions of dead, living and living secondary polymer with discrete chain length i, then

$$\mu_r^P = E(w_P^r) = \sum_{i=1}^{\infty} i^r w_{P,i}$$

is called the r-th moment of the chain length distribution (in the equation above: the dead polymer distribution) about zero. The zeroth moment is equivalent the average weight fraction, the first moment can be seen as number average molecular weight, and the third moment the skewness or asymmetry of the distribution.

Using these moments, it is easy to compute the average chain length or width of the distribution. The average chain length (or degree of polymerization) can be evaluated by

$$P_n = \frac{\mu_1^P}{\mu_0^P},$$

i.e. the mean of the probability distribution about zero over its sum. The polydispersity (or width of the distribution) is calculated by

$$PD = \frac{\frac{\mu_2^P}{\mu_1^P}}{P_n} = \frac{\mu_0^P \mu_2^P}{(\mu_1^P)^2}. \tag{2.57}$$

In general the following equation holds for all moment balance equations ($k =$

$[P; R; R, sec]$):

$$\frac{d(m_R \mu_r^k)}{dt} = \sum_{i=1}^{\infty} i^r \frac{d(m_R w_i^k)}{dt} = -A_R dz \left(\varrho v \frac{\partial \mu_r^k}{\partial z} + \mu_r^k \frac{\partial (\varrho v)}{\partial z} \right) + \mu_{r,reac}^k \qquad (2.58)$$

with

$$\mu_{r,reac}^k = \sum_{i=1}^{\infty} i^r \dot{m}_{i,reac}^k = \dot{m}_{1,reac}^k + \sum_{i=2}^{\infty} i^r \dot{m}_{i,reac}^k. \qquad (2.59)$$

Living Polymer (Primary) In order to determine the summands of (2.59), the following two parts are used, one for a single molecule and one for the remainder $(2 \ldots \infty)$. For the single molecule, one can derive from the reaction scheme (Eqns. (2.1)–(2.13))

$$\begin{aligned} i = 1 : M_{R,1} A_R dz \Bigg(& 2 k_{th} c_M^3 + \sum_{\nu=1}^{3} k_{p,I_\nu} c_M c_{RI_\nu} + k_{p,X} c_{RX} c_M - k_p c_M c_{R,1} \\ & + k_{tr,M} c_M \sum_{j=1}^{\infty} c_{R,j} - k_{tr,M} c_M c_{R,1} - k_{tr,X} c_X c_{R,1} \\ & - k_{t,c} c_{R,1} \sum_{j=1}^{\infty} c_{R,j} - k_{t,d} c_{R,1} \sum_{j=1}^{\infty} c_{R,j} - k_{bb} c_{R,1} + k_{bb} c_{R,1} \\ & - k_{tr,P} c_{R,1} \sum_{j=1}^{\infty} j \, c_{P,j} + k_\beta \sum_{j=2}^{\infty} \frac{c_{R,j,sec}}{j-1} \Bigg), \end{aligned}$$

and analogous, the second part reads

$$\begin{aligned} i \geq 2 : M_{R,i} A_R dz \Bigg(& k_p c_M c_{R,i-1} - k_p c_M c_{R,i} + k_{p,sec} c_M c_{R,i-1,sec} \\ & - k_{tr,M} c_M c_{R,i} - k_{tr,X} c_X c_{R,i} \\ & - k_{t,c} c_{R,i} \sum_{j=1}^{\infty} c_{R,j} - k_{t,d} c_{R,i} \sum_{j=1}^{\infty} c_{R,j} - k_{bb} c_{R,i} + k_{bb} c_{R,i} \end{aligned}$$

$$-k_{tr,P}c_{R,i}\sum_{j=1}^{\infty} j\,c_{P,j} + k_\beta \sum_{j=i+1}^{\infty} \frac{c_{R,j,sec}}{j-1}\Bigg).$$

Inserting both parts in (2.59) and finally in (2.58) yields for the zeroth of the three moments of the living polymer distribution:

$$\begin{aligned}\frac{\partial \mu_0^R}{\partial t} + v\frac{\partial \mu_0^R}{\partial z} = \frac{\varrho}{M_M}\Bigg[&2k_{th}\frac{\varrho}{M_M}w_M^3 + \sum_{\nu=1}^{3} k_{p,I_\nu}\frac{M_M}{M_{RI_\nu}}w_M w_{RI_\nu} - k_{tr,P}\mu_0^R\mu_1^P \\ &- \left(k_{t,c}+k_{t,d}\right)(\mu_0^R)^2 + k_\beta\frac{M_M}{\varrho}w_{R,sec} + k_{p,sec}w_M w_{R,sec} \\ &+ k_{p,X}\frac{M_M}{M_{RX}}w_M w_{RX} - k_{tr,X}\frac{M_M}{M_X}w_X\mu_0^R\Bigg] \qquad (2.60)\end{aligned}$$

$$IC: \mu_0^R(z,0) = \mu_{0,0}^R(z) \qquad (2.61)$$

$$BC: \mu_0^R(0,t) = \mu_{0,in}^R(t) \qquad (2.62)$$

Note that the following assumption is used in the derivation of that equation: $M_{R,i} = M_M$. Naturally, one would expect something like $M_{R,i} = i\,M_M$. But if this is assumed, most of the infinite sums could not be calculated by inserting the appropriate moments. Hence the model could not be simplified since one would have to compute infinite sums numerically.

The first and second moment equation are computed similarly and their model equation is listed in the Appendix B. Note that for the derivation of those equations, the relations on finite and infinite summations listed in Appendix A are used.

Living Polymer (Secondary) As previously mentioned, secondary living polymer is an indication for the long-chain branching in the polymer. Hence it has a high impact on the physical properties of the product. To derive the model equations for it, the general equation for the moment equations (2.58) is used. The reaction term $\mu_{r,reac} = \mu_{r,reac}^{R,sec}$ of (2.58) is computed by

$$A_R dz \sum_{i=1}^{\infty} M_{R,sec,i}\left(ik_{tr}c_R c_{P,i} - k_{p,sec}c_M c_{R,sec,i} - k_\beta c_{R,sec,i}\right).$$

And with $M_{R,sec,i} \equiv M_M$ this gives for the r-th moment

$$\frac{\partial \mu_r^{R,sec}}{\partial t} + v\frac{\partial \mu_r^{R,sec}}{\partial z} = \frac{\varrho}{M_M}\Big[k_{tr,P}\mu_0^R\mu_{r+1}^P - \big(k_{p,sec}w_M + k_\beta\frac{M_M}{\varrho}\big)\mu_r^{R,sec}\Big] \quad (2.63)$$

$$IC : \mu_r^{R,sec}(z,0) = \mu_{r,0}^{R,sec}(z) \quad (2.64)$$

$$BC : \mu_r^{R,sec}(0,t) = \mu_{r,in}^{R,sec}(t) \quad (2.65)$$

Note that the moment equations of both, the living primary (listed in detail in App. B) and the living secondary polymer do close, since the r-th living primary/secondary polymer moment does not depend on its higher moments.

Dead Polymer The moments of the distribution of dead polymer are also calculated by (2.58) using the following expression for the computation of $\mu_{r,reac} = \mu_{r,reac}^P$:

$$\begin{aligned} i = 1 \quad M_{P,1}A_R\,dz\Big(&k_{tr,M}c_M c_{R,1} + k_{tr,X}c_X c_{R,1} + k_{td}c_R c_{R,1} \\ &+ k_{tr,P}c_{R,1}\sum_{j=1}^{\infty} j\,c_{P,j} - k_{tr,P}c_R c_{P,1} + k_\beta\sum_{j=2}^{\infty}\frac{c_{R,j,sec}}{j-1}\Big). \end{aligned}$$

Higher indices lead to

$$\begin{aligned} i \geq 2 \quad M_{P,i}A_R\,dz\Big(&k_{tr,M}c_M c_{R,i} + k_{tr,X}c_X c_{R,i} + k_{td}c_R c_{R,i} \\ &+ \frac{1}{2}k_{tc}\sum_{k=1}^{i-1} c_{R,k}c_{R,i-k} + k_{tr,P}c_{R,i}\sum_{j=1}^{\infty} j\,c_{P,j} \\ &- i\,k_{tr,P}c_R c_{P,i} + k_\beta\sum_{j=i+1}^{\infty}\frac{c_{R,j,sec}}{j-1}\Big). \end{aligned}$$

Inserting this in the general form of the moment equations (2.58) one obtains e.g. for the first moment of the dead polymer distribution

$$\frac{\partial \mu_1^P}{\partial t} + v\frac{\partial \mu_1^P}{\partial z} = \frac{\varrho}{M_M}\left[\frac{1}{2}k_\beta \frac{M_M}{\varrho}\mu_1^{R,sec} + k_{tr,P}\left(\mu_1^P \mu_1^R - \mu_0^R \mu_2^P\right) + k_{tr,M} w_M \mu_1^R + \left(k_{tc} + k_{td}\right)\mu_0^R \mu_1^R + k_{tr,X}\frac{M_M}{M_X} w_X \mu_1^R\right] \tag{2.66}$$

$$IC : \mu_1^P(z,0) = \mu_{1,0}^P(z) \tag{2.67}$$

$$BC : \mu_1^P(0,t) = \mu_{1,in}^P(t) \tag{2.68}$$

It is important to note that the higher ($r \geq 0$) moment equations for the dead polymer do not close, i.e.

$$\mu_r \neq f(\mu_0, \mu_1, \ldots, \mu_{r-1}, \mu_r),$$

but the r-th moment depends on higher moments. To overcome that situation, a technique introduced by Hulburt and Katz (1964) is used. They proposed an artificial closure, which circumvents the problem above. Hence

$$\mu_3^P = \frac{\mu_2^P}{\mu_1^P \mu_0^P}\left(2\,\mu_0^P\,\mu_2^P - \mu_1^P\right) \tag{2.69}$$

2.2.3 Discretization

Since the model equations for the peripheral units (see Section 2.3) are represented by systems of differential and algebraic equations, the flowsheet simulator DIVA is used for the numerical solution of the equation system. Hence the partial differential and algebraic equations of the tubular reactor model have to be transformed into a system of differential and algebraic equations. For this transformation an adaptive method of lines approach with a finite differences scheme is used. First order backward differences are taken for first order derivatives, for second order derivatives a second order central scheme is chosen. The adaptation can be done statically or dynamically.

In a *static* adaptation scheme, for some time integration steps, the grid is fixed. Then in an additional regridding step a new grid point distribution is calculated, where

grid points may be inserted or dropped. This recalculated grid point distribution is kept fixed for the successive time integration steps until a new regridding is required. Hence the number of grid points might change during simulations, whereas it remains constant if a *dynamic* adaptation mechanism is used. For the second approach no additional regridding step is required, the grid moves continuously during the time integration. The dimension of the system is increased by the additional partial differential equation for the grid movement. Hence the overall system increases by the number of grid points. The flowsheet simulator DIVA requires a fixed number of states during the simulation run, hence, for the discretization of the partial differential and algebraic equation system the dynamical adaptation scheme has to be used.

The discretization with a Method of Line approach utilizes a variable grid with N_z grid nodes

$$0 = z_1 < z_2(t) < \ldots < z_{N_z-1}(t) < z_{N_z} = L,$$

i.e., the first and the last grid node are fixed to the boundaries. The position of the grid nodes are continuous functions and have to be introduced as additional state variables, that add to the number of system state variables.

For the considered adaptive Method of Lines approach, the position of the grid nodes follows the equidistribution principle introduced by Dorfi and Drury (1987). They suggested an adaptive grid which has regions of high resolution where necessary. This allows larger steps for the time integration. For this purpose, the model equations are transformed to the new moving grid according to

$$\left.\frac{\partial x_j}{\partial t}\right|_{z_n(t)} = \frac{dx_{j,n}}{dt} - \left.\frac{\partial x_j}{\partial z}\,\frac{dz}{dt}\right|_{z_n(t)}. \tag{2.70}$$

This formulation represents the Lagrangian of the time derivative of any state x_j in the tubular reactor at a grid node $z_n(t)$. At the boundaries, $z_1(t)$ and $z_{N_z}(t)$ the grid nodes are fixed and

$$\left.\frac{\partial x_j}{\partial t}\right|_{z_\nu(t)} = \frac{dx_{j,\nu}}{dt} \qquad \nu = 1, N_z. \tag{2.71}$$

Additional equations are required to determine the positions of the inner grid points.

The general form of these equations reads

$$\tau \mathbf{E}(\mathbf{x}, \mathbf{z}, \kappa) \frac{d\mathbf{z}}{dt} = \mathbf{g}(\mathbf{x}, \mathbf{z}, \kappa), \tag{2.72}$$

where τ and κ are temporal or spatial regularization parameters and $\mathbf{z} \in \mathbb{R}^{N_z}$ is a vector containing the inner grid points. Grid smoothing (spatial or temporal) is necessary in order to avoid numerical problems caused e.g. by an overlapping of grid point trajectories or by oscillations of the grid point movement. Both, matrix $\mathbf{E} \in \mathbb{R}^{N_z \times N_z}$ and the function vector $\mathbf{g} \in \mathbb{R}^{N_z}$ are based on the spatial equidistribution principle, where a monitor function $M(\mathbf{x})$ for the estimation of the discretization error is used and the grid nodes are placed such that this error is small. In this work, an arc-length monitor function is used,

$$M(z, \mathbf{x}) = \sqrt{1 + \frac{L}{J} \sum_{j=1}^{J} \left(\frac{1}{\hat{x}_j} \frac{\partial x_j}{\partial z} \right)^2}. \tag{2.73}$$

It is also possible to use higher order derivatives in the monitor function. Taking the second derivative e.g. monitors not the gradient but the curvature of the graph of the state variables. This results in

$$M(z, \mathbf{x}) = \sqrt{1 + \frac{L^2}{J} \sum_{j=1}^{J} \left(\frac{1}{\hat{x}_j^2} \frac{\partial^2 x_j}{\partial z^2} \right)^2}.$$

Therein, $\hat{x}_j$ is used to make each of the summands dimensionless. Moreover, the value of $\hat{x}_j$ should be chosen such that all summands contribute with a similar magnitude to the monitor function. L denotes the length of the reactor. Of course not all states have to be included into that function, in fact, including all states just enlarges the number of entries into the Jacobian (we would have a sub-matrix with a dense structure) and hence increases the computation time and storage requirement.

In an ideal grid node arrangement the discretization error is distributed uniformly across the spatial coordinate. The equidistribution principle postulates that integrals over adjacent sub-domains of a monitor function have to be equal, i.e. are constant

over the whole domain. Hence

$$\int_{z_{n-1}}^{z_n} M(z,\mathbf{x})\,dz = \int_{z_n}^{z_{n+1}} M(z,\mathbf{x})\,dz \qquad \forall\, n \in [2, N_z - 1]. \tag{2.74}$$

A discrete form of Eq. (2.74) is

$$\frac{\zeta_{n-1}}{M_{n-1}} = \frac{\zeta_n}{M_n} \qquad \forall\, n \in [2, N_z - 1] \tag{2.75}$$

with the discrete form of the monitor function,

$$M_n = \sqrt{1 + \frac{L}{J}\sum_{j=1}^{J}\left(\frac{1}{\hat{x}_j}\frac{x_j(z_{n+1}) - x_j(z_n)}{z_{n+1} - z_n}\right)^2} \tag{2.76}$$

and with the grid point concentration $\zeta \in \mathbb{R}^{N_z-1}$

$$\zeta_n = \frac{1}{z_{n+1} - z_n}. \tag{2.77}$$

Since Eq. (2.75) is algebraic, it is not yet of the form that is proposed in (2.72) (see Dorfi and Drury (1987)). To avoid an overlapping of grid points, the spatial movement of the grid nodes is controlled. Introducing the spatial smoothing parameter $\kappa > 0$ the grid point concentration ζ_n is replaced by their numerically anti-diffused counterpart $\tilde{\zeta}_n$,

$$\tilde{\zeta}_1 = \zeta_1 - \kappa(\kappa+1)(\zeta_2 - \zeta_1) \tag{2.78a}$$

$$\tilde{\zeta}_n = \zeta_n - \kappa(\kappa+1)(\zeta_n - \zeta_{n-1}) \qquad n \in [2, N_z - 1] \tag{2.78b}$$

$$\tilde{\zeta}_{N_z} = \zeta_{N_z} - \kappa(\kappa+1)(\zeta_{N_z-1} - \zeta_{N_z}). \tag{2.78c}$$

Then one can substitute (2.75) using the Eqns. (2.78)

$$\frac{\tilde{\zeta}_{n-1}}{M_{n-1}} = \frac{\tilde{\zeta}_n}{M_n} \qquad \forall\, n \in [2, N_z - 1]. \tag{2.79}$$

The spatial smoothing parameter κ influences the ratio of adjacent grid points and

gives a simple handle to avoid overlapping or a high concentration of grid nodes locally. Verwer et al. (1989) have shown, that if κ satisfies the following condition

$$\frac{\kappa}{\kappa+1} \leq \frac{\zeta_n}{\zeta_{n-1}} \leq \frac{\kappa+1}{\kappa},$$

then a non-smooth grid point distribution is impossible. In particular, $\kappa \gg 1$ almost fixes the grid points to their initial position, whereas $0 < \kappa \leq 1$ allows an aggressive placement of the grid nodes.

Still, the introduction of $\tilde{\zeta}_n$ yields no differential equation. So, besides spatial smoothing, also temporal smoothing is used to avoid numerical problems. Therefore, the algebraic equations (2.79) are transformed into ordinary differential equations introducing the smoothing parameter τ,

$$\frac{\tilde{\zeta}_{n-1} + \tau \frac{d\tilde{\zeta}_{n-1}}{dt}}{M_{n-1}} = \frac{\tilde{\zeta}_n + \tau \frac{d\tilde{\zeta}_n}{dt}}{M_n}. \tag{2.80}$$

Substituting (2.78) into (2.80) and using

$$\frac{d\zeta_n}{dt} = \zeta_n^2 \Big(\frac{dz_{n+1}}{dt} - \frac{dz_n}{dt} \Big), \tag{2.81}$$

it is straightforward to derive the matrix $\mathbf{E}$ in the following form (cf. Eq. (2.72))

$$\underbrace{\begin{bmatrix}
e_{1,1} & 0 & 0 & 0 & 0 & 0 & 0 & \cdots & 0 \\
e_{2,1} & e_{2,2} & e_{2,3} & e_{2,4} & 0 & 0 & 0 & \cdots & 0 \\
e_{3,1} & e_{3,2} & e_{3,3} & e_{3,4} & e_{3,5} & 0 & 0 & \cdots & 0 \\
0 & \ddots & \ddots & \ddots & \ddots & \ddots & 0 & \cdots & 0 \\
\vdots & \cdots & e_{n,n-2} & e_{n,n-1} & e_{n,n} & e_{n,n+1} & e_{n,n+2} & \cdots & \vdots \\
0 & \cdots & 0 & \ddots & \ddots & \ddots & \ddots & \ddots & 0 \\
0 & \cdots & 0 & 0 & e_{N_z-2,N_z-4} & e_{N_z-2,N_z-3} & e_{N_z-2,N_z-2} & e_{N_z-2,N_z-1} & e_{N_z-2,N_z} \\
0 & \cdots & 0 & 0 & 0 & e_{N_z-1,N_z-3} & e_{N_z-1,N_z-2} & e_{N_z-1,N_z-1} & e_{N_z-1,N_z} \\
0 & \cdots & 0 & 0 & 0 & 0 & 0 & 0 & e_{N_z,N_z}
\end{bmatrix}}_{:=\mathbf{E}}$$

The elements of $\mathbf{E}$ are listed in detail in App. C (Eqns. (C.1)). Moreover, the elements of the right hand side vector $\mathbf{g}$ of (2.72) are specified there (Eq. (C.2)).

In order to reduce the error prone work of discretizing all equations manually, the tool SyPProT (Köhler (2002)) has been used to transform the system of partial differential equations into a system of differential and algebraic equations, as this is required for the simulator DIVA. For the initiator weight fractions, the method is applied in detail in the next section.

2.2.3.1 Example

Here, the partial differential equations for the initiators (according to Eq. (2.24)) are used to illustrate the application of the moving grid scheme. In particular, Eq. (2.24) applied to the initiators $I_\nu, \nu = 1, 2, 3$ yields

$$\frac{\partial w_{I_\nu}(z,t)}{\partial t} + v(z,t)\frac{\partial w_{I_\nu}(z,t)}{\partial z} = -k_{I_\nu}(z,t)w_{I_\nu}(z,t). \tag{2.82}$$

Discretizing this equation with a fixed, equidistant grid, using first order backward differences, one ends up with

$$w_{I_\nu}(0,t) = w_{I_\nu}(z_1,t) = w_{I_{in}} \tag{2.83}$$

$$\frac{dw_{I_\nu}(z_n,t)}{dt} + v(z_n,t)\frac{w_{I_\nu}(z_n,t) - w_{I_\nu}(z_{n-1},t)}{z_n - z_{n-1}} = -k_{I_\nu}(z_n,t)w_{I_\nu}(z_n,t)$$
$$\forall\, n \in [2, N_z], \tag{2.84}$$

or, (2.84) rewritten in the semi-implicit notation DIVA requires

$$\frac{dw_{I_\nu}(z_n,t)}{dt} = -v(z_n,t)\frac{w_{I_\nu}(z_n,t) - w_{I_\nu}(z_{n-1},t)}{z_n - z_{n-1}} - k_{I_\nu}(z_n,t)w_{I_\nu}(z_n,t). \tag{2.85}$$

Alternatively, Eq. (2.82) can be discretized using an adaptive grid following the equidistribution principle. Then the partial differential equations for the initiators yield in semi-implicit discretized form

$$\frac{dw_{I_\nu}(z_n,t)}{dt} - \frac{w_{I_\nu}(z_n,t) - w_{I_\nu}(z_{n-1},t)}{z_n(t) - z_{n-1}(t)}\frac{dz_n(t)}{dt}$$
$$= -v(z_n,t)\frac{w_{I_\nu}(z_n,t) - w_{I_\nu}(z_{n-1},t)}{z_n(t) - z_{n-1}(t)} - k_{I_\nu}(z_n,t)w_{I_\nu}(z_n,t) \quad \forall\, n \in [2, N_z]. \tag{2.86}$$

Note that in this equation, the grid position $z_n(t)$ is not a constant but a state variable.

The monitor function in the LDPE model is only a function of one state variable, namely the zeroth living polymer moment, $\mu_0^R(z,t)$. Hence the discrete monitor function is

$$M_n = \sqrt{1 + L\left(\frac{1}{\hat{\mu}_0^R}\frac{\mu_0^R(z_n,t) - \mu_0^R(z_{n-1},t)}{z_n(t) - z_{n-1}(t)}\right)^2}. \tag{2.87}$$

Note that increasing the number of monitored state variables, does not increase the model size itself. Instead, this influences the number of Jacobian elements and hence also leads to a higher memory consumption.

Moreover, the values of the spatial and temporal smoothing parameters κ and τ is chosen with 2.0 and 0.1 respectively. So the distance between adjacent grid points may vary in an interval of $[\frac{2}{3}; \frac{3}{2}]$.

2.2.4 Validation

In the next two sections, the validation of the tubular reactor as the main process unit in the LDPE production plant is shown. The reference profile is the result of the steady state simulator *Luposim* T, developed by the BASF company for Basell. For simplicity, at first, the coolant flux direction is co-current wise, since in *Luposim* T, the counter current coolant flux is approximated iteratively using a shooting method.

At first, only one module is used for the comparison between the two simulation tools. After that, using the model for the whole tubular reactor, the influence of the discretization is discussed.

2.2.4.1 Validation of one Module

For the validation of one module, a high resolution fixed grid with 1000 grid nodes is compared to data given by the cooperation partner. Those results have been obtained using the steady state simulator *Luposim* T. According to the cooperation partner, these results show very good agreement with measured real plant data. Hence their steady state simulator results serve here as reference data for model validation. For that validation data of only one module with a coolant flux that is operated co-current wise is used. In Fig. 2.9 on top the temperature profile in the reactor is plotted on the

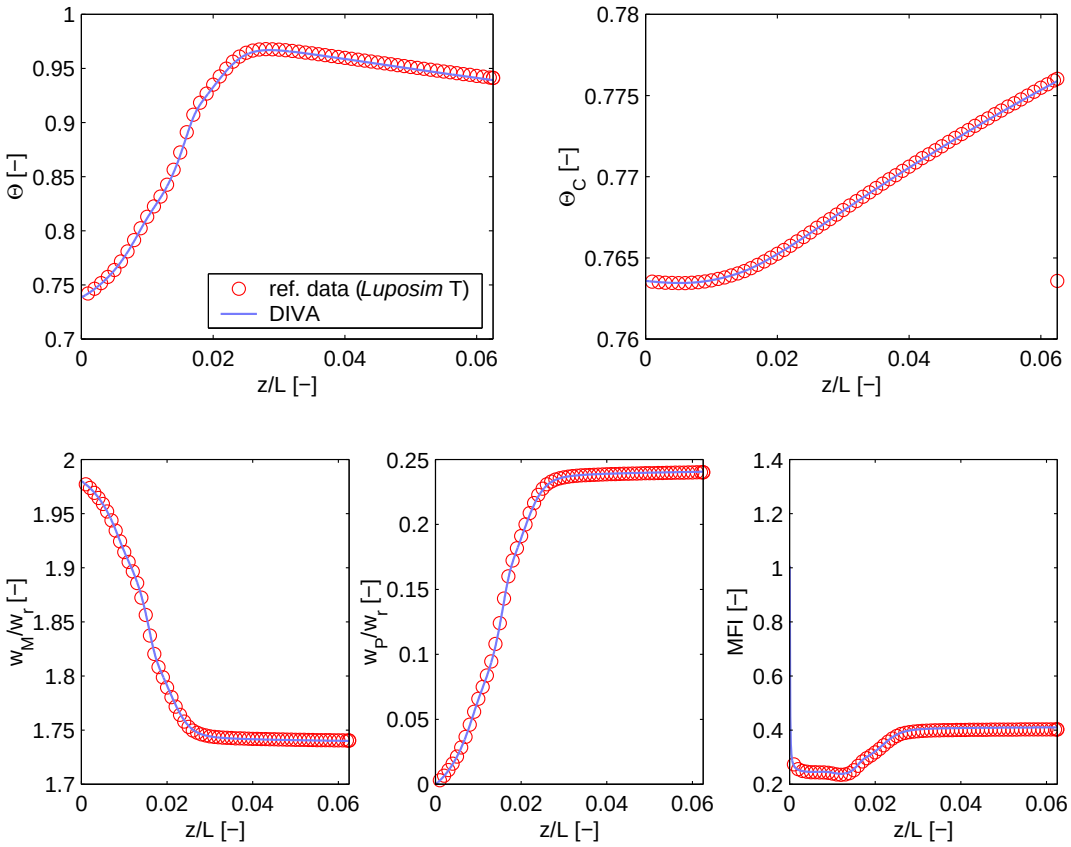

Figure 2.9: Temperature profiles, the mass fractions of monomer and polymer and the melt flow index at steady state conditions

left. On the right the coolant temperature is depicted. Please note, that the temperature profiles in the top row of the diagram are made dimensionless using the reference temperature T_{ref}. Hence $\Theta = \frac{T}{T_{ref}}$ and $\Theta_C = \frac{T_C}{T_{ref}}$. In the bottom row on the left the mass fraction of monomer and in the middle the one of polymer can be seen. Again, the values are divided by a "reference weight fraction" w_r. Moreover, the bottom right graph shows one physical property of the polymer, the melt flow index. The values obtained by *Luposim* T are indicated by red circles, simulation results of DIVA is drawn with a solid blue line. It has to be pointed out, that the simulator tools solving the equations in either DIVA or *Luposim* T are completely different from each other. The flowsheet simulator DIVA solves the whole set of system equations simultaneously for each time integration step, whereas the steady state simulator *Luposim* T integrates along the spatial coordinate, and hence only has to solve approx. 30 ODEs

at the same time. Despite of the difference in numerical solution methods the results match very precisely in steady state.

The important quantities for the product are not only melt flow index, but also the moments of the chain length distributions. They are depicted in Fig. 2.10. In the left column the moments of the dead polymer chain length distribution are shown. The middle column depicts the moments of the living primary, the left one the moments of the living secondary polymer chain length distribution. Again, the simulation results obtained with DIVA match the industrial data precisely. The graph of the dead polymer always has a positive gradient, since in neither of the reactions (2.1)–(2.13) polymer is consumed. In contrast to that, the graphs of the living primary and secondary polymer moments have distinct local minima and maxima. This can be explained by the different initiator types that are used. The profiles of their weight fractions are depicted

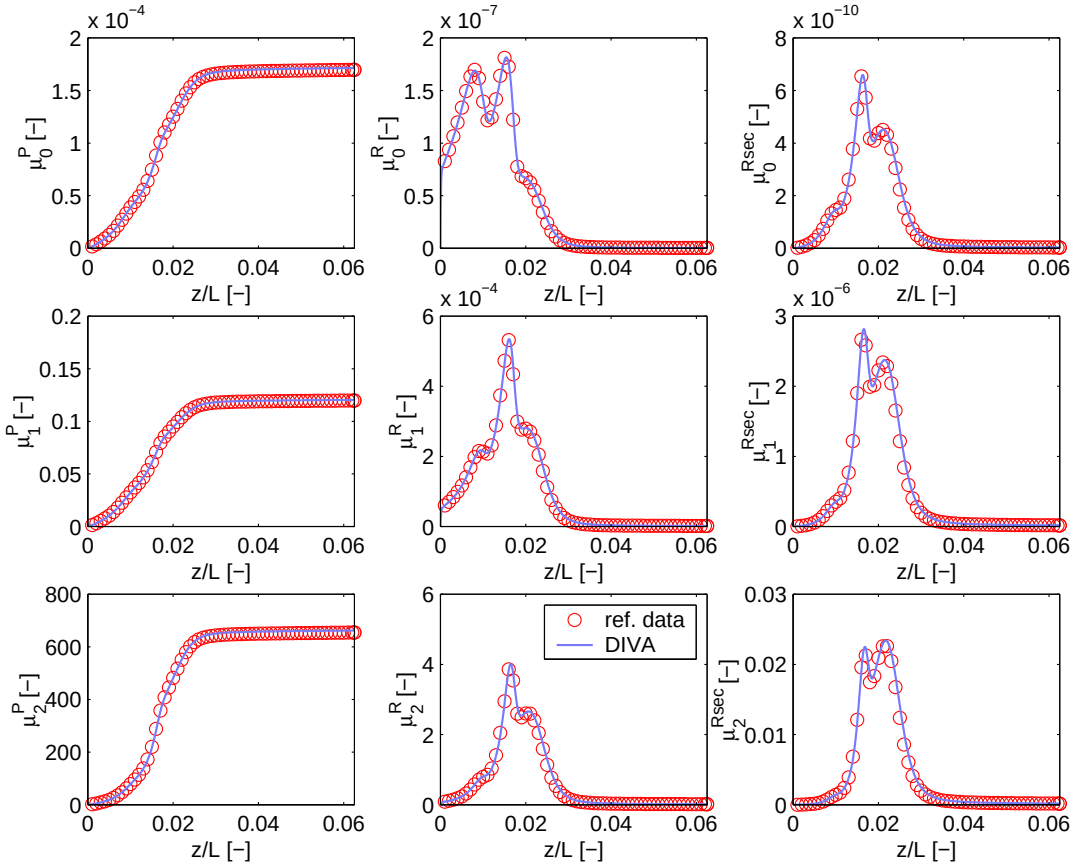

Figure 2.10: Zeroth, first and second moments of the chain length distributions.

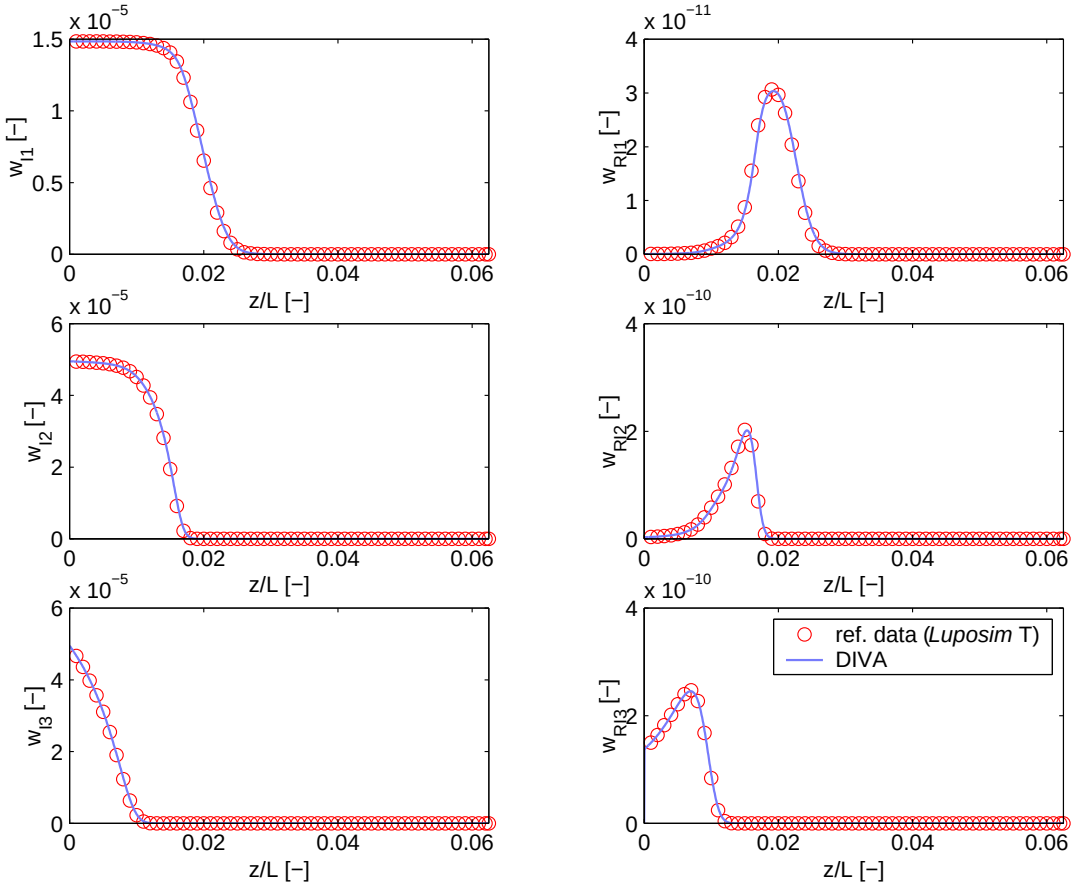

Figure 2.11: The weight fractions of initiator and their radicals.

in the left column of Fig. 2.11, the right column shows their radicals. The initiator three instantaneously decomposes into radicals, resulting in the first "propagation wave" and the first maximum in the zeroth moments of living radicals. The radicals are rapidly consumed along the reactor and since the growth reaction is exothermic, also initiator two and one start building radicals. The decomposition rate of those radicals is higher than the termination rate of dead polymer, hence the second maximum in the zeroth moment evolves. Then no reaction (except thermal initiation) provides new radicals, hence the moment of living polymer decreases to zero.

It has been shown, that the rigorous dynamical model (without an energy balance for the reactor wall) is able to reproduce precisely the reference values of the steady state simulator *Luposim* T. The number of grid points used for this comparison is

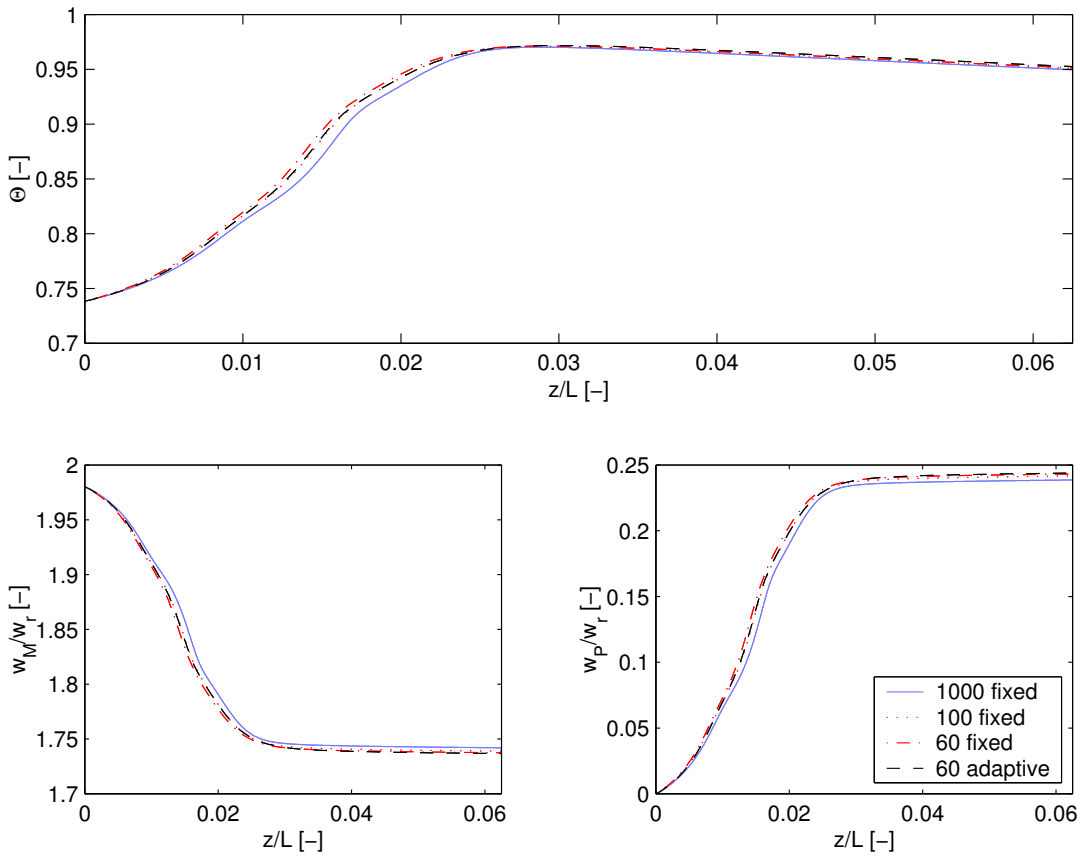

Figure 2.12: Temperature profiles and the mass fractions of monomer and polymer at steady state conditions using different discretization schemes and grid points

unrealistic high. A model of the tubular reactor, with its 29 partial differential and algebraic equations for each of the 16 modules would result in a system of $464 \cdot 10^3$ ordinary differential and algebraic equations. Such a system is far too large for standard computers systems available right now. So, in a next step, the influence of the selected discretization method on the simulation result of one module is discussed.

2.2.4.2 Influence of Discretization

The previous section proves the validity of the detailed model for one module. Here, the influence of the discretization will be discussed in detail. In order to select the best discretization method for the purpose of this work, the fully featured rigorous model

is used for this comparison, i.e. the energy balance equation for the wall is included. Moreover, the coolant is operated counter-current wise. For this configuration no simulation data from *Luposim* T is available, hence the detailed dynamical model with a high resolution fixed grid serves as reference.

The following configurations are compared to each other,

- high resolution *fixed* grid (1000 grid nodes),
- intermediate resolution *fixed* grid (100 grid nodes),
- low resolution *fixed* grid (60 grid nodes) and
- low resolution *adaptive* grid (60 grid nodes).

In Fig. 2.12, process variables, such as dimensionless temperature Θ and weight fractions of monomer w_M and LDPE w_P are depicted along the spatial coordinate. Both, w_M and w_P are made dimensionless using a reference weight fraction w_r. Again, only one module i.e. one cooling jacket, is considered here. The reference profile, which is the result of the simulation using the high resolution fixed grid is drawn in all three graphs with a solid blue line. The dash-dotted red line represents the intermediate resolution grid, the dotted red line the low resolution fixed and the dashed black line the low resolution adaptive grid. As one can observe, the number of grid points of either fixed or moving grid does not influence the profile of those process variables significantly. Only in regions of the tubular reactor where larger temperature gradients occur, some slight deviations between the four discretization schemes are visible.

But for such issues as optimization or control, also product properties play an important role. These properties can be expressed in terms of the number average,

$$P_n = \frac{\mu_1^P}{\mu_0^P} \tag{2.88}$$

variance

$$\sigma^2 = \frac{\mu_0^P \mu_2^P - (\mu_1^P)^2}{(\mu_0^P)^2} \tag{2.89}$$

and skewness

$$\gamma = \frac{\mu_3^P}{\sigma^2}. \tag{2.90}$$

They are depicted in the left column of Fig. 2.13. Number average means here an average chain length, variance is the averaged squared deviation from the arithmetic mean. The standard deviation is defined as the square root of the variance. Both standard deviation and variance describe the spread of a distribution, as does the polydispersity defined in (2.57). To describe, whether a distribution is asymmetric, the skewness can be used. If the distribution is normal, then the skewness calculated with centralized moments is zero, if the right tail is longer than the left one, then the skewness is negative, otherwise it will be positive. In Fig. 2.13 right column shows the second moments of the living primary and secondary and the dead polymer chain-length distribution. Again, the solid line represents the grid with 1000 fixed grid points, the dash-dotted line the fixed grid with 60 nodes and the dashed line the adaptive grid with the same number of grid nodes.

From this picture it is obvious, that there exist significant differences between the high and the low resolution grids in general. But if one compares these differences in magnitude, the adaptive low resolution grid performs considerably better than the fixed one. E.g. the error in the variance of the distribution is approx. 25% using the fixed grid, whereas with the adaptive grid it is 10% less. The reason for these large deviations in the properties of the distributions can be seen in the right column of Fig. 2.13. Even though the zeroth moment of the living polymer chain length distribution is used in the monitor function $M(z, \mathbf{x})$ (Eq. (2.73)), the number of fixed grid points is too small to resolve the formation of living polymer precisely. Hence these deviations sum up in higher moments of living polymer and naturally the error is transferred to the moments of the dead polymer chain length distribution.

In Tab. 2.1 the simulation times with the different discretization schemes are compared. The fastest calculation time, utilizing a low-resolution fixed equidistant grid is chosen as the reference time ($t_{disc,ref} = 42.42\ s$ on a standard PC equipped with an AMD Athlon™ 64 Processor 3500+ and $1GB$ RAM). In order to make the results of this comparison transferable to other computer systems, not the absolute values of the simulation time but multiples of the fastest solution are shown. In the upper row, the

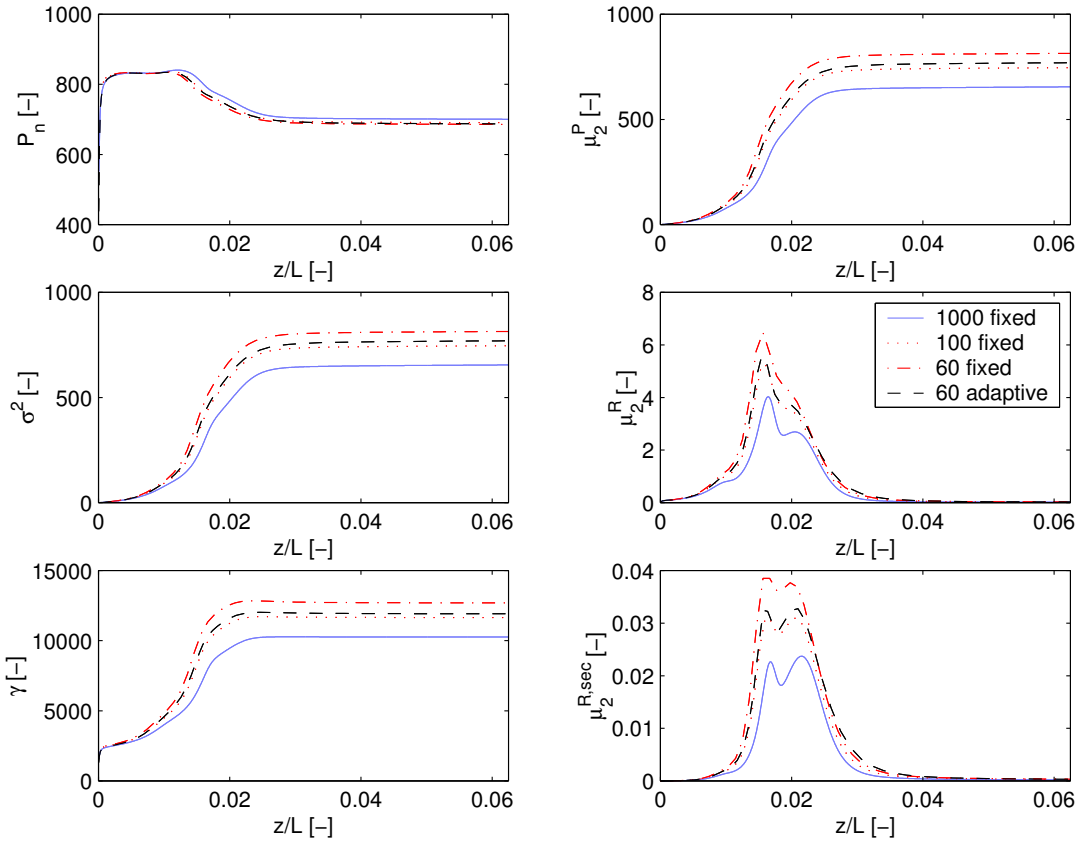

Figure 2.13: Temperature profiles and the mass fractions of monomer and polymer at steady state conditions using different discretization schemes and grid points

results for the validation of one module are tabulated (see Sec. 2.2.4.1). There, the model without energy balance for the wall has been used and that the coolant is assumed to flow co-current wise. It is interesting to see, that the fixed grid with 100 grid nodes and the low-resolution grid both have similar simulation times, even though the

Wall energy balance	Coolant flux direction	Fixed 1000	Fixed 100	Fixed 60	Adaptive 60
–	co-current	83.3	1.9	1.0	2.0
✔	counter-current	110.7	4.0	1.8	12.6

Table 2.1: Comparison of simulation times $\frac{t_{disc}}{t_{disc,ref}}$ on a standard with an AMD Athlon™ 64 Processor 3500+ and $1GB$ RAM.

number of state variables is lower by a factor of 1.6. Moreover, the high-resolution scheme, which is larger in size by a factor of 16.7, takes 83.3 times longer to be solved. In general, the effort of solving equation systems numerically increases exponentially with system size. Additionally, also the type of equations and back-mixing effects increase simulation times. This can be seen in the bottom row of the table, which tabulates the results of a simulation with the energy balance equation for the wall and with the counter-current flow. Both effects contribute to an almost doubled simulation time for the fixed low-resolution grid. The fixed intermediate-resolution grid scales with the same factor, but the adaptive grid now takes three times as long as the fixed grid with the same error. Even though, the simulation is much faster, it is not possible to use the fixed grid with 100 grid nodes, since this adds up to $29 \cdot 16 \cdot 100 = 46000$ equations, which has not been possible to solve on a standard PC. Here, the adaptive

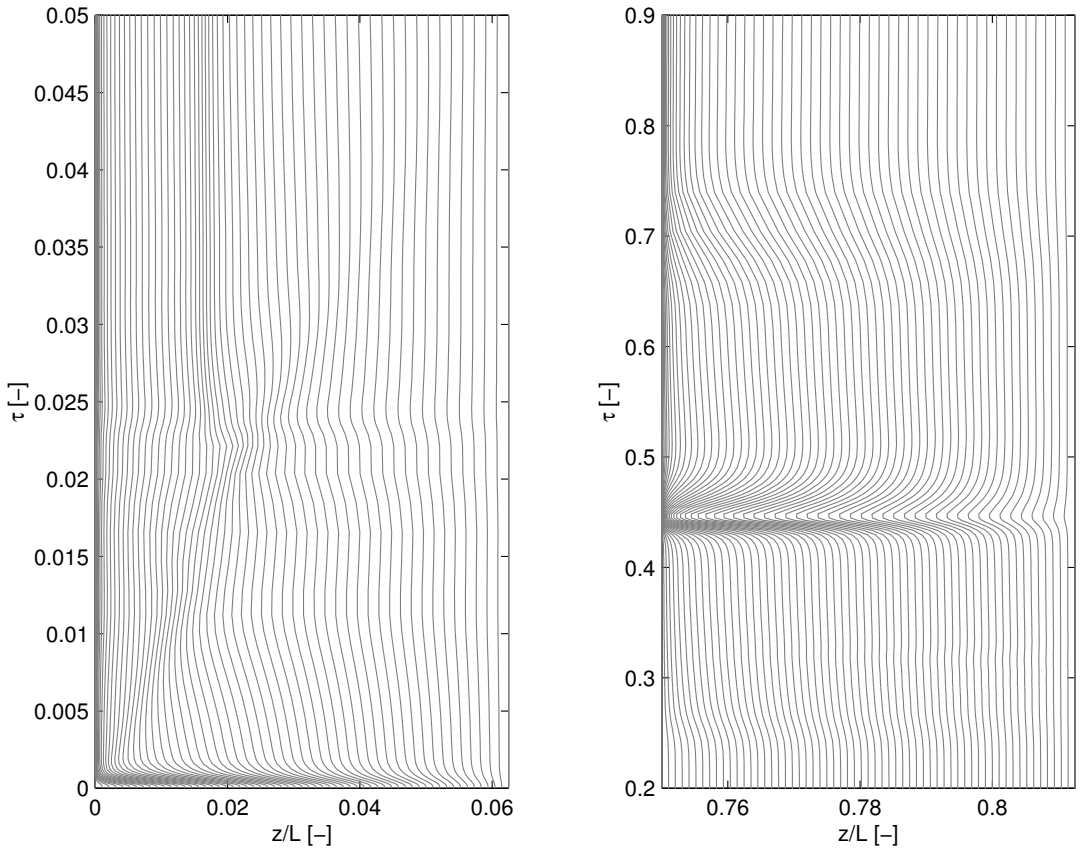

Figure 2.14: Movement of grid nodes during the startup of the tubular reactor

grid is smaller by a factor of 1.6 ($30 \cdot 16 \cdot 60 = 28800$).

To see how the grid node distribution evolves with simulation time, Fig. 2.14 displays the movement of the grid nodes of two modules during the startup of the tubular reactor. The abscissa displays the dimensionless axial coordinate, the y-axis the simulation time $\tau = \frac{t_{sim}}{t_{res}}$. This is a dimensionless number accounting for the real simulation time t_{sim} and the residence time of the reactor t_{res}. One grey line represents the position of a grid node. The left figure shows the grid node distribution right after the initiator injection in the first module, the right one shows the arrival of a wave at the fourth section, in particular, at the thirteenth module. In both figures it can be seen that the grid node concentration moves rapidly to the left boundary of the plot and after only a few milli-τ the steady-state is established. It is important to see, that in the left figure, the grid nodes are not exclusively locked to the left picture boundary, there is also a higher concentration at $z/L \approx 0.02$, which is due to the fact, that the zeroth living polymer moment is used for the monitor function. And from Fig. 2.10 follows directly, that there a higher resolution is required.

Disregarding the longer simulation times, the low-resolution adaptive grid offers both reasonable model size (which has been important because of memory constraints of standard PCs at that time) and sufficient accuracy. So, this discretization method is used throughout the remainder of this work.

2.3 Peripheral Units

The periphery of the tubular reactor can be summarized in a few single units. First of all the mixing units, then the compressors, the separators and some heat exchangers. Ideal controllers are assumed, that keep the controlled variables at the desired set point, e.g. temperatures in the separators, where the model equations and underlying assumptions are given in Section 2.3.3.

2.3.1 Mixer

In the plant there are several units for mixing different streams, e.g. mixing fresh ethylene with the recycle from the low pressure separator, or the injection of new initiator into the reactor tube. All of these units have in common that they are assumed

not to have storage capacities. Thus, the different fluxes mix instantaneously, meaning that the mixer is modeled as a continuous stirred tank reactor with infinitely small volume. Hence these systems can be described by algebraic equations solely. Therefore all mixers in the plant are described by algebraic mass, component and energy balances.

$$0 = \dot{m}_{mix} - \sum_{j=1}^{J} \dot{m}_{in,j}, \tag{2.91}$$

$$0 = \dot{m}_{mix} w_{mix,i} - \sum_{j=1}^{J} \dot{m}_{in,i,j} w_{in,i,j} \qquad \forall\ i = 1, \ldots, I-1. \tag{2.92}$$

It is assumed, that the heat capacity of modifier is the same as the one of ethene. Moreover, the heat capacity of the monomer is assumed to be constant in those mixers, hence

$$0 = T_{mix} \dot{m}_{mix} - \sum_{j=1}^{J} \dot{m}_{in,j} T_{in,j}. \tag{2.93}$$

2.3.2 Compressor

There are three compressors in the plant, a so-called 'booster', which compresses the ethylene gas from the low pressure recycle to the feed pressure of the freshly added monomer/modifier mixture. The feed is followed by a pre-compressor, which brings this gas stream to an intermediate pressure. Afterwards, the hyper-compressor, which compresses the monomer/modifier mixture up to the operating pressure of approx. 3000 bar. The booster consists of two successive stages, the pre-compressor consists of three stages, the final pressure is reached after another two stages in the hyper-compressor.

A rating model of compressors in general correlates the behavior of real gases to the behavior of ideal gases. The change of state of ideal gases can be described by the polytropic exponent, which the The American Society of Mechanical Engineers

(1997) define in their test code as

$$n = \frac{\log\left(\frac{p^{out}}{p^{in}}\right)}{\log\left(\frac{\dot{V}^{in}}{\dot{V}(p^{out},\dot{H}^{out})}\right)}, \tag{2.94}$$

where p_{in} and p_{out} are inlet and outlet pressure and $\dot{V}$ is the volumetric flow rate at inlet and real outlet conditions p_{out} and T_{out}. However, for such a description it is necessary to use performance map curves. These curves correlate machine efficiency and machine head to volumetric flow rate and either inlet guide vane or angular speed, depending on whether the machine is angle or speed controlled. Since both, performance map curves for the efficiency and for the head of all compressors are not specified by the cooperation partner, it is assumed that temperature and pressure are controlled ideally. Then, in general, the k-th stage of a compressor consists of the following equations

$$\begin{aligned}
0 &= \dot{m}_{in,k} + \gamma\,\dot{m}_{in,rec} - \dot{m}_{out,k} \\
\varrho_{i,k} V_{R_k,i} \frac{dw_{i,k}}{dt} &= \dot{m}_{in,k} w_{in,i,k} + \gamma\,\dot{m}_{in,rec} w_{in,i,rec} - \dot{m}_{out,k} w_{i,k}, \quad i = 1,\ldots,N_C - 1 \\
0 &= \sum_{i=1}^{N_C} w_{i,k} - 1.0
\end{aligned}$$

with

$$\gamma = \begin{cases} 1 & \text{for } k = 1 \\ 0 & \text{else.} \end{cases}$$

Moreover, $m_{in,k+1} = m_{out,k}$. Note that in these compressor units only two components are present, namely $ethylene$ and $modifier$. Both are either freshly fed to the process or come from the recycle lines. Moreover, it is supposed that the physical properties of both modifier and ethylene are identical. Since both, pressure and temperature are controlled ideally, they are assumed to be constant at a given set point, i.e. $T_k = const.$ and $p_k = const.$.

2.3.3 Separator

The separators are required to split up the mixture of monomer, modifier and polymer. It is assumed that monomer and modifier are removed ideally from the mixture, meaning that only polymer leaves the plant.

In the plant, there are two separating units, one where the mixture at high pressure is relaxed to an intermediate pressure and a succeeding one, where relaxation to a moderate pressure, slightly higher than ambience pressure takes place. The two different pressure levels are introduced to save compression energy from the low to the intermediate pressure level.

High pressure separator To fully describe the high pressure flash unit, mass balance, component mass balance and energy balance equations are required. The global mass balance is assumed to be quasi-stationary, so are the component mass balances for the three components (monomer, modifier and polymer) and the energy balance. Moreover, the liquid phase contains all three components, where the gaseous phase (which is recycled in subsequent recycle lines) does not contain any product. Using an reasonable fast controller, the flash will be both isothermal and isobaric. To describe the vapor-liquid-equilibrium a generic equation (which was fitted to given measured data) is used

$$w_{liq,M} = w_{liq,M}(p_{flash}, T_{flash}).$$

Hence the model reads

$$\begin{aligned}
0 &= \dot{m}_{in,hp} - \dot{m}_{vap} - \dot{m}_{liq} \\
0 &= \dot{m}_{in,hp} w_{in,hp,X} - \dot{m}_{vap} w_{vap,X} \\
0 &= \sum_{i=1}^{N_C} w_{vap,i} - 1.0 \\
0 &= \sum_{i=1}^{N_C} w_{liq,i} - 1.0 \\
0 &= w_{vap,P} \\
0 &= w_{liq,X}
\end{aligned}$$

$$0 = \dot{m}_{in,hp} h_{in,hp} - \dot{m}_{vap}(h_{vap} + \Delta h_{vap,M}) - \dot{m}_{liq} h_{liq}.$$

Note that from the energy balance equation not the temperature is calculated (remember that isothermal behavior was assumed), but the mass flux of the vapor phase. Moreover, it is assumed that polymer and modifier are separated ideally, i.e. no polymer but all modifier is recirculated in the high pressure recycle ($w_{vap,P} = w_{liq,X} = 0$).

Low pressure separator The low pressure flash is modelled to separate ideally the polymer P from the unreacted monomer M, hence only polymer is withdrawn from the plant and all monomer is recycled. So the model equations for this unit read

$$\begin{aligned} 0 &= \dot{m}_{in,lp} - \dot{m}_M - \dot{m}_P \\ 0 &= w_{in,lp,M} \dot{m}_{in,lp} - \dot{m}_M. \end{aligned}$$

Additionally, the flash is temperature controlled, so that $T_{lp} = const.$.

2.3.4 Recycles

The recycle lines of Fig. 2.1 are assumed to be lag systems and the heat exchangers can be used to control the temperature at arbitrary set points. So the volume of the recycles is modeled by simple tank units.

$$0 = \dot{m}_{in} - \dot{m}_{rec} \tag{2.95}$$

$$\varrho_{rec,M} V_{rec} \frac{dw_{rec,M}}{dt} = \dot{m}_{in} w_{in,M} - \dot{m}_{rec} w_{rec,M} \tag{2.96}$$

$$0 = w_{rec,X} + w_{rec,M} - 1.0 \tag{2.97}$$

$$0 = T_{rec} - T_{set}. \tag{2.98}$$

Note, that in the high pressure recycle line, the only components are monomer M and modifier X. The low pressure recycle consists of pure ethene, so there the component mass balance and the closure are not required to describe the unit model.

2.4 Simple Model of the Plant

The simplified model only includes the essential process characteristics and is therefore only suitable for a qualitative but not a quantitative prediction of the process behavior.

Due to it's simplicity it is well suited for a numerical bifurcation analysis using the methods and tools described in Mangold et al. (2000a). The influence of the most important process parameters is studied systematically. These are: the feed flow rate, the feed concentration of monomer and the heat exchange.

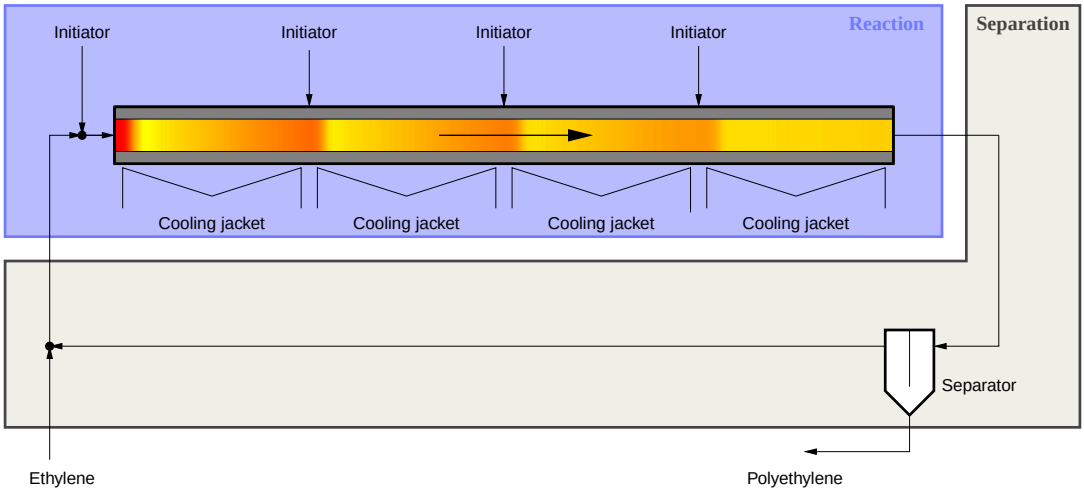

Figure 2.15: Flowsheet representation of the simple mathematical model

Fig. 2.15 shows the flowsheet of the simplified plant for the production of low density polyethylene using a tubular reactor. The simplified tubular reactor is 1000 m long and has a inner diameter of 4 cm. Fresh monomer is fed to the plant and mixed with the recycle from the separator. The free radical polymerization of LDPE is carried out in the tubular reactor. Therefore initiators are added to the monomer stream at the inlet of the tubular reactor. The reaction starts, the temperature rises, initiator decompose into radicals, radicals bind monomer and hence monomer gets consumed, whereas polymer is produced. The reaction heat is removed using four different cooling jackets. Here, the length of each of the four cooling zones is identical. A cooling zone is located in between two injectors.

At the outlet, unreacted ethylene is separated from the polymer in one flash unit,

the polymer is withdrawn from the plant, whereas the monomer is recycled to the system.

For comparison, the flowsheet of the real production plant is depicted in Fig. 2.1. Next, the main differences in the plant structure are listed in detail.

As one can observe, compressors are neglected completely. Additionally, the pressure in the tubular reactor is assumed to be constant ($p = 3000\ bar$). This implies, that the simple model does not need two recycle lines. Recall, that in the real production process the only reason for having two recycle lines are savings in compression energy. Hence, the recycle lines are operated at that pressure to which the flash unit expands the ingoing monomer/polymer mixture. Since the pressure drop in the reactor is neglected, the simple model only has one flash unit and only one recycle line. This has no effect on the total recycle flow rate.

The next difference which is obvious just by comparing Fig. 2.15 to Fig. 2.1, is the number of coolant jackets. In the real production process, there are in total 16 different coolant cycles which can be operated co- or counter current wise. For the simplified process the number of jackets is decreased to four. Moreover, the simple model assumes a constant coolant temperature, which of course saves an additional partial differential equation.

Additionally, the initiator mixture consisting of three different initiators, which decompose at different temperature levels, is substituted by a single initiator, resolving at intermediate temperature levels.

2.4.1 Reaction Scheme

The reaction scheme used for the simplified model of the tubular reaction differs significantly from the very detailed scheme in the rigorous dynamic model. Here only the main reactions, characteristic for all polymerization reactions are taken into account. Side reactions are completely neglected. Hence only the following reactions are considered,

$$I_v \xrightarrow{k_{I_v}} 2\ R_{I_v} \qquad \text{initiator decomposition,} \tag{2.99}$$

$$R_{I_v} + M \xrightarrow{k_{p,I_v}} R_1 \qquad \text{initiation,} \tag{2.100}$$

$$R_i + M \xrightarrow{k_p} R_{i+1} \qquad \text{propagation,} \tag{2.101}$$

$$R_i + R_j \xrightarrow{k_{t,c}} P_{i+j} \qquad \text{termination by combination and} \tag{2.102}$$

$$R_i + R_j \xrightarrow{k_{t,d}} P_i + P_j \qquad \text{termination by disproportion.} \tag{2.103}$$

Buback (1980) reported that the rate of thermal initiation of ethylene is much lower compared to the other initiation reactions, so that reaction is neglected. There are two more differences when comparing the reaction scheme (2.99)-(2.103) to the more detailed one (2.1)–(2.7), the number of components is reduced by six, since only one initiator equation is required and the modifier is neglected. Even though two different initiators (I_ν for $\nu = 1, 2$) are used (decomposing at low and intermediate temperatures), one component mass balance equation is sufficient, since initiator decomposing at low temperatures is injected only at the inlet of the tubular reactor, the second initiator is added at all successive injection pumps. All initiator is consumed in the section where it is injected. Moreover, the additional counter for the occurrence of double bonds is not included in the termination reaction (2.103).

2.4.2 Model Equations

2.4.2.1 Tubular Reactor

Both in the rigorous and in the simpler dynamical model of the tubular reactor in the LDPE production process, it is supposed that the following assumptions hold

- one homogeneous liquid phase and
- plug flow.

In order to reduce both complexity and model size more simplifications have to be taken into account, such as

- a constant pressure drop over the reactor length
- reduction of the number of coolant jackets down to four, that are additionally operated at a constant temperature level
- a constant average heat transfer coefficient

- reduction of the number of initiators to two
- a constant temperature and a negligible time delay in the recycles
- a negligible energy balance equations for coolant and inner reactor wall

So there are seven components in the reactor, two initiators, their radicals, monomer and living and dead polymer. Adding the energy balance for the reactor temperature, the models compare in their size as tabulated in Tab. 2.2.

For the simple model, only data available from literature is be used. There, the parameters are usually published based on concentrations rather than on weight fractions. Hence the simple model equations are formulated in terms of concentrations and the component mass balances for the species are

- initiator concentrations

$$\frac{\partial c_{I_\nu}}{\partial t} + v\frac{\partial c_{I_\nu}}{\partial z} = -k_{I_\nu}\, c_{I_\nu} \qquad \forall\, \nu = 1,2, \tag{2.104}$$

- initiator radicals concentrations

$$\frac{\partial c_{R_\nu}}{\partial t} + v\frac{\partial c_{R_\nu}}{\partial z} = 2k_{I_\nu}\, c_{I_\nu} - k_{p,I_\nu} c_{R_\nu} c_M \qquad \forall\, \nu = 1,2, \tag{2.105}$$

- monomer concentration

$$\frac{\partial c_M}{\partial t} + v\frac{\partial c_M}{\partial z} = -\sum_{\nu=1}^{2} k_{p,I_\nu}\, c_{R_\nu}\, c_M - k_p\, c_M \lambda_0^R, \tag{2.106}$$

	Detailed model	Simplified model
Number of modules	16	4
Number of PDAEs per module	30	7
Grid resolution	60	50
Total number of DAEs	≈ 30000	≈ 1000

Table 2.2: Comparison of model sizes of the tubular reactor – rigorous versus simplified model

- overall concentration of living polymer

$$\frac{\partial \lambda_0^R}{\partial t} + v\frac{\partial \lambda_0^R}{\partial z} = \sum_{\nu=1}^{2} k_{p,I_\nu}\, c_{R_\nu}\, c_M - \big(k_{tc} + k_{td}\big)(\lambda_0^R)^2, \tag{2.107}$$

- overall concentration of dead polymer (product)

$$\frac{\partial \lambda_0^P}{\partial t} + v\frac{\partial \lambda_0^P}{\partial z} = \big(0.5k_{tc} + k_{td}\big)(\lambda_0^R)^2. \tag{2.108}$$

Knowing that the energy balance for the wall is neglected and that the coolant temperature T_C is constant, it is straightforward to derive the energy balance

$$\varrho c_p\big(\frac{\partial T}{\partial t} + v\frac{\partial T}{\partial z}\big) = \Delta h\Bigg(k_p c_M \lambda_0^P + \big(\frac{1}{2}k_{tc} + k_{td}\big)(\lambda_0^P)^2 + \sum_{\nu=1}^{2} k_{I_\nu} c_{I_\nu}\Bigg) - \frac{U}{\pi r^2}(T - T_C). \tag{2.109}$$

In the equations above, c_j denotes the concentration of species j. These state variables are distributed over the domain. v is the flow rate of the reaction mixture, which is a concentrated variable. Both, $\varrho = 540\frac{kg}{m^3}$ and $c_p = 2.7\frac{kJ}{kgK}$ are constant over the length of the reactor. So are the heat of reaction $\Delta h = 95\frac{kJ}{mol}$ and the heat transfer coefficient $U = 80\frac{W}{mK}$.

For all state variables $\mathbf{x} = [c_i \quad \lambda_0^j \quad T]^T$, the following initial and boundary conditions hold

$$IC: \qquad \mathbf{x}(z, t = t_0) = \mathbf{x}_0(z) \tag{2.110}$$

$$BC: \qquad \mathbf{x}(z = 0, t) = \mathbf{x}_{in}(t) \tag{2.111}$$

The reaction rates and their parameters are given in Tab. 2.3. The values for the initiator decomposition have been reported by Kim and Iedema (2004) and the values for all propagation and termination reactions are taken from Lee and Marano (1979).

initiator decomposition	$k_{I_1} = 1.35 \cdot 10^{13} \exp\left(\frac{-117476-0.2805\cdot 10^{-5} p}{\mathbb{R}T}\right)$	$\left[\frac{1}{s}\right]$
	$k_{I_2} = 2.89 \cdot 10^{14} \exp\left(\frac{-138237-1.012\cdot 10^{-5} p}{\mathbb{R}T}\right)$	$\left[\frac{1}{s}\right]$
propagation	$k_p = 5.88 \cdot 10^{4} \exp\left(\frac{-29704+2.325\cdot 10^{-5} p}{\mathbb{R}T}\right)$	$\left[\frac{m^3}{gmol\ s}\right]$
initiation	$k_{p,I_1} = k_{p,I_2} = k_p$	
termination by combination	$k_{tc} = 1.075 \cdot 10^{6} \exp\left(\frac{-1247+1.422\cdot 10^{-5} p}{\mathbb{R}T}\right)$	$\left[\frac{m^3}{gmol\ s}\right]$
by disproportion	$k_{td} = k_{tc}$	

Table 2.3: Kinetic rate expressions used in the simple model

2.4.2.2 Peripheral Units – Simple Model

For the description of the rigorous dynamic mathematical model of the low-density polyethylene production plant, additional units for compression, separation and heat exchange are used. Though these units do not contribute significantly to the size of the model, most of the units are neglected or simplified. In particular, the two different flash units of the detailed model operated at different pressure levels for recovery of compression energy, are concatenated into a single flash unit. Additionally, this flash unit ideally separates product from unreacted monomer, which makes it unnecessary to include a equilibrium correlation into that model,

$$0 = \dot{n}_{in} - \dot{n}_{rec} - \dot{n}_{LDPE} \tag{2.112}$$

$$0 = \dot{n}_{in} x_{M,in} - \dot{n}_{rec} x_{M,rec} \tag{2.113}$$

$$0 = \dot{n}_{in} x_{I_v,in} - \dot{n}_{rec} x_{I_v,rec} \tag{2.114}$$

$$0 = \dot{n}_{in} x_{R,in} - \dot{n}_{rec} x_{R,rec} \tag{2.115}$$

$$0 = T_{rec} - T_{fix}. \tag{2.116}$$

Since only one recycle line is used for the simple model, the compressors can be neglected as well. Hence, only a mixing unit is required, which ideally mixes the incoming feed and the recycled material from the flash unit. The model equations for

this unit read

$$0 = \frac{\dot{n}_{rec}}{M} + \dot{V}_F - \dot{V}_R \tag{2.117}$$

$$0 = \dot{n}_{rec} x_{M,rec} + \dot{V}_F c_{M,F} - \dot{V}_R c_M \tag{2.118}$$

$$0 = \dot{n}_{rec} x_{I_v,rec} + \dot{V}_F c_{I_v,F} - \dot{V}_R c_{I_v} \tag{2.119}$$

$$0 = \dot{n}_{rec} x_{R,rec} + \dot{V}_F c_{R,F} - \dot{V}_R c_R \tag{2.120}$$

$$0 = T_R - T_{fix}. \tag{2.121}$$

Note that in (2.117) a volume balance occurs, however, in this mixing unit no reaction takes place which changes the mole number, hence a general mass balance may also be stated in terms of volume.

So far for both, the rigorous and the simpler model, the mathematical model equations have been derived. The next chapter shows simulation results for both steady state and dynamical solution of the LDPE production line.

Chapter 3

Simulation Results

It does not matter how slowly you go, so long as you do not stop.
– Confucius

In this chapter, simulation results of both, the detailed and the simple model will be presented. At first, in Sec. 3.1, results of the rigorous model are compared to the reference, which is the solution of a simulation run of the steady state simulator *Luposim* T. For the steady state comparison, the system without an additional energy balance for the thick reactor wall is used, since *Luposim* T does not account for this effect. Then dynamic simulation results with the detailed mathematical model are shown in Sec. 3.2. These include simulations of only the tubular reactor during startup operations or disturbances, as well as disturbances in input variables of the whole production process from the given nominal operating point. Finally, in Sec. 3.3, the detailed model is compared to a simpler one. Since the agreement between simple and rigorous model is very good, the nonlinear analysis of the process is carried out using the simpler and hence smaller model.

3.1 Steady State Simulation Results – Rigorous Model

First, the focus is on the validation of the rigorous model of the tubular reactor. As it has been already shown in Sec. 2.2.3, the results of the rigorous dynamic model of one module match perfectly the results of the steady state simulator *Luposim* T, inspite of the different solution strategy and the large difference in the number of equations of

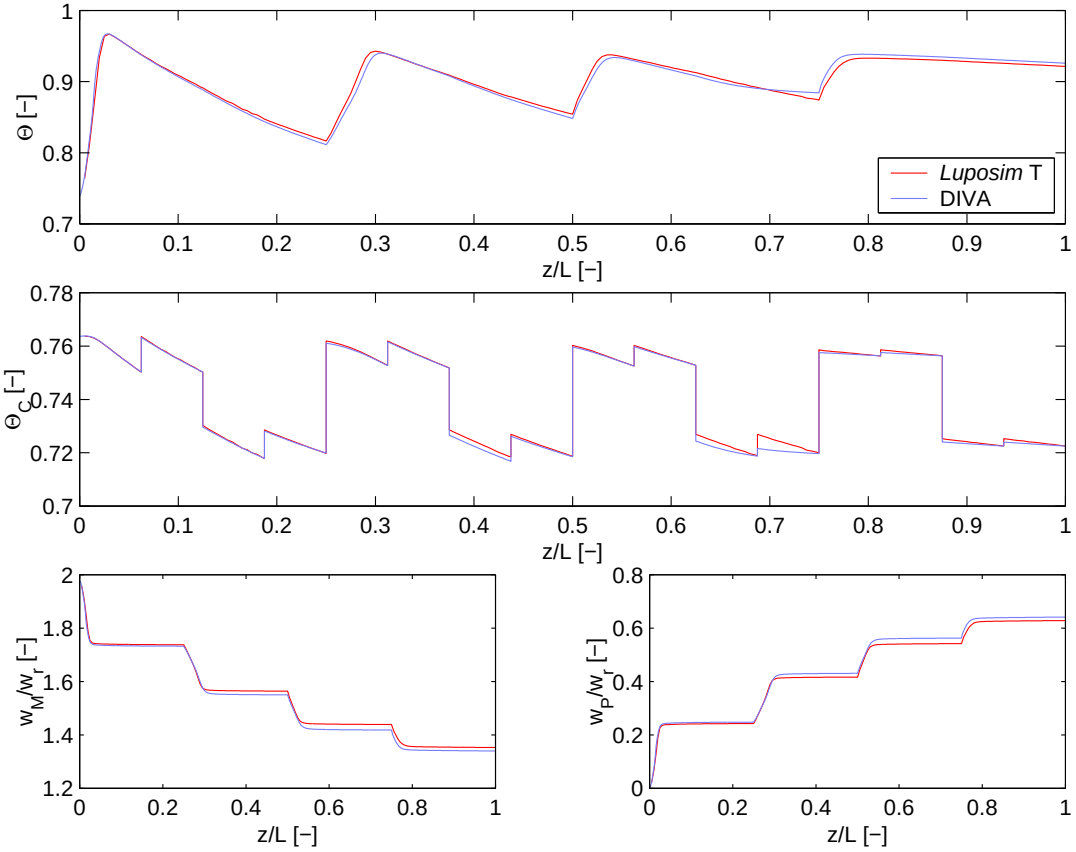

Figure 3.1: Comparison of steady state simulation results from *Luposim* T and DIVA – temperatures, monomer and polymer weight fractions

the systems, that are solved numerically. DIVA on the one hand side is an equation based simulator that solves DAE systems simultaneously in each integration step. The steady state simulator *Luposim* T on the other side integrates along the spatial coordinate and implements the counter-current coolant flow via a shooting method. Clearly, the numerical effort for *Luposim* T is much smaller compared to the state-of-the-art simulator DIVA, but of course its commitment is different. Whereas *Luposim* T only solves the steady state equations, DIVA additionally solves dynamic systems and can be used for dynamic and steady state optimizations and for nonlinear analysis. These results will be presented in Sec. 3.3.

3.1.1 System Without Energy Balance for the Wall

In this section, the steady state simulation results of *Luposim* T are compared to the results of DIVA. Note that *Luposim* T only simulates the tubular reactor, hence only simulation results of this unit are considered. Moreover, coolant is operated counter-current wise. Remember that *Luposim* T approximates a counter-current coolant operation using a shooting method. Looking at Fig. 3.1 it is obvious that the results of both simulators show very good agreement. Only at the end of the tubular reactor, there are some larger deviations in the coolant temperature. In particular at $z/L = 0.75$, the inlet temperature of the coolant is the same, but the outlet temperature of this cooling zone at $z/L \approx 0.69$ differs quite significantly. This is due to the fact, that DIVA requires all variables to be elements in $\mathbb{C}^1$, unless implicit event functions are defined

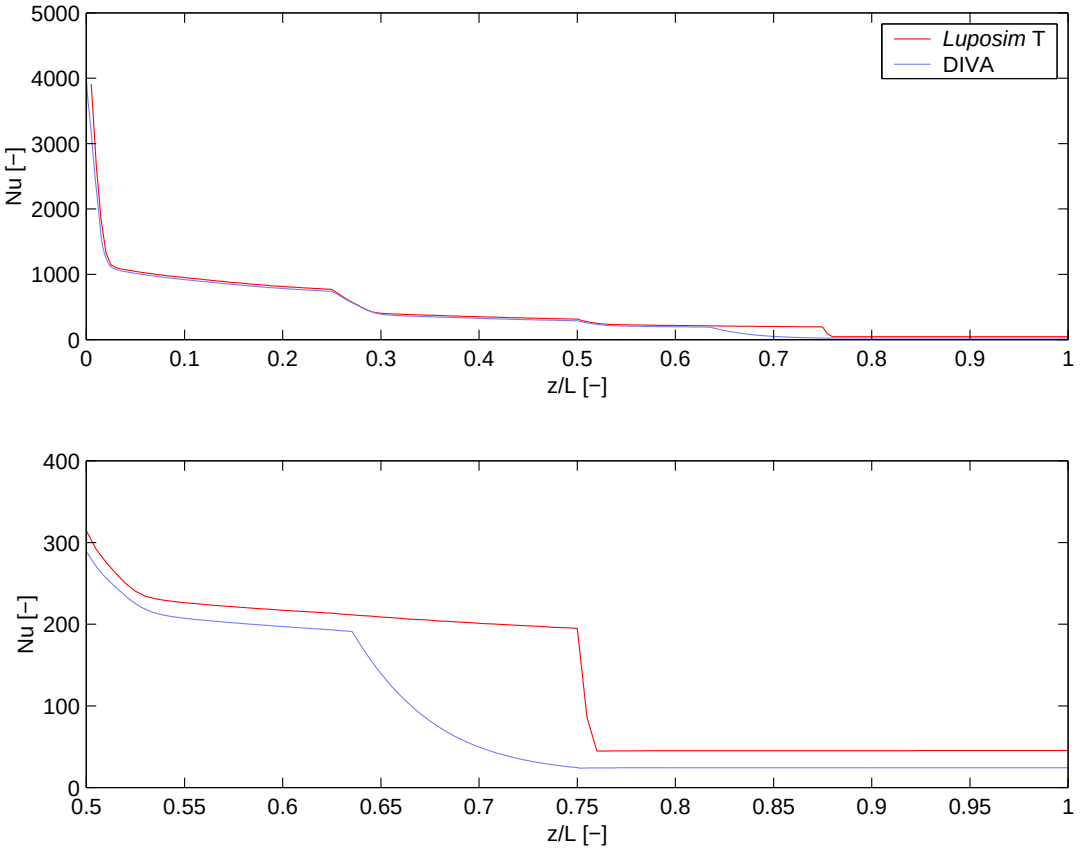

Figure 3.2: Comparison of steady state simulation results from *Luposim* T and DIVA – Nusselt number in the tubular reactor.

for these variables ($\mathbb{C}^1$ is the set of functions that are continuous and have a continuous *first* derivative). Since all variables in the tubular reactor are spatially distributed, that would imply numerous distributed event functions. Each event causes a local iterative search for the exact point in time, at which that event occurs. Therefore, simulation times would exceed an acceptable limit, so such a procedure is not practical for a distributed parameter system. To avoid this, the discontinuous correlations have been converted into functions in $\mathbb{C}^1$. Both, the effect of such a transformation (which is applied to the Reynolds number) and the effect of slight deviations at a transition point can be seen in Fig. 3.2. There, the Nusselt number ($Nu = f(Re, Pr)$) is plotted against the length of the reactor. In the top figure, the whole reactor and in the bottom figure only the relevant sector is graphed. Again, the red and blue line represent simulation results of *Luposim* T and DIVA. To a large extent, there is good agreement between the two profiles. Only in the region with large deviations in coolant temperature, a significant difference is visible. This can be explained first by small deviations in the Reynolds number of the rigorous model, since this implies an earlier transition from the turbulent to the turbulent-laminar domain. Moreover, the implementation of this transformation to a $\mathbb{C}^1$ function changes the limit points of the transient region from turbulent to laminar Reynolds numbers. The region of transition becomes slightly larger, leading to the effect depicted in Fig. 3.2.

Another point which is very interesting from Fig. 3.2 in general, is the strong dependency of the Nusselt number on the location within the reactor. The Nusselt number decays from almost 4000 (for turbulent flows) down to 20, where the flow is laminar. Since Nu directly influences the heat transfer resistor R_i as one summand in the overall heat transfer coefficient from reactor to coolant (Eq. (2.43) or (2.48)), it is obvious, that the profile of the coolant temperature has almost no gradient with respect to reactor length in section four (c.f. Fig. 3.1).

Apart from that difference, and despite of the fact, that only the adaptive low-resolution discretization scheme is used, the profiles in Fig. 3.1 match very well. Nevertheless, in Sec. 2.2.4.2 it has been shown, that even though there are only minor deviations in process variables such as temperature or weight fractions, in some properties of the distribution there may well occur larger deviations. Hence, Fig 3.3 shows these properties, such as number average P_n, variance or skewness. Moreover, the melt flow index is shown in the bottom right graph. As one can observe,

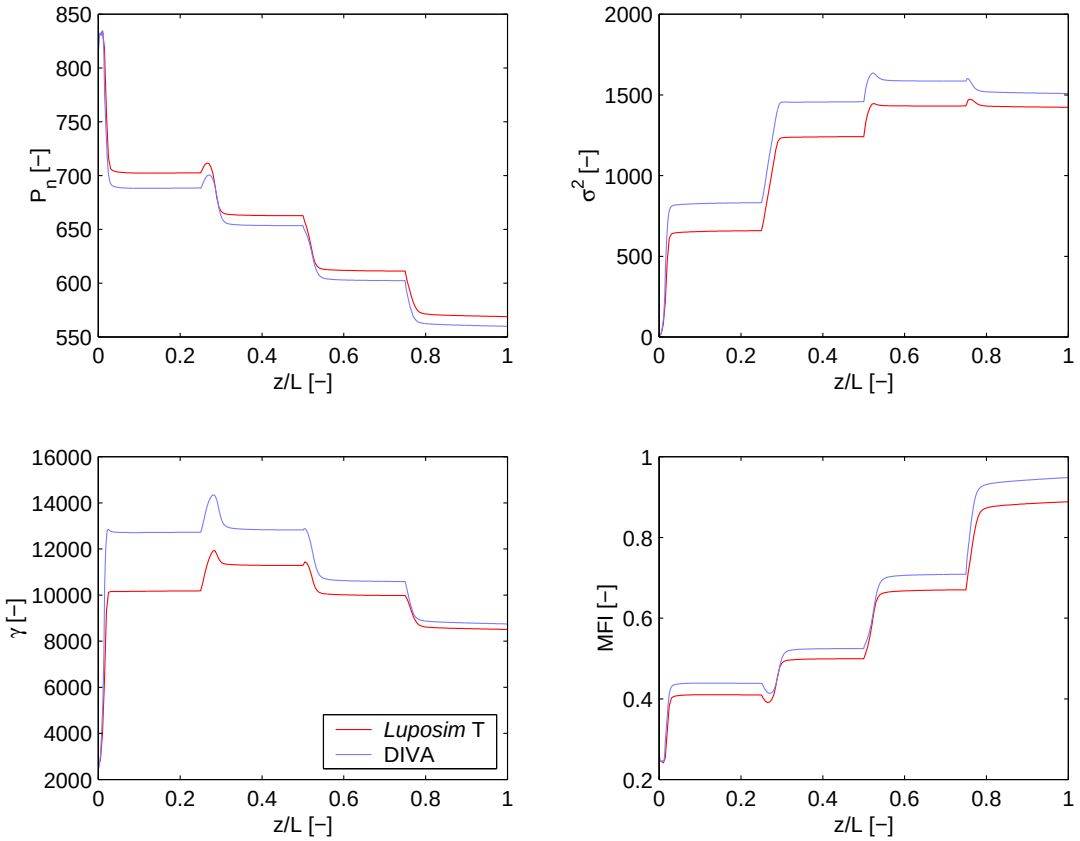

Figure 3.3: Comparison of steady state simulation results from *Luposim* T and DIVA – properties of the dead polymer distribution and the melt flow index.

the deviations in the product ($z/L = 1$) are only in a range of $3-6\%$. But during the polymerization, the properties of the distribution such as variance and most of all skewness show larger deviations up to 30%. This error is introduced by the discretization. Recall, that for a high-resolution scheme, the moments calculated by DIVA and *Luposim* T match accurately, whereas for lower resolutions, in all moments of the radical distribution and hence also of the dead polymer distribution a discretization error becomes visible. In general, due to the discretization, DIVA "produces" longer chains in the beginning. The influence of this effect becomes smaller, the longer the reaction takes place. Hence, at the outlet, both simulation results agree quite well and using the low-resolution adaptive discretization scheme does not introduce deviations in the product with are unacceptable. In the sequel, the adaptive Method of Lines is used for all simulations using the rigorous dynamic model for the tubular reactor.

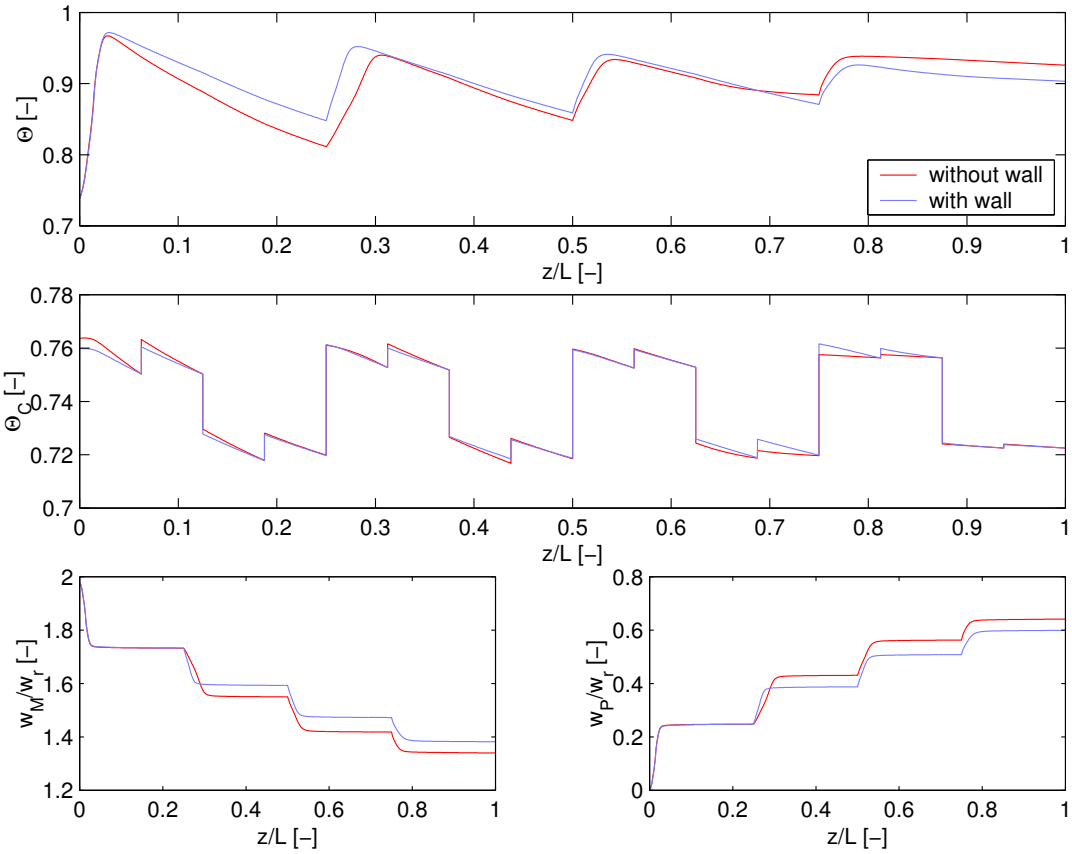

Figure 3.4: Comparison of steady state simulation results neglecting the energy balance for the wall and including it – temperatures and weight fractions of monomer and polymer.

3.1.2 System With Energy Balance for the Wall

In this section, the energy balance for the reactor wall is included into the mathematical description of the tubular reactor. First the influence of the wall in steady state is discussed. In Fig 3.4 the steady state profiles of dimensionless temperatures and normalized weight fractions are depicted. The red lines represent the model without, the blue lines the model with additional partial differential equation for the wall. One can see from the top graph in Fig. 3.4 that the reactor temperature in the first section and in the last section is significantly influenced by the reactor wall equation, even though the heat transfer coefficient of the wall is included into the model without the additional equation. These deviations are due to the fact that the model with wall

energy balance allows heat transport also in axial direction, which causes peaks and minima to smooth out. This is most obvious in the first and last section of the tubular reactor. In the first section the highly exothermic reaction starts and the coolant is used to lower the reactor temperature. Since in the second section the reaction is re-ignited by adding new initiator, again temperature rises. But in the case with energy balance for the reactor wall, the wall allows heat transport in axial direction. Hence the temperature before and after the injector is higher. This effect additionally causes the initiator injected at $z/L = 0.25$ to decompose faster, producing more heat of reaction. So even though the energy balance for the wall should chop off peaks, the maximum temperature in sections two and three are higher.

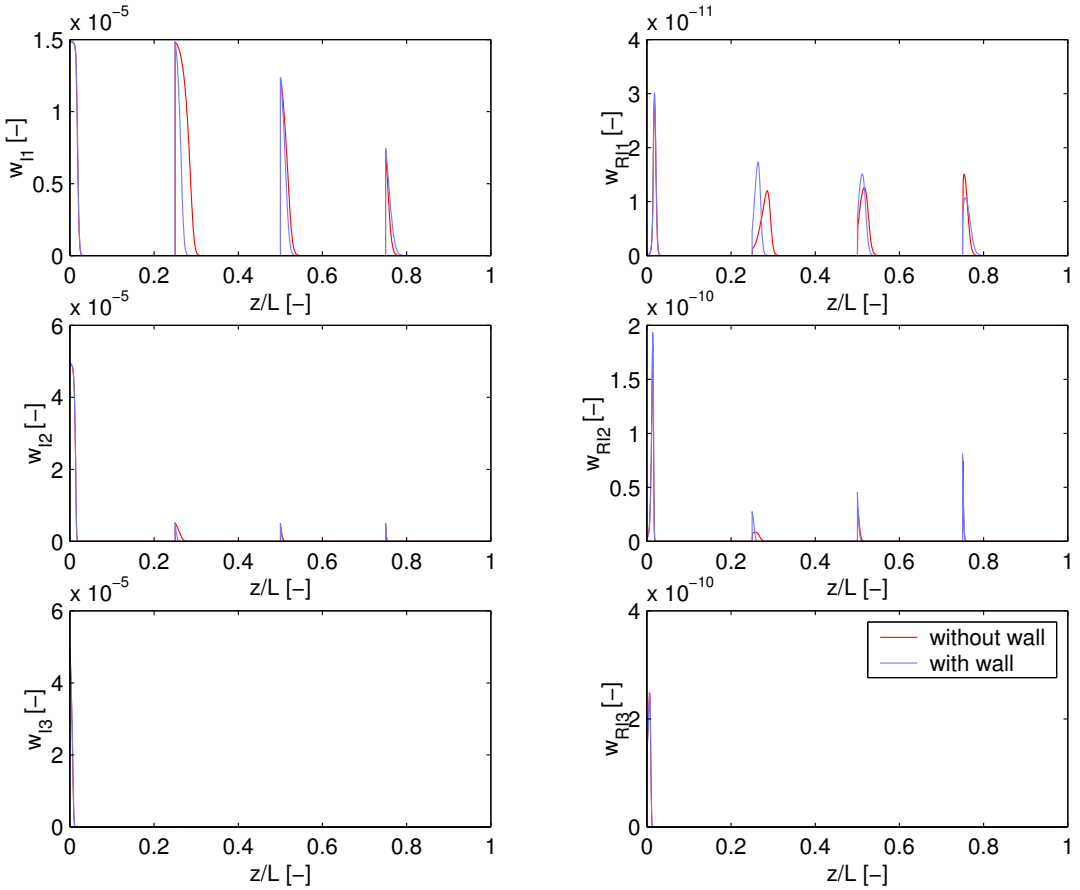

Figure 3.5: Comparison of steady state simulation results neglecting the energy balance for the wall and including it – weight fractions of initiator and their radicals

Looking only on the steady state results, it cannot yet be decided, whether an energy balance for the wall is required to describe the main features of the production process of low-density polyethylene. However, since the inner wall adds an enormous thermal capacity to the system, the transient behavior should be more affected by the addition of the wall balance. Therefore, in the next section, dynamic simulations with both models are performed.

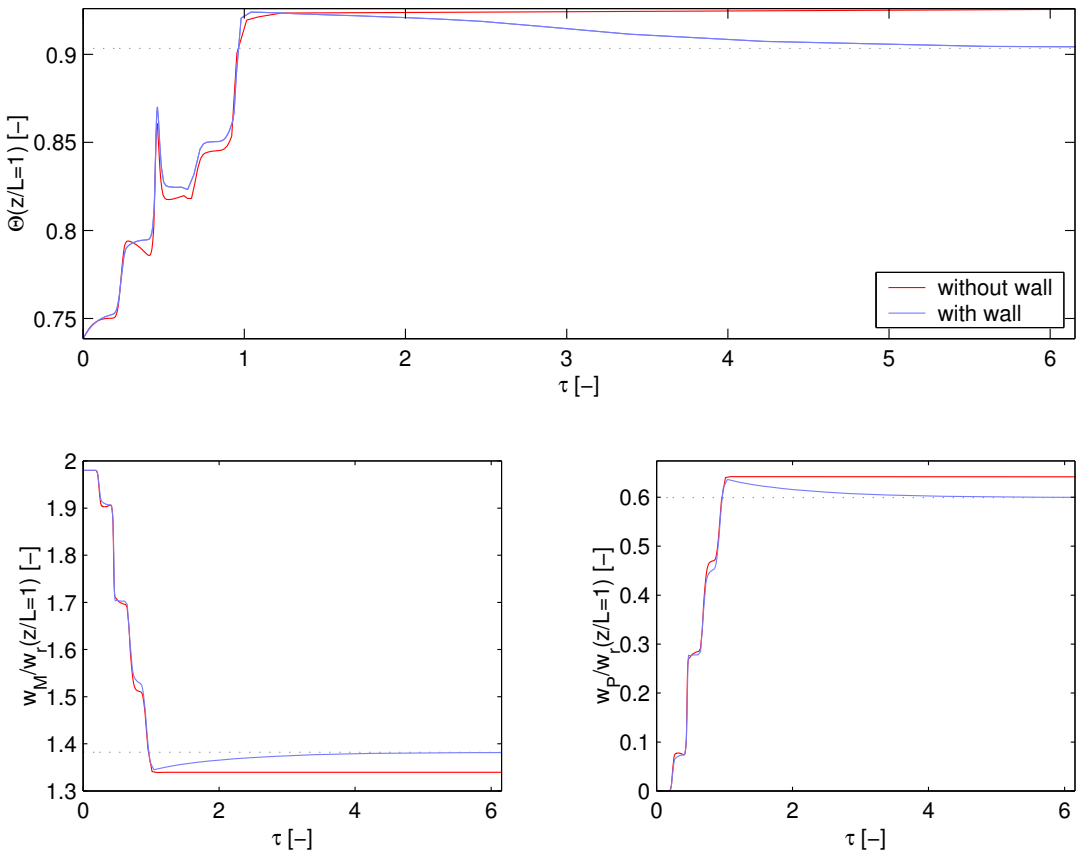

Figure 3.6: Comparison of dynamic simulation results neglecting the energy balance for the wall and including it – temperature and weight fractions of monomer and polymer

3.2 Dynamic Simulation Results – Rigorous Model

In this section, at first, the two dynamic rigorous models with and without energy balance equation are compared to each other in their transient behavior. In the beginning, only the tubular reactor will be considered, then in Sec. 3.2.2 the recycles are closed and the dynamic behavior of the uncontrolled LDPE production plant will be investigated.

3.2.1 System Without Recycle

Here, two cases are discussed, the startup of the tubular reactor when there are no material recycles, and the transient behavior when disturbances are applied to the inlet of the reactor. For both models, the adaptive Method of Lines approach is used for the discretization of the PDAE system.

3.2.1.1 Startup

At first, a comparison in the transient behavior of the startup of the uncontrolled tubular reactor with and without energy balance for the wall is shown. From the steady state behavior, it is obvious that there exists almost no difference, hence for simplicity, that equation might be dropped. Fig 3.6 depicts process variables such as dimensionless temperature or normalized weight fractions at the outlet of the tubular reactor. The red line represents the model without an additional energy balance for the wall, the blue line represents the model which includes that equation. Of course, the result is not very surprising, indeed the transient behavior is affected. In the beginning of the simulation, both models act very similar, in fact in Θ only slight differences become visible for the first few τ time units. But after $\tau = 1$, in the model where the heat capacity is neglected, the steady state is reached. However, the model with energy balance needs approx. 6τ until the steady state establishes. Hence, even though the influence of the reactor wall on the steady state is of minor importance (see Fig. 3.4), it is not admissible to neglect it for the transient behavior.

So, for the simulation of a startup of the tubular reactor, the model which accounts for the heat conduction in the wall is used. Fig. 3.7 shows the dynamic profiles for the startup already graphed in Fig. 3.6. Except for the coolant, for the startup simulation

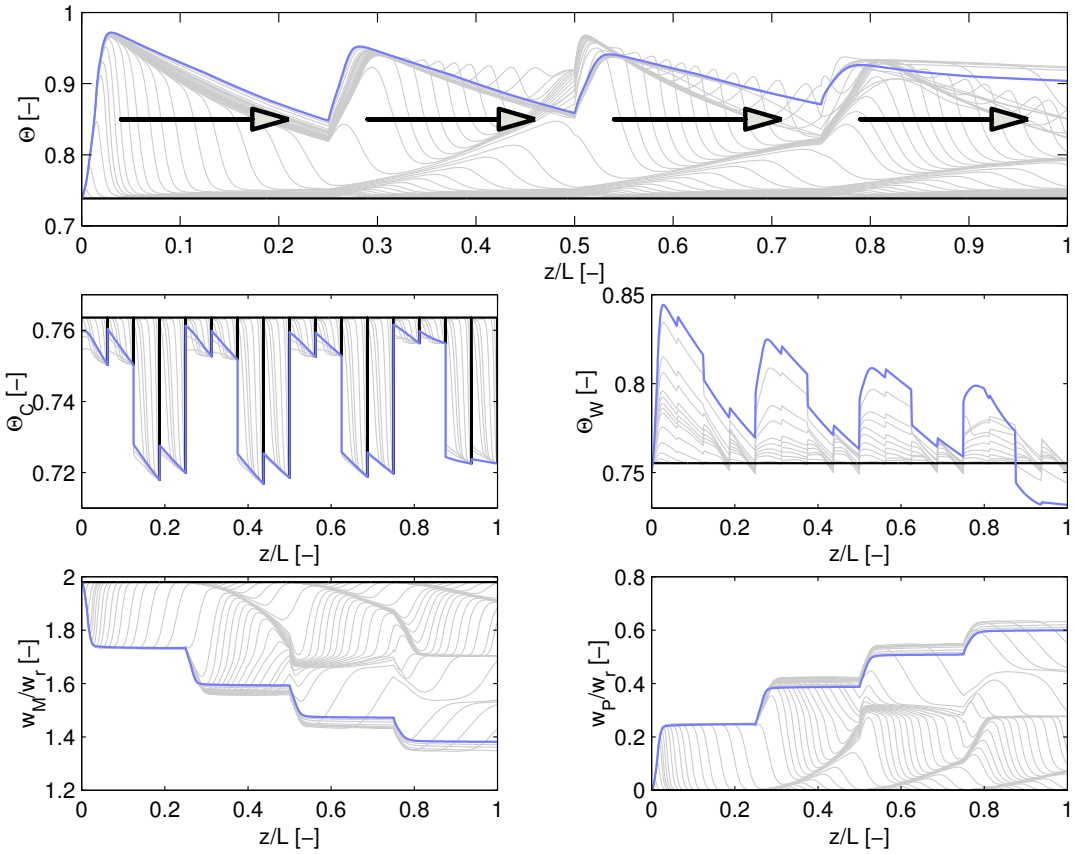

Figure 3.7: Profiles of process variables during startup operation, plotted over the reactor length

it is assumed, that the initial values of the distributed parameters are already at feed condition. Hence the initial profile, indicated by the black solid line, is constant. Moreover this implies, that in the reactor no initiator, no radicals and no polymer exists. Since the coolant is operated at different levels, for the coolant only the inlet is at steady state conditions, whereas the initial values of the distributed state variables are set to an arbitrary but reasonable temperature. Then for $\tau > 0$, initiator is added at all four injectors. Since initiator decomposing at a low temperature level is only added at the inlet of the tubular reactor, there the reaction starts. The reaction is highly exothermic and so the temperature rises and one front propagates through the reactor. At the same time, at the second injection valve initiator is added but very few is consumed, hence the reaction is in an extinguished state. As soon as the front

from the first injector passes by the second one, also there the reaction starts, because of the higher temperature level. The accumulation of unconsumed initiator and the arrival of the reaction front at the third injector causes temporarily a high temperature peak after the addition of initiator. But as initiator gets consumed, the sharp peak is smoothened which prevents that product decomposition takes place. Then the front leaves the reactor and after 6τ the steady state profile is established.

Since startup is time consuming, a case study is performed, that gives some insight to the potential of dynamic optimization. The following cases will be considered

- case 1: the case, which has been introduced in the previous paragraph, all initiators are added simultaneously at steady state flow rates,
- case 2: as case one, but additionally, for $\Delta\tau = \frac{1}{4}$, the third initiator resolving at low temperatures is added in all injectors,
- case 3: as case two, the feed flow rate of the third initiator is doubled,
- case 4: as case three, the amount of the third initiator is doubled again,
- case 5: initiators are added sequentially after $\Delta\tau = \frac{1}{4}$, $\frac{1}{2}$ and $\frac{3}{4}$ at steady state flow-rates,
- case 6: initiators are added sequentially after $\Delta\tau = 1$, $\frac{7}{4}$, $\frac{9}{4}$ and $\frac{5}{2}$ at steady state flow-rates.

Herein, the difference $\Delta\tau$ is always the absolution difference related to the start of the simulation, i.e. $\tau = 0$. Hence for case five, initiator is always added when the reaction front reaches the injector. In case six, first a steady state has to be reached. Since this holds for the tubular reactor without any material recycles when the reaction front leaves the reactor, one has to wait $\Delta\tau_1 = 1$ time units for the first wave, then additional $\Delta\tau_2 = \frac{3}{4}$ time units ($\Delta\tau = \Delta\tau_1 + \Delta\tau_2$) etc..

Fig. 3.8 shows the simulation results of this case study. The graphs show process variables at the outlet of the tubular reactor. In the top row, the dimensionless temperature $\Theta = \frac{T}{T_{ref}}$ is shown in both the left and the right picture. The right plot is a magnification of the first 2τ time units. The bottom row graphs the melt flow index as one property of the product. Also here, the right diagram is a magnification of the first

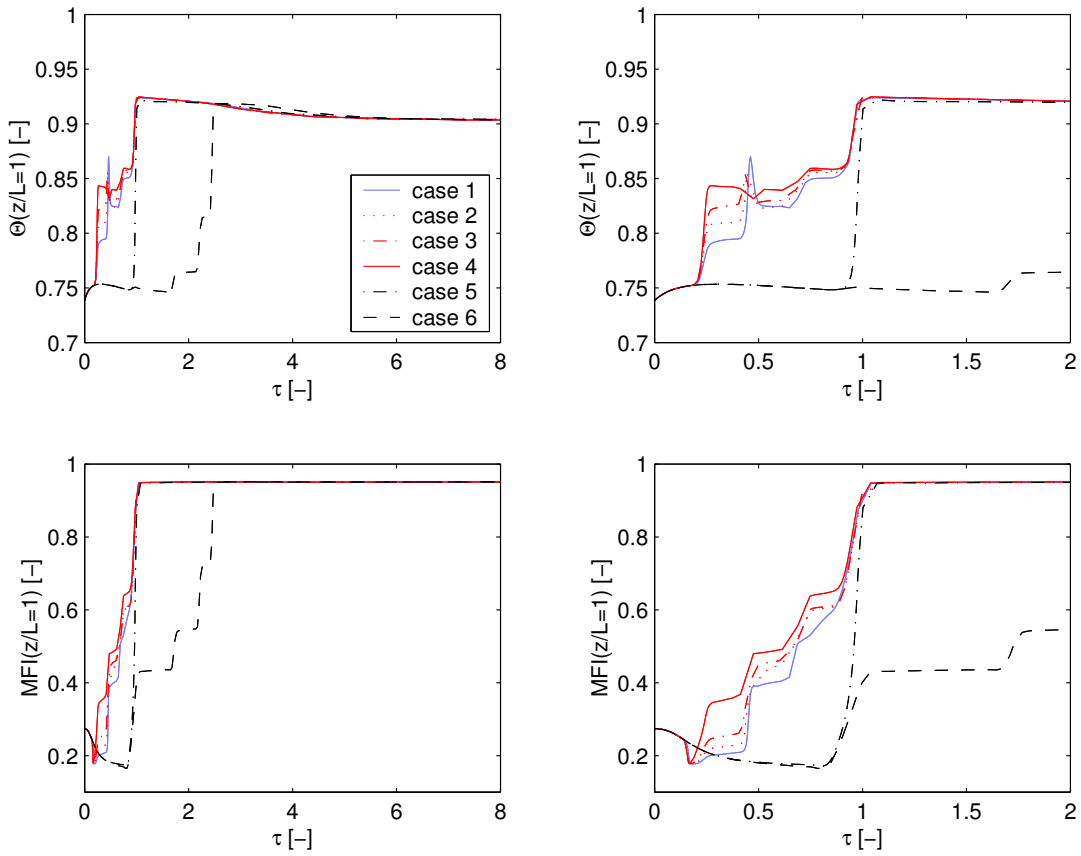

Figure 3.8: Comparison of time constants for different startup strategies of the tubular reactor

time units. The blue solid line represents case one which has already been used in the comparison of the transient behavior with and without wall. The red color indicates that for these cases the initiator decomposing at a low temperature level is used in all injectors and the black lines indicate that the initiators are added sequentially. What becomes obvious is that of course case six takes longest to reach the steady state. Another interesting observation can be made from Fig. 3.8. Although the reactor temperature has not reached a steady state, product in terms of melt flow index is already within the specification limits after only 1.8 τ. Moreover, the different strategies do not significantly improve the startup of the tubular reactor, except for the fact, that method six takes by far longest. But looking in more detail at the right column, one can see, that the case studies marked in red color (all injection valves add the initiator

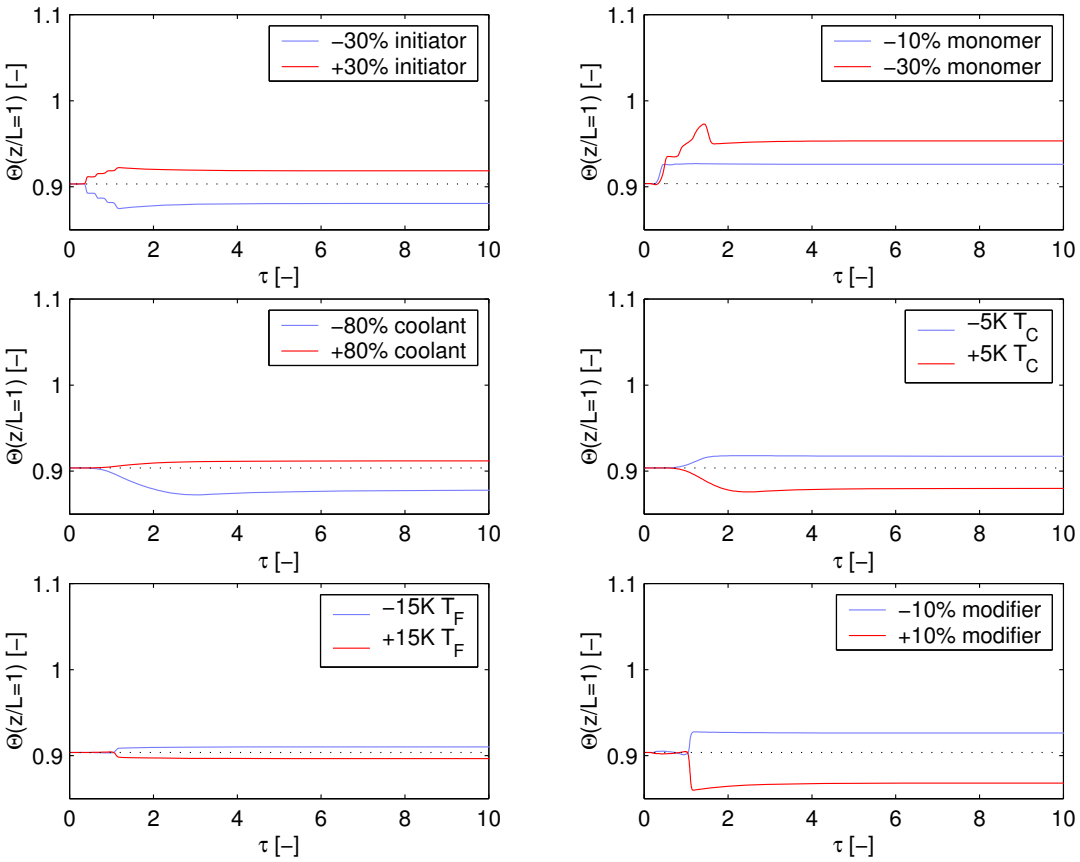

Figure 3.9: Influence of disturbances on the outlet temperature – without recycles

resolving at low temperature for $\tau = \frac{1}{4}$) are slightly ahead of the other strategies. And among each other, the case study which adds most of the third initiator is performing better than the others. Hence, even by simple case studies, there is some improvement visible, so there is potential for a dynamic optimization of the startup operation.

3.2.1.2 Disturbances

The influence of the disturbances on the transient behavior will be discussed utilizing the rigorous mathematical model of the tubular reactor with energy balance for the reactor wall. Characteristic disturbances to be considered were specified by the cooperation partner. In particular,

- step change in feed flow rate of monomer (-30%),

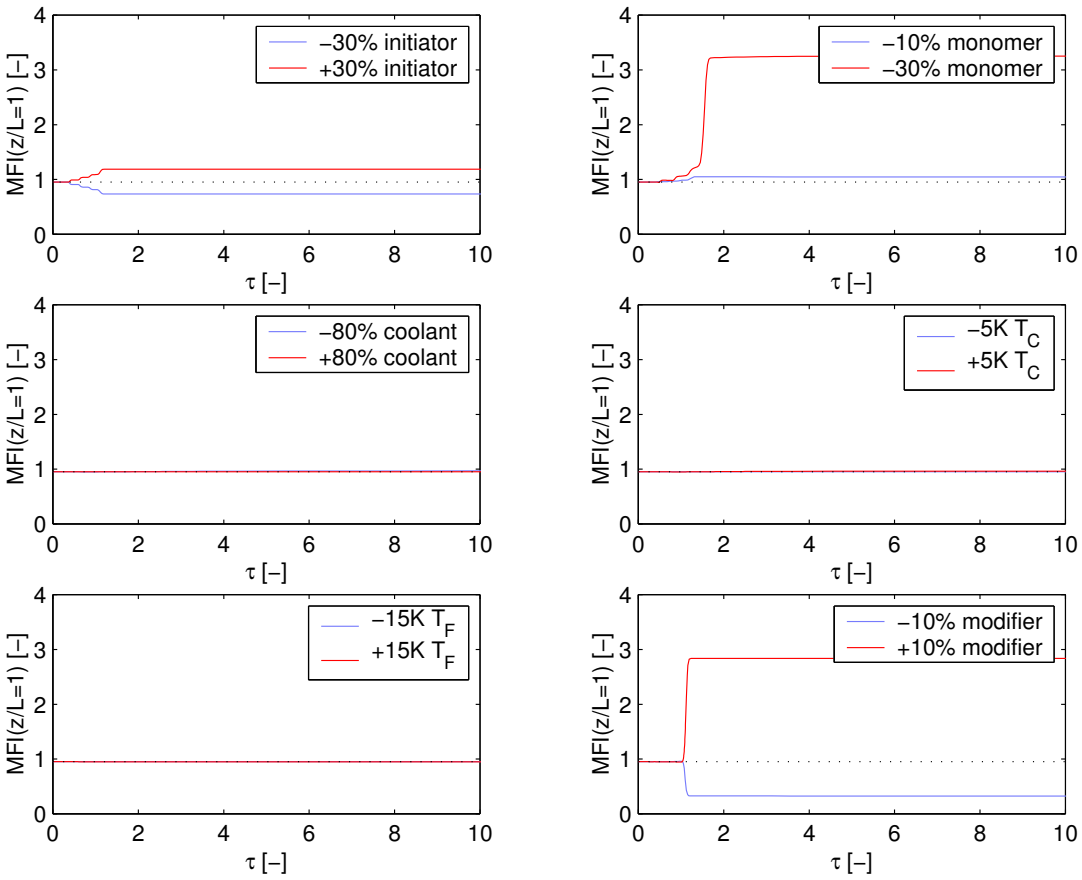

Figure 3.10: Influence of disturbances on the melt flow index – without recycles

- step change in feed flow rate of coolant ($\pm 80\%$),
- step change in feed flow temperature ($\pm 5K$),
- step change in feed flow rate of modifier ($\pm 50\%$),
- step change in feed flow rate of initiators ($\pm 30\%$).

Results of this simulations are depicted in Fig. 3.9 and 3.10. There the black dotted line refers to a simulation without any disturbances. So the initial value for the simulations indeed is a steady state. In all graphs, in general, the blue line denotes a negative, the red line a positive sign of the step change, except for the feed rate of the monomer (top diagram in the right column). This feed flow rate is only disturbed in the direction towards smaller feeds, hence the blue line indicates the smaller, the red

line the larger step change. From all diagrams in Fig. 3.9 it follows immediately, that the system is nonlinear, since step changes of the same size into different directions do not lead to a symmetric shape of the graphs (symmetric with respect to the steady state value). Moreover, looking at the second row in Fig. 3.9, a higher cooling capacity (either caused by increase in the coolant flow rate or by a decrease of the coolant temperature) results in higher outlet temperatures at the reactor end. This can be explained using the Nusselt number of the reactor flow. Increasing the cooling capacity causes the first temperature maximum to be shifted downstream. This means that at the injector in the second section the reactor temperature is already at a higher initial value. Thereby in section two, the reaction is more intense and more monomer gets converted. The same holds for the third section, so that the rector content becomes more viscous and the transition to a laminar flow regime moves upstream. Recall that laminar flow always implies smaller Nusselt numbers and the overall heat transfer coefficient becomes worse. So, a higher coolant capacity in section four has only little influence on the outlet temperature, resulting in a rise of that temperature.

Fig. 3.10 shows the influence of the step changes on the melt flow index, one characteristic property of the produced low-density polyethylene. What is most striking there, is that although the effect of e.g. step changes in initiator feed flow rate and coolant flow rate have a similar effect on the outlet temperature, the MFI is only slightly affected by that disturbance. But the modifier and the monomer feed flow rate show a significant impact on that physical property. However, this is an expected result, since in general modifiers are used to control the chain length distribution. The chain length distribution has large impact on the physical properties and the melt flow index is one way to measure the physical properties of the polymer. Hence, both feed flow rates (monomer and modifier) must have a large influence on the physical properties.

Generally speaking, the rigorous model for the uncontrolled system with no recycles proves to be robust, all given disturbances can be simulated, although the simulation times tend to be considerably large. Depending on the kind of disturbance, simulation runs with a duration of more than $8h$ can occur.

The dominating time constant in the detailed dynamic model without recycles is introduced by the inclusion of a “semi-distributed” energy balance equation for the reactor wall. Hence the energy balance equation for the reactor wall cannot be

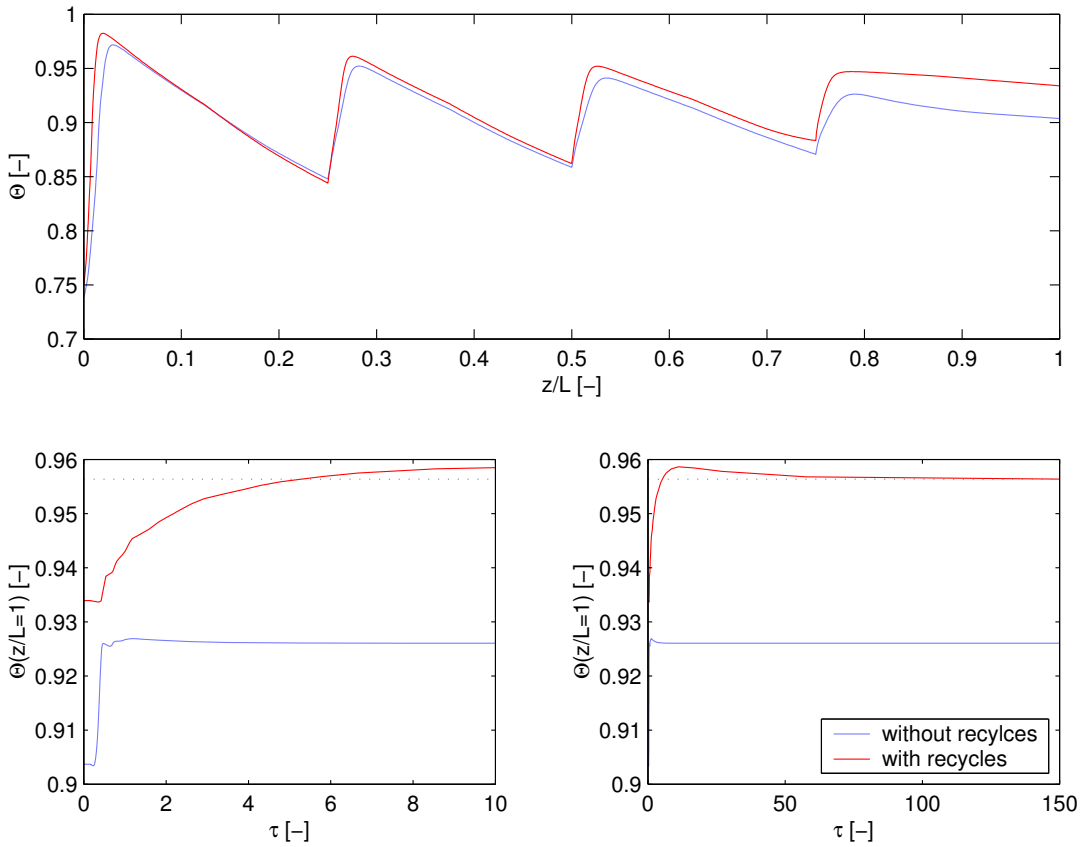

Figure 3.11: Influence of the recycles on the time constant of the tubular reactor

neglected.

3.2.2 System With Recycle

In the sequel, the recycle lines are closed, but still the reactor is operated uncontrolled, except for the assumptions that have been made in Chap. 2, e.g. compressor is always capable to track any given inlet pressure. Main issue of this section is the investigation on how the recycles influence both the time constant and the stability of the system. Therefore step tests are performed. First the steady state profile of the model with recycles and the profile of the model without recycles are compared. This comparison and the simulation results of the same step change in the feed rate is done in Fig. 3.11. In the top of that figure, the temperature profile are graphed. In the first two sections, these profiles match very well, although in the last section there are larger deviations.

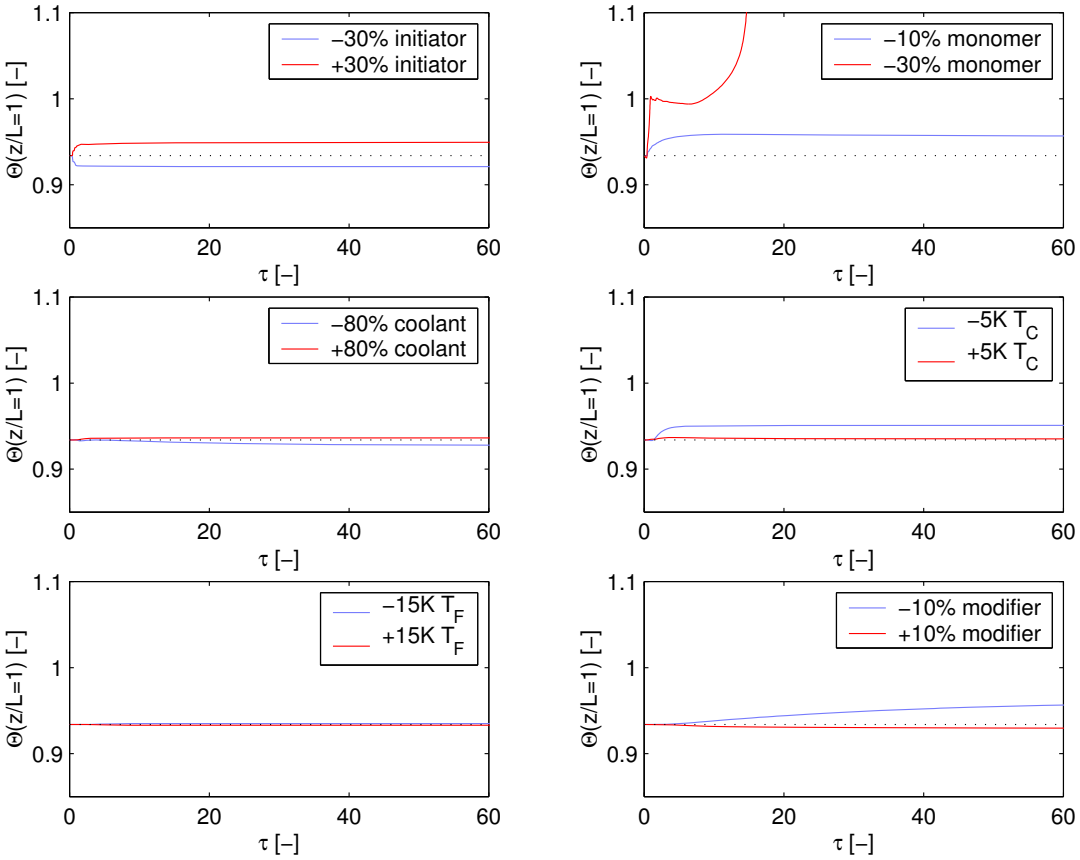

Figure 3.12: Influence of disturbances on the outlet temperature – with recycles

As in Sec. 3.1.1, the reason for the larger deviations in section four of the tubular reactor can be found in the Nusselt number. Slight changes in Reynolds number lead to large changes in the Nusselt number and so the overall heat transfer coefficient becomes worse. Then the coolant jackets are not able to remove the heat of reaction as efficiently as before. Nevertheless, feed into the tubular reactor is the same, hence it is assumed that the agreement of both models is well enough.

The influence of the recycles on the overall time constant is shown in the bottom row of Fig. 3.11. There the simulation result of a small decrease in the feed flow rate of monomer on both systems is depicted. The right graph shows a magnification of the first 10τ time units, the left one displays the whole simulation time. Since steady state profiles of the reactor temperature differ at the outlet of the tubular reactor, the initial value of the dimensionless temperature Θ is different. In fact, $\Theta(\tau = 0)$ in

the bottom row is equal to $\Theta(z/L = 1)$ in the top row. From the two diagrams it follows immediately, that the recycles increase the overall time constant of the low-density polyethylene production process by a factor of 10–15. For the considered disturbance, the system without recycles reaches a new steady state after approx. 5τ time units, whereas the system with recycles needs more than 50τ until the steady state is reached. Hence, not the large heat capacity of the reactor wall, but the volume of the recycle lines determines the largest time constant in the LDPE production plant.

3.2.2.1 Disturbances

Each of the disturbances that have been already introduced in Sec. 3.2.1.2 is now also imposed on the system with material recycles. In Fig. 3.12 and Fig. 3.13 the results are shown. In both figures, the scale of the ordinate is the same, but the scale of the abscissa is different. It has been shown in the previous section, that the material recycles considerably increase the dominating time constant in the system. So, in order to reach a steady state, the simulation time has to be increased. In fact, the simulation time is even larger than depicted in the graphs ($\tau = 150$), but for a better overview, in the plots it is zoomed into 60τ. For all disturbances, except the larger decrease in the monomer feed rate, a new steady state settles. Also the simulation with the step change in the modifier feed rate reaches a new steady state, but the time constant is $\approx 100\tau$ for that disturbance.

In the system with material recycle, the effect of a change in the coolant capacity is smaller compared to the system without recirculation. This behavior is caused by the recycle lines. From Sec. 3.2.1.2 it has been concluded, that the outlet temperature of the reactor is higher for an increase in the heat capacity of the coolant. This leads to less conversion, and the mean of the chain length distribution $P_n = \frac{\mu_1^P}{\mu_0^P}$ is lower. A lower mean results in higher densities, hence the overall heat transfer worsens and the outlet temperature will be higher. On the other hand, less conversion means higher recycle flow rates, which means that the reactor flow rate is also higher and hence the laminar region with a small overall heat transfer coefficient will be shorter. So, the coolant is able to withdraw more heat of reaction. Both effects compensate and so a step change in the coolant capacity shows less impact on the outlet temperature.

The most interesting effect of the recycles is the influence on the stability of the

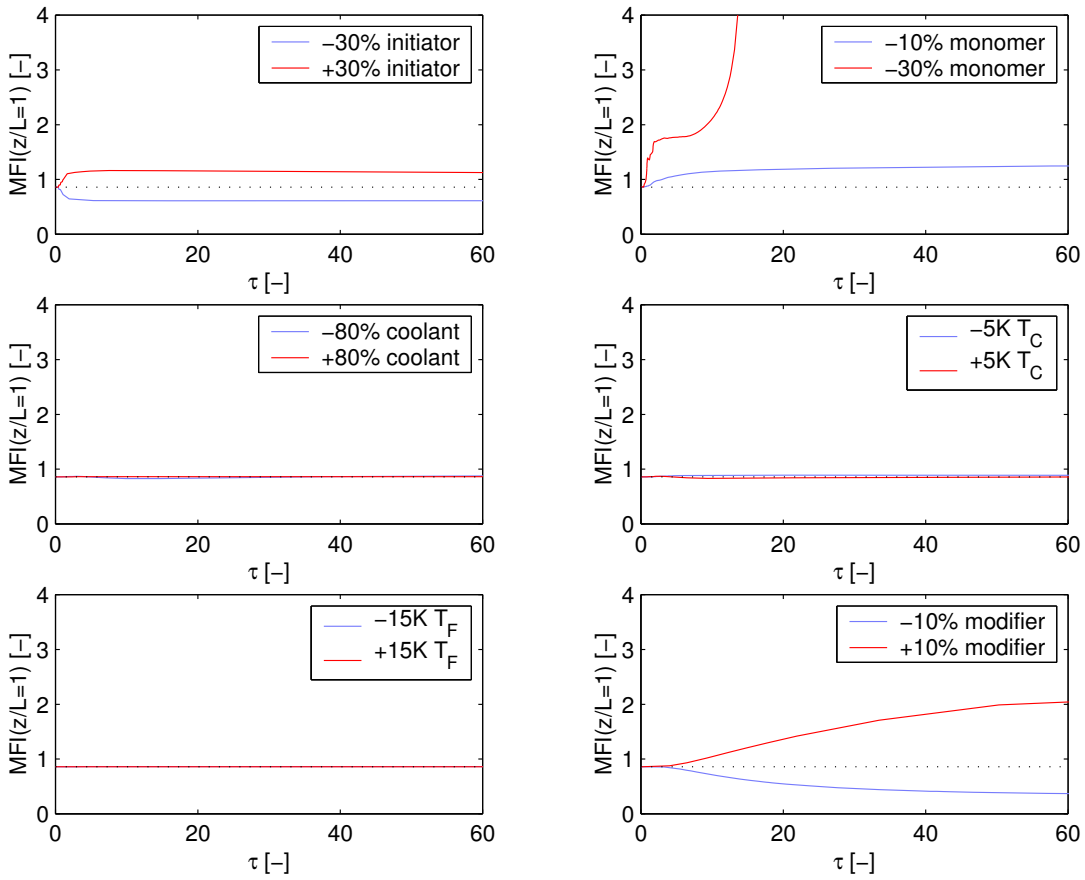

Figure 3.13: Influence of disturbances on the melt flow index – with recycles

overall system. This can be seen in the top right diagram in both Fig 3.12 and 3.13. The small step change in the monomer feed rate has no influence on the stability of the system, after approx. 10τ, a new steady state is obtained. But a large step in the monomer feed rate renders the rigorous mathematical model of the LDPE production process unstable. The direct effect of the step change results in a higher end temperature. The temperature rise is drastically from $\Theta = 0.93$ to $\Theta \approx 1$. Since the outlet temperature drops, initially it looks as if also for the large step a new steady state could be attained. However, the high temperature also causes more monomer to be converted, hence the recycle flow rate is smaller and so the feed to the reactor becomes less. Higher residence times also imply that the region of laminar Nusselt number increases. As a consequence, after $\tau \approx 10$, the temperature rises again, the heat of reaction cannot be removed by the coolant, the product decomposes. The ther-

mal runaway behavior however cannot be observed in the controlled plant, hence this phenomenon is a feature of this uncontrolled model implementation.

This observation though is the starting point for a thorough nonlinear analysis of the mathematical model of the LDPE production plant. For this purpose, the rigorous model turned out to be unmanageable. The size of the model, even though a low resolution discretization scheme has already been selected, is too large for the application of the nonlinear analysis methods available in DIVA. Hence the simple model of Sec. 2.4 has been derived.

3.3 Nonlinear Analysis – Simple Model

The nonlinear analysis in DIVA examines the behavior of the mathematical model using continuation methods. These methods calculate the steady state solution of a system (1.1) as a function of one or two model parameters. Such a procedure is called a parameter continuation. The continuation algorithm contains methods for the stability analysis and for the detection of singularities. For the stability analysis in DIVA there are two methods available, a k-step Arnoldi method (Sorensen, 1992) and a QR algorithm of the LAPACK collection (`DGEEV`). The latter routine is a replacement of the `EB07AD` routine from the Harwell Library, as the developers of the Harwell Library state that their routine is outdated. Hence, for the purpose of this work, both the latest stable version of the Arnoldi algorithm (as a replacement for the previous beta version) and the `DGEEV` routine have been implemented. One advantage of the Arnoldi method is, that only the dominating eigenvalues are calculated, which reduces computation times considerably for large systems. In fact, the Arnoldi method calculates approximations to a few eigenvalues with their corresponding eigenvectors. These approximations are called Ritz values or Ritz vectors respectively. However, these approximations sometimes give inaccurate results for the stability analysis of the steady states. So for this method it is recommended to validate the results of the stability analysis by dynamic simulations.

Nonlinear dynamics of reactor separator systems has received considerable interest during the last few years and various types and combinations of different reaction and separation processes were investigated. In particular, Pushpavanam and Kienle (2001) studied a first order exothermic reaction in a CSTR in combination with an

isothermal, isobaric flash which is used for the recycle of unreacted reactant. In addition, intermediate heat exchangers are used for energetic decoupling of the reactor and the separator unit. It was found that the behavior of such a system strongly depends on the flow control strategy. Most complicated patterns of behavior were found for a fixed feed flow to the reactor. In that case a total number of twenty-four different bifurcation diagrams were predicted using singularity theory and it was shown that the behavior of such a reactor separator system is completely different from the stand alone reactor investigated earlier in Uppal et al. (1974), for example.

In particular, it was found that at high Damköhler numbers,

$$Da = \frac{t_{process}}{t_{reaction}}, \tag{3.1}$$

two steady state solutions exist, which merge and disappear at a limit point if the Damköhler number is decreased. Hence, large operation regions were found with no steady state at all. In these regions the recycle flow rate will increase continuously. In addition, isolated branches of steady state solutions (isolas) and Hopf bifurcation points were found. The latter are the origin of oscillatory behavior. Clearly, multiplicity and instability of steady states is caused primarily by the exothermicity of the chemical reaction.

Recently, a similar system, a loop reactor for the polymerization of vinyl acetate was investigated by Melo et al. (2003). They found that the transition from operation without material recycles to an operation with a partial recirculation of polymer solution is characterized by the evolution of oscillatory behavior. At low recycle rates they observed complex dynamics, including chaos. Moreover they predicted as many as seven steady states for the reactor model. They identified the overall heat transfer coefficient as one of the key influence factors on the dynamic behavior.

Similar steady state solution curves with a single turning point were found for a plug flow reactor with a first order exothermic reaction by Kiss et al. (2003). As a practical application example, a LDPE reactor separator system was considered. The plant configuration is very similar to the one considered here. It includes a tubular reactor with four different initiator feeds. This is equivalent to a system with four different tubular reactors in series leading to sequential bifurcations with multiple hysteresis. The analysis was based on a steady state model only and no prediction

of dynamic behavior including stability was possible. Moreover, implications for practically relevant operating conditions were not discussed.

This gap has been closed by Häfele et al. (2005). There, the simple model, derived in Sec. 2.4 has been used for the nonlinear analysis of the model. In this work, these results will briefly be discussed.

3.3.1 Comparison – Rigorous Model and Simple Model

First the validity of the simple model should be checked using the steady state profile of the reactor temperature. Both profiles are shown in Fig. 3.14, the blue line indicates the rigorous model with energy balance equation for the wall, the red line represents the solution of the simple model. Note that the initial conditions for both models, i.e.

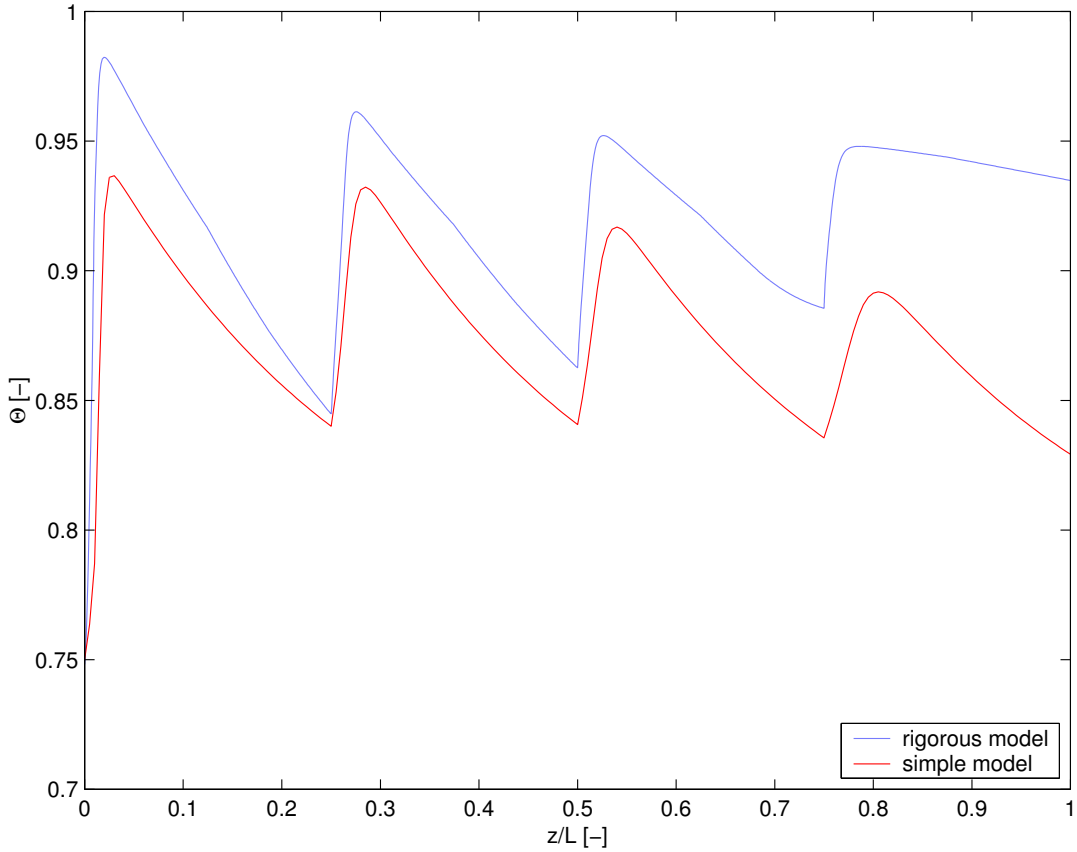

Figure 3.14: Comparison of the steady state reactor temperature profile of the simple and the rigorous model

feed temperature and feed flow rate of monomer are approximately the same. In contrast to the rigorous model, the simple model utilizes only two different initiators, one decomposing at a moderate and one decomposing at a intermediate temperature level. Moreover, the first injection valve only adds initiator resolving at low temperatures. All other injectors add only the intermediate initiator, whereas in the rigorous model, always a mixture of at least two different initiators is used. From this difference, most of the steady state deviations between the two models can be explained, such as size of peaks and gradient *after* an injector. But also the influence of a constant heat transfer coefficient is clearly visible in section four of the tubular reactor ($z/L \geq 0.75$). In the rigorous model, the heat transfer is reduced by a factor > 10, whereas the simple model assumes constant heat transfer. Hence, as soon as a laminar flow establishes, the difference in the reactor temperature of the two models becomes larger. Corre-

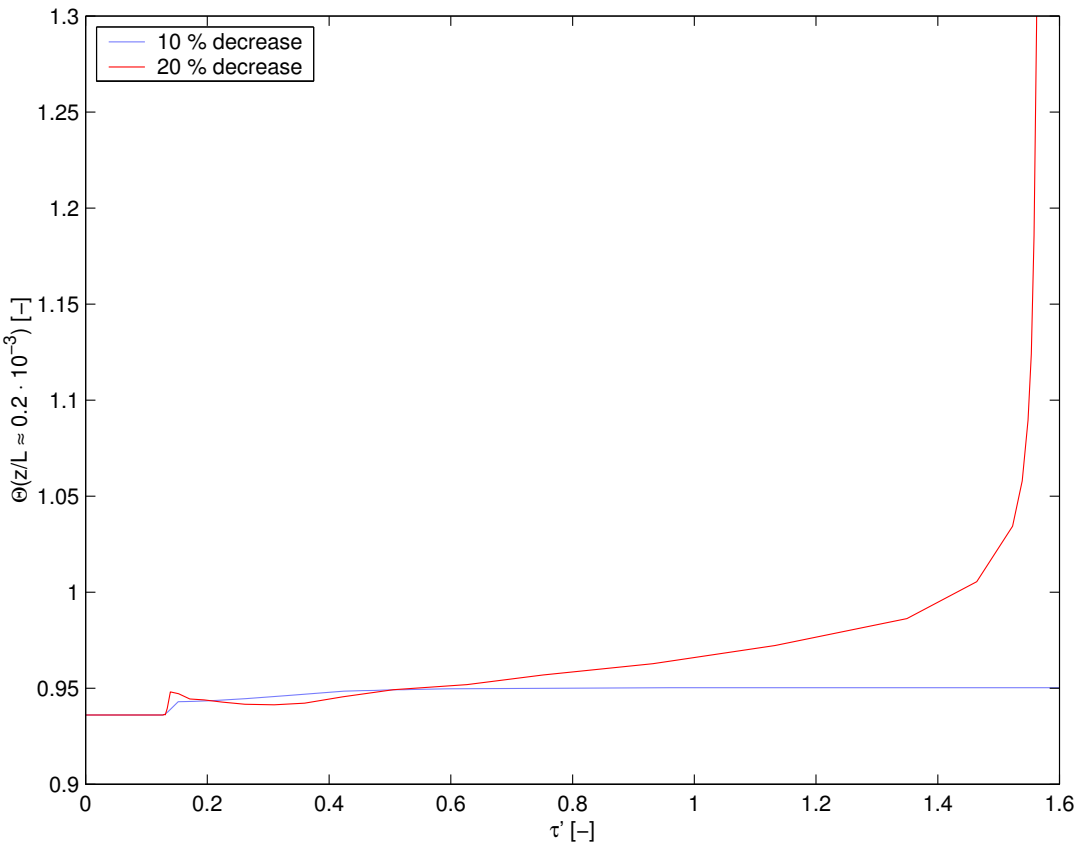

Figure 3.15: Thermal runaway of the simple model

lating the heat transfer coefficient to the polymer concentration would account for an decrease in the overall heat transfer in the simple model as well. Nevertheless, though quantitatively there are some deviations, the simple model is quantitatively a good approximation of the rigorous reference model.

This becomes even more obvious when looking at the responses on step changes in the monomer feed concentration, which is depicted in Fig. 3.15. The abscissa shows the dimensionless temperature $\Theta(\frac{z}{L} = 0.2 \cdot 10^{-3}) = \frac{T(0.2 \cdot 10^{-3})}{T_{ref}}$ over the dimensionless time $\tau' = \frac{t}{t_{res,F}}$. Herein $t_{res,F} = \frac{V_R}{\dot{V}_{M,F}}$ with the monomer feed rate $\dot{V}_{M,F}$. For this figure both a smaller (-10%) and a larger (-20%) decrease in the fresh feed flow rate has been applied to the uncontrolled simple model. Whereas for the small step change a new steady state is obtained, the temperature rises exponentially for the 20% decrease. This result matches the simulation results using the rigorous model with closed material recycles. In particular, the top right diagram of Fig. 3.12 also shows the thermal runaway of the tubular reactor as a result of a large step change in the monomer feed flow rate. It should be noted, that even though both models predict the thermal runaway phenomenon, the location is different. The detailed model shows the runaway phenomenon at the end of the tubular reactor ($z/L = 1$), the simple model just after the first injector ($z/L \approx 0.2 \cdot 10^{-3}$). Moreover, in practice, a proper control strategy prevents the occurrence of such phenomena in the plant. However, the phenomenon might be explained by means of nonlinear analysis.

3.3.2 Bifurcation and Stability Analysis

Here, the bifurcation and stability analysis is applied to the simplified model of the LDPE tubular reactor production process. The variable that is selected for the parameter continuation is the monomer feed flow rate, since this parameter seems to have most effect on the stability of the overall system. The result of a parameter continuation is shown in Fig. 3.16. There, the blue solid line represents the stable solutions, the dashed red line indicates unstable solution branches. The normal operating point is marked by the black circle filled with a grey pattern, where $\tau' = 1$. The left diagram shows the dimensionless temperature, the right diagram the result of variations in τ' on the conversion in the plant. Note that for residence times less than 0.2, except of the trivial solution no other steady state solution exists. Trivial means that no reaction

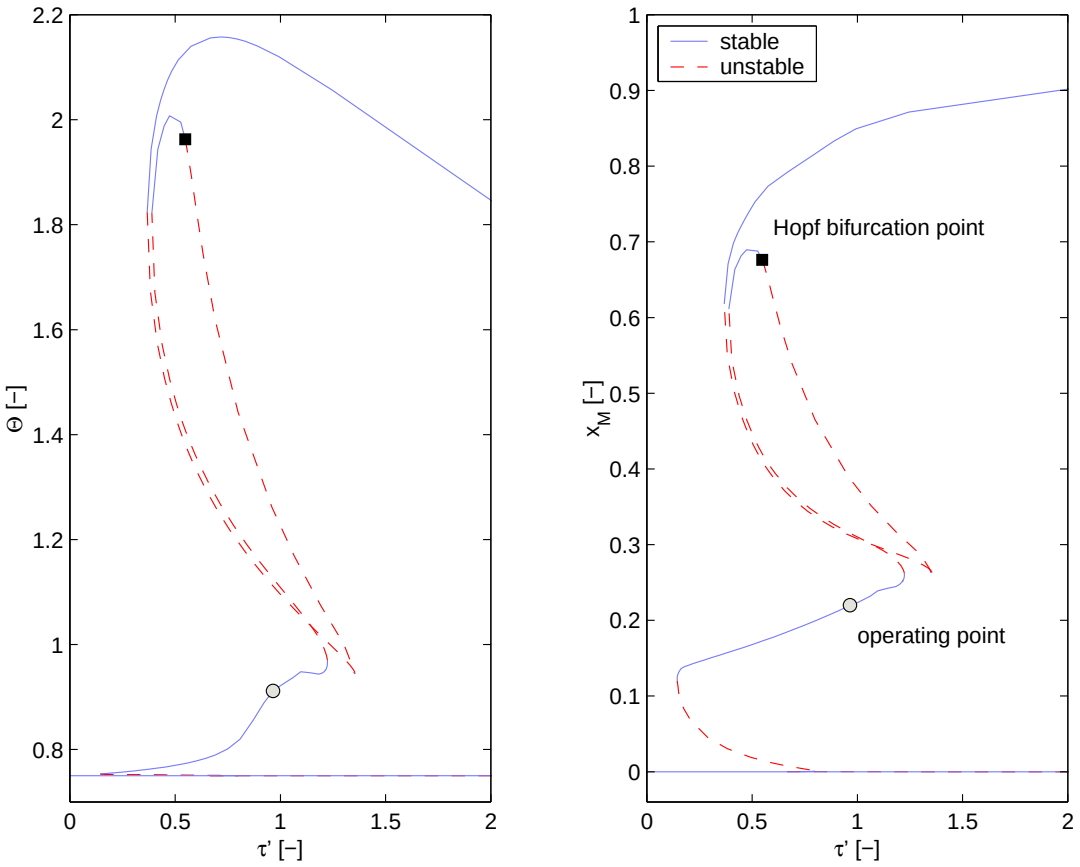

Figure 3.16: Stability and bifurcation diagram

takes place, the reactor is extinguished, hence $x_M = 0.0$, and $\Theta = 0.75$. This is a good agreement with the results of Kiss et al. (2003). Stable solution branches beyond a conversion level of 0.26 are not feasible, since the temperature level in the reactor would be too high.

In particular, the highest conversion that could be obtained in an economical reasonable region of operation is 0.26, whereas in commercial plants this limit is higher than 0.30. However, at this operating point, a small decrease in the feed flow rate, i.e. an increase in the residence time, forces the reactor to the upper stable branch. This solution branch though is far above its upper limit for safe operation. In fact, it is higher than the decomposition temperature of polyethylene. However, for the transition of a stable branch to an unstable one in the high temperature regime, at $\tau' \approx 0.5$, a Hopf bifurcation point occurs, which leads to an oscillatory behavior. This has been

shown in detail in Häfele et al. (2005).

The large difference of at least 4% less conversion in the simple model compared to a commercial plant can be explained by

- the initiator mixtures, which release more radicals, hence more monomer can be converted and
- the temperature level in the last section of the reactor, where the rate of termination is lower than in the rigorous model.

The first item can be addressed by adding a initiator mixture to the reactor, the second point is a matter of a heat transfer coefficient that correlates to conversion. Hence, the influence of the heat transfer coefficient should be studied using a two parameter continuation with residence time as first and heat transfer coefficient as second parameter. Additionally, in contrast to the constant value, a variable heat transfer coefficient could be used for receiving a better agreement between the simple and the rigorous models.

Chapter 4

Outlook on Optimization

Engineering is the professional art of applying science to the optimum conversion of natural resources to the benefit of man.
– Ralph J. Smith

In this section, the first step towards a dynamic optimization is introduced, in particular, a sensitivity analysis is performed. In general, optimization problems can be classified into dynamic and steady state applications. In steady state, the operating point is subject of the optimization, i.e. reduction of energy or maximization of yield at the nominal operating point. Dynamic optimization problems address the transient behavior of the plant, i.e. for grade or throughput changes. In the following, only dynamic optimization problems are considered, which can be further divided into online and offline optimizations. For online optimization applications, such as model predictive control, rather simple, most often linear mathematical representations for the process are used. This is a concession to the requirement of fast computation times. In contrast to that, for offline optimizations more sophisticated models are used, as this application has no limitations on computation times. The optimization calculates in advance suitable strategies of the input parameters for given pre-defined scenarios, e.g. grade changes from one to the other product or load changes in the plant. The result of the offline optimization are sequences for the input parameters, which can be stored as a "recipe" in process control systems. These recipes are then used by plant operators to carry out transitions in a reproducible and repeatable manner.

For the sequel, it is assumed that a change in the feed flow rate occurs, e.g. re-

quired by market demands. Despite of that change, the plant still should produce the same grade.

Therefore, a brief review on dynamic optimization will be given in Sec. 4.1. Because the selection of a suitable objective is non-trivial, three different objective functions are defined. In Sec. 4.2, the sensitivity analysis as an important step in identifying key input parameters is introduced. Results of the sensitivity analysis with respect to the different objective functions are then presented in Sec. 4.3.

4.1 Problem Statement

The general formulation of a dynamic optimization problem is

$$\min \Phi(\mathbf{x}, \mathbf{p}, \mathbf{u}, t), \tag{4.1}$$

with constraints on parameter and input variables

$$\mathbf{p}_{min} \leq \mathbf{p} \leq \mathbf{p}_{max}, \tag{4.2}$$

$$\mathbf{u}_{min} \leq \mathbf{u}(\mathbf{t}) \leq \mathbf{u}_{max}. \tag{4.3}$$

Therein, for a given t_{end}, the objective $\Phi \in I\!R$ is defined by

$$\Phi = \int_{t_0}^{t_{end}} g(\mathbf{x}, \mathbf{p}, \mathbf{u}, t)dt. \tag{4.4}$$

The vector of all state variables of the system is denoted by $\mathbf{x} \in I\!R^{N_x}$. The parameter vector is represented by $\mathbf{p} \in I\!R^{N_p}$ and the input variables are $\mathbf{u} \in I\!R^{N_u}$.

In DIVA, this problem formulation is solved using SQP methods from the NAG library (NAG, 1993).

As already mentioned in the introduction of this chapter, one formulation of a dynamic optimization problem is that product properties have to remain constant, despite of load changes in the tubular reactor imposed by either up- or downstream processes. If one assumes that the product properties are measured in terms of

- the number average molecular weight (μ_1^P) and

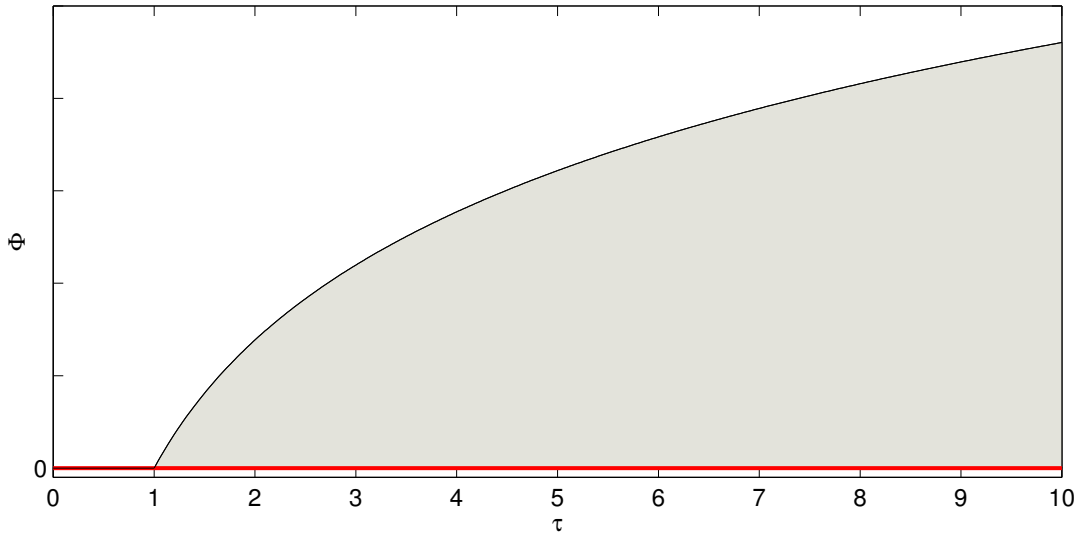

Figure 4.1: Graphical representation of the objective function for load changes

- the width or spread of the distribution (PD),

then the dynamic optimization problem is to find an appropriate set and sequence of input variable values, that compensates for the disturbances in the feed flow rate keeping the product at the desired mean and the desired width of the chain length distribution. Thus, the objective (4.4) for this optimization problem is

$$\begin{aligned}\Phi_1(z/L=1) &= \int_{t_0}^{t_{end}} \sum_{n=1}^{N} \gamma_i (x_i(1) - \tilde{x}_i(1))^2 dt \\ &= \int_{t_0}^{t_{end}} \left[\gamma_\mu (\mu_1^P(1) - \tilde{\mu}_1^P(1))^2 + \gamma_{PD}(PD(1) - \tilde{PD}(1))^2\right] dt, \quad (4.5)\end{aligned}$$

where γ_i are weight factors that have to be chosen such, that ideally neither of the summands outnumbers the other significantly. Moreover $\tilde{x}_i$, in particular $\tilde{\mu}_1^P$ and $\tilde{PD}$ denote the *initial* values of their corresponding state variables, since those values define the product at the nominal feed rate. Using definition (4.5) it follows, $\Phi_1 > 0$ and Φ_1 is monotonically increasing.

A qualitative graph of the objective (4.5) is depicted in Fig. 4.1. The red line marks the ideal solution, meaning no deviations in the two quantities μ_1^P and PD during the load change. However, the real graph of the objective function without optimization

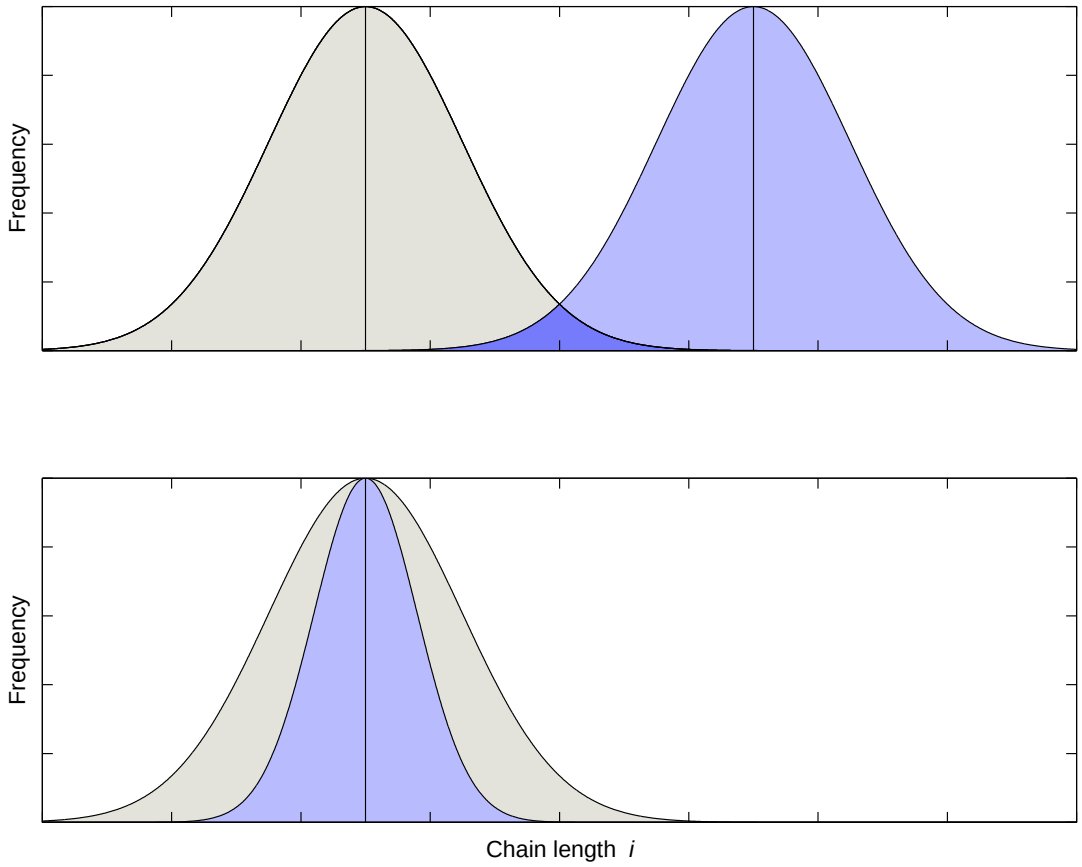

Figure 4.2: Measures of a distribution

might be the one marked by the black line. Hence the optimization problem is to minimize the grey area.

The variables μ_1^P and PD are chosen, because both, mean and width characterize the distribution. This characterization is not unique, if only one of the two is solely taken into account, see e.g. Fig. 4.2. There different normal distributions are depicted representing chain length distributions of different grades. The first grade, indicated by the gray area in the top row has the same spread as the second grade, indicated by the light blue area in the top row. However, their average, marked by the vertical line is significantly different. In the diagram in the second row, both chain length distributions have the same mean, but the spread is different. Hence in both cases, even though one characteristic of the distribution is identical, the grades differ in their physical properties such as density and melt flow index.

This shows, that it is important to select a *suitable* objective for the dynamic optimization. In order to study the validity of the sensitivity analysis for different objective functions, two additional objective functions

$$\Phi_2(z/L=1) = \int \left(\gamma_M(w_M(1)-\tilde{w}_M(1))^2 + \gamma_P(w_P(1)-\tilde{w}_P(1))^2\right)dt \qquad \text{and} \tag{4.6}$$

$$\Phi_3(z/L=1) = \int (MFI(1)-\tilde{MFI}(1))^2 dt \tag{4.7}$$

are defined. The second objective Φ_2 does not include any relevance for the chain length distribution, whereas the third objective maps the distribution to a measurable physical property, the melt flow index.

Not only a suitable objective function but also the set of input parameters are important for a successful dynamic optimization. Using all model input variables as optimization parameters in general increases the optimization problem without an additional benefit. Thus it is important to identify the significant input parameters, which is done using the sensitivity analysis. The sensitivity analysis determines the influence of parameter or input variables with respect to a state variable of the mathematical model. For an optimization, this state variable is the objective function. The set of the most important parameters is then used as optimization parameters. Note that in this work, the optimization step is not carried out, since the rigorous dynamic model is too large for DIVA to handle.

4.2 Sensitivity Analysis

The sensitivity analysis is an important step in a dynamic optimization. In order to have a tractable optimization problem, only the relevant input variables should be selected as optimization parameters, because the sensitivity equation enlarges the systems' Jacobian considerably. Hence, fewer optimization parameters reduce the size of the optimization problem.

In general, sensitivities are defined by

$$\mathbf{W} = \frac{\partial \mathbf{x}}{\partial \mathbf{p}} \tag{4.8}$$

with the vector of all state variables $\mathbf{x}$ and the vector of all input parameters $\mathbf{p}$. Hence the sensitivity matrix $\mathbf{W}$ is element in $\mathbb{R}^{N_p \times N_x}$. The equation based simulator DIVA solves systems of the following type

$$\mathbf{B}(\mathbf{x}, \mathbf{p}, \mathbf{u}, t)\dot{\mathbf{x}} = \mathbf{f}(\mathbf{x}, \mathbf{p}, \mathbf{u}, t) \tag{4.9}$$

with the initial condition

$$\mathbf{x}(t = t_0) = \mathbf{x_0}. \tag{4.10}$$

Here, $\mathbf{B} \in \mathbb{R}^{N_x \times N_x}$ and $\mathbf{u} \in \mathbb{R}^{N_u}$. Note that $\mathbf{B}$ might be singular. $\mathbf{u}$ are external input variables, e.g. set points for controllers or feed conditions. The total derivative of Eq. (4.9) with respect to the parameters $\mathbf{p}$ is

$$\mathbf{B}\dot{\mathbf{W}} = -\mathbf{J_x}\mathbf{W} - \mathbf{J_p} \tag{4.11}$$

with the initial conditions

$$\mathbf{W}(t = t_0) = \mathbf{W_0}, \tag{4.12}$$

the Jacobian $\mathbf{J_x} \in \mathbb{R}^{N_x \times N_x}$ with respect to $\mathbf{x}$

$$\mathbf{J_x} = \frac{\partial(\mathbf{B}\dot{\mathbf{x}} - \mathbf{f})}{\partial \mathbf{x}}, \tag{4.13}$$

and the Jacobian $\mathbf{J_p} \in \mathbb{R}^{N_x \times N_p}$ with respect to $\mathbf{p}$

$$\mathbf{J_p} = \frac{\partial(\mathbf{B}\dot{\mathbf{x}} - \mathbf{f})}{\partial \mathbf{p}}. \tag{4.14}$$

In DIVA, only one numerical integration algorithm is able to generate and solve the augmented system consisting of (4.9) and (4.11) simultaneously, namely the sparse implementation by M. Mangold of the (dense) DDASAC (Caracotsios and Stewart, 1985). Unfortunately, this algorithm does not solve the LDPE problem, and the current implementation of the linear implicit extrapolation algorithm LIMEX (Ehrig

et al., 1999) is not capable of calculating sensitivities. More recent versions of the LIMEX (Schlegel et al., 2002) overcome that problem, but are not available right now within DIVA.

However, as the sensitivity equations Eq. (4.11) are decoupled from the overall system (Eq. (4.9)), the following method is proposed to calculate the sensitivities *after* the simulation runs. The parameters, that can be changed independently from each other in both, the detailed model and the real production site are

- all cooling capacities, i.e. $\dot{m}_{C,k}$ or $T_{C,in,k}$ with $k = 1, \ldots, 16$,
- the amount of initiators added at each injector, i.e. $\sum_{n=1}^{N_{init}} \dot{m}_{I,n,k}$ with $N_{init} = 3$ and $k = 1, \ldots, 4$,
- the outlet pressure of the hyper compressor, p_F,
- the total amount of feed to the plant, i.e. $\dot{m}_F$ and
- the feed temperature, i.e. T_F.

Note that the composition of the initiator mixture cannot be changed independently, only the total amount of those flow rates. Hence 39 input parameters could be selected as optimization parameters, so for the proposed procedure 40 simulation runs are required. However, this number can be reduced, since the effect of changes in $\dot{m}_{C,k}$ and $T_{C,in,k}$ is equivalent. Still 23 individual simulations have to be made, where one parameter is changed at a time.

Using the simulation results, it is possible to calculate the sensitivities of the changed parameters at the outlet of the tubular reactor ($z/L = 1$) with respect to the objective function Φ_i according to

$$\frac{\partial \Phi_i(1)}{\partial \mathbf{p}} = \lim_{\Delta \mathbf{p} \to 0} \frac{\Phi_i(1, \mathbf{p} + \Delta \mathbf{p}) - \Phi_i(1, \mathbf{p})}{\Delta \mathbf{p}}, \qquad \forall\, i = 1, 2, 3, \tag{4.15}$$

which is approximated for each individual parameters by

$$\frac{\partial \Phi_i(1)}{\partial p_j} \approx \frac{\Phi_i(1, p_j + \Delta p_j) - \Phi_i(1, p_j)}{\Delta p_j}, \qquad \forall\, j = 1, \ldots, N_p. \tag{4.16}$$

For the simulations with the perturbed system, each of the 22 parameters is reduced by 1%, i.e. $\Delta p_j = -0.01 p_j$.

In the model of the LDPE production plant, the objective function has not yet been taken into account. Hence, the objective itself has to be evaluated *after* the simulation run. Therefore, the integral in (4.4) is approximated using the left Riemann sum

$$\Phi(1) \approx \sum_{n=1}^{N_T} \Phi\Big(\mathbf{x}_{n-1}, \mathbf{p}_{n-1}, \mathbf{u}_{n-1}, t_{n-1}\Big)(t_n - t_{n-1}). \tag{4.17}$$

Since (4.5) is monotonically increasing, the left Riemann sum (4.17) is always an underestimate of the true value of the integral (4.5), hence the real sensitivities of the process are higher. However, for this study the qualitative influence of the parameters on the sensitivities not the precise quantitative influence is investigated, so that this systematic error has no significant effect on the outcome.

It is important to know, that values for the sensitivities received by Eq. (4.15) are not dimensionless. So for comparing the sensitivities amongst each other, one has to be very careful. One approach of comparing sensitivities more easily is to introduce scaling. However, since scaling parameters are not unique, the ratio of different sensitivities strongly depends on the scaling factor. In this work, only absolute values of the sensitivities are considered.

4.3 Results

In this section, the results of the sensitivity analysis using the procedure suggested in the previous section are presented. As already mentioned, the perturbation in the parameter vector is -1%, and the objective function is evaluated using (4.17).

The first two diagrams that are presented in this section, have a similar structure, in the first, second and third column they show the sensitivities with respect to the first, second and third objective function (Eqns. (4.5)–(4.7)). In Fig. 4.3 the influence of the feed flow rate of initiator at the four injection valves is shown. Each row represents one injector location, the first row at $z/L = 0$ down to the last row at $z/L = 1$. The scale of the ordinate is in all diagrams the same, the scale of the abscissa is identical in each column, i.e. for each objective function. Looking at the sensitivities with respect to the first objective (combination of number average and width) it is clear that the last injector has the highest sensitivity on the product. The sensitivities with respect

to the second objective function (adding weight fraction of polymer and monomer) additionally emphasizes this observation, here the sensitivity of the last injection valve is higher by a factor of at least 10 than the one of all other valves. This however is a strong contrast to the sensitivities with respect to the (statistical) properties of the distribution. There except for the first initiator injection all other sensitivities are in a similar range, which is additionally confirmed if one looks at the sensitivities with respect to the melt flow index. Also there all sensitivities are within a tight range.

Adding less initiator to the reactor causes less radicals to form. However, the conversion of monomer to polymer is approximately the same, which can be seen in the top three graphs of the middle column. Hence, the formation of less initial radicals generates less but longer polymer chains, which result in LDPE with different physical

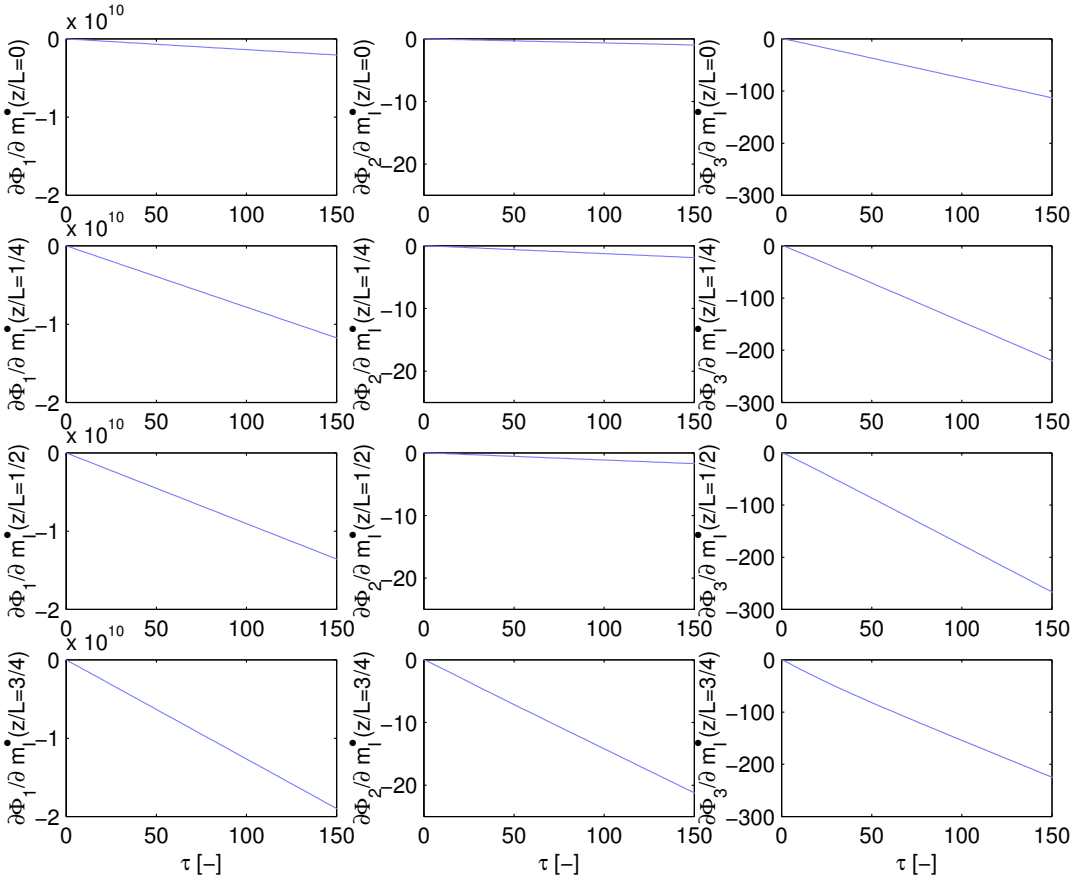

Figure 4.3: Sensitivities of initiator feed flow rates with respect to Φ_1, Φ_2 and Φ_3

properties. Hence, the effect of adding initiator is only slightly visible in the weight fractions of monomer and polymer, but has impact on the moments of the distribution or derived physical properties. However, in the bottom sensitivity plot with respect to the weight fractions of monomer and polymer, a large influence of a perturbed feed flow rate of initiator is visible. Adding more or less initiator at the last injection valve obviously influences the weight fraction of polymer and monomer. Since this is the reactor section with a laminar flow, which means that the heat transfer is very small, the heat of reaction cannot be removed as well as in the turbulent sections. So little variations in the radical generation, causes a significant variation in the reactor temperature. However, changes in the reactor temperature affect the thermal initiation of monomer (2.4), which results in a different conversion rate of monomer to polymer and is shown in that sensitivity diagram.

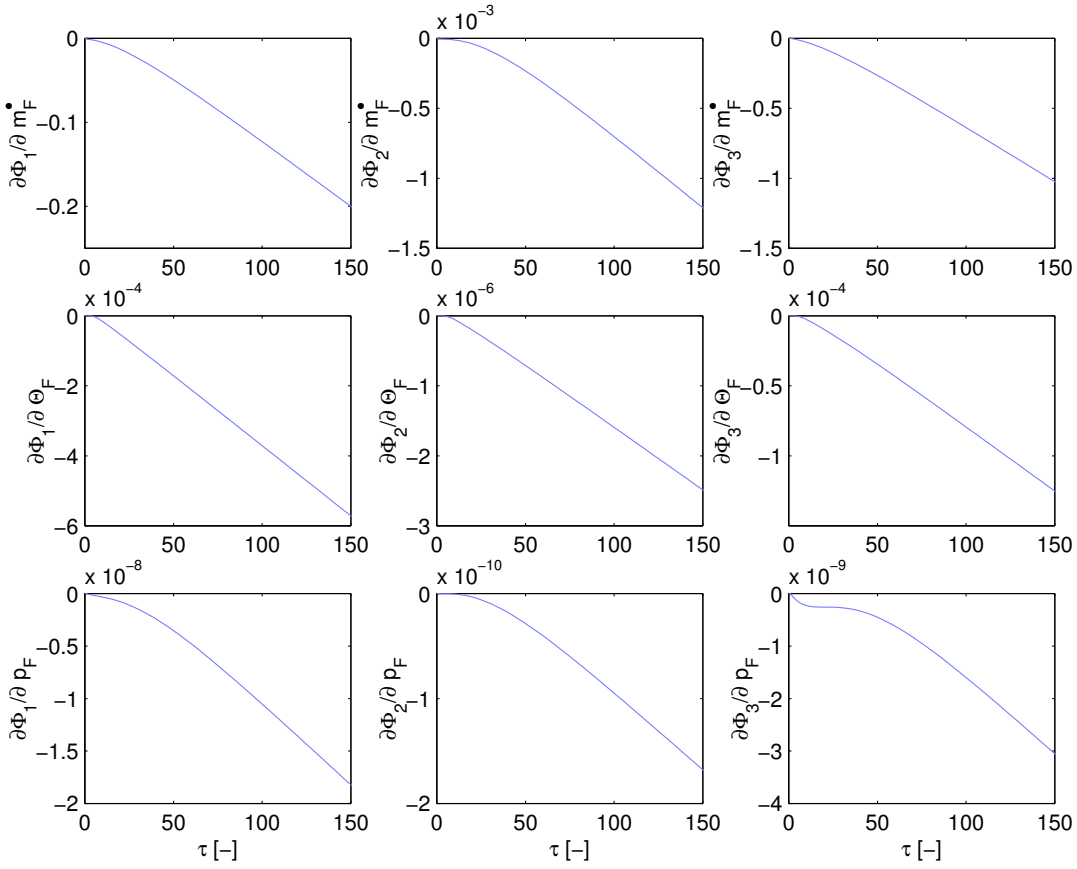

Figure 4.4: Sensitivities of feed parameters with respect to Φ_1, Φ_2 and Φ_3

In Fig. 4.4, the sensitivities of three feed parameters on the three objective functions are shown. All three objectives qualitatively show a similar influence on the three parameters. However, the third objective accounting for the melt flow index shows that from $\tau \approx 10-40$, the sensitivity with respect to the inlet pressure remains constant, whereas the first and second objective do not show this behavior. This phenomenon cannot be explained so far.

Which of the three parameters is now the most important one? The influence of the three parameters on the objective functions at $\tau = 150$ is listed in Tab. 4.1. Hence, changing the feed flow rate $\dot{m}_F$ by one unit, the first objective changes its value by -0.20608. The influence of p_F seems to be very small, but the pressure is measured in Pa, so changing the pressure by $1\,Pa$ changes the objective by $-1.88296 \cdot 10^{-8}$. However, $10^5\,Pa = 1\ bar$, so perturbing the pressure by 1 bar changes the value of the objective function twice as effectively as changing the feed temperature by 1 K.

Since the influence of the parameters on the objectives Φ_1 and Φ_3 is comparable and because the result of Fig. 4.3 has been misleading for Φ_2, for the remaining parameters only the third objective is taken into account. The sensitivities of the those 16 parameters, namely the coolant temperatures with respect to the melt flow index are depicted in Fig. 4.5. In this figure, the diagrams can be grouped into categories. Within each category, all graphs have the same scale, however, the scale of the y-axis is different for the categories. The top two rows have a *larger* scale ($-4.0 \cdot 10^{-5}$), whereas the scale of the bottom two rows is 50 times finer ($-8.0 \cdot 10^{-7}$). The columns refer to the position of the coolant jacket within one section, the rows represent the four sections of the tubular reactor. Hence the right-most two columns represent the "cold" coolant. It is interesting to see that in sections with a high Nusselt number the cold coolant has a significantly higher impact on the melt flow index of the poly-

	Φ_1	Φ_2	Φ_3
$\dot{m}_F$	-0.20608	$-1.25023 \cdot 10^{-3}$	-1.05410
Φ_F	$-5.87075 \cdot 10^{-4}$	$-2.55611 \cdot 10^{-6}$	$-1.28721 \cdot 10^{-4}$
p_F	$-1.88296 \cdot 10^{-8}$	$-1.73594 \cdot 10^{-10}$	$-3.16672 \cdot 10^{-9}$

Table 4.1: Sensitivities of feed parameters with respect to the objectives Φ_1, Φ_2 and Φ_3.

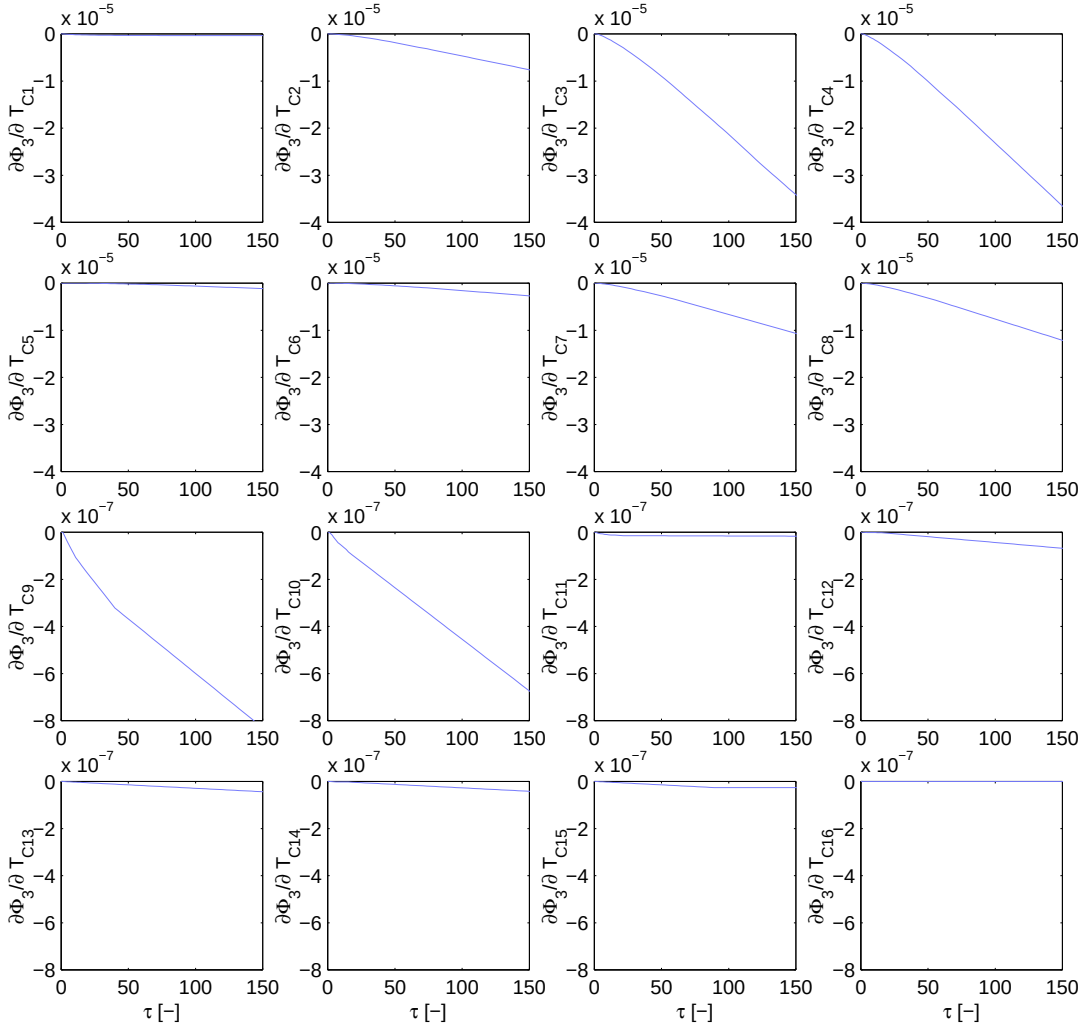

Figure 4.5: Sensitivities of coolant feed temperatures with respect to Φ_3. Note the different scale of the ordinate in the top two and in the bottom two rows.

mer than the warmer two (left-most) coolant jackets. Moreover, the influence of the coolant capacity on the melt flow index decays with the length of the tubular reactor. Whereas the maximum is in the first section, the last section shows almost no influence on changes in the coolant capacity. This result is well expected, since already Fig 3.2 showed, that the Nusselt number is very small in the laminar region compared to the turbulent regime. Moreover, the heat transfer also explains the reduction of the coolant sensitivity with larger distances from the inlet. As Fig. 3.2 shows, at the inlet of the tubular reactor, where the Reynolds number predicts a turbulent mixture, a high

Nusselt number takes care for a good heat transfer from coolant to the reactor. Hence the sensitivity is high. As the viscosity of the mixture in the reactor rises, the Nusselt number decreases, which results in a reduced sensitivity to the coolant capacity, until the reactor temperature is almost insensitive to the coolant temperature.

From the observations above, the input variables with highest influence on the physical properties of the polymer, determined by the melt flow index, are the feed flow rate, all initiator flow rates (their nominal value is of the order of $10^{-3}\ \frac{kg}{s}$), feed temperature and feed pressure. However, for the case studied here, the disturbance is introduced by changes in the feed flow rate. Hence, it is suggested to select the initiator flow rates and temperature controller which sets the inlet temperature of the tubular reactor as optimization parameters. Such a temperature control is e.g. given in the intercoolers of the compressors, so this controller is a good choice for a successive optimization.

Chapter 5

Future Work

The best way to predict the future is to invent it.
– Theodore Hook

As the production process of LDPE in a tubular reactor is very complex and highly nonlinear, a detailed dynamic model is essential for applications like

- engineering studies,
- dynamic optimization of grade and/or load changes,
- process control addressing safety and operation issues and
- operator training in dedicated operator training systems.

So, in order to explore new concepts for the production process of LDPE the rigorous model serves various purposes. However, a rigorous dynamic model as derived in this work currently is only directly applicable to the first two items of the list above, as for engineering studies and offline dynamic optimization of transitions between different steady state operation points simulation time is no limiting factor. This does not hold for advanced process control algorithms like model predictive control, as the underlying optimization has only limited simulation time to predict the plant behavior for a limited time horizon and calculate from this prediction the optimal control strategy. Also operator training is time critical since there always at least real time simulation speed has to be guaranteed.

For such applications, simplified dynamic mathematical models have to be derived and the rigorous model serves as reference process. The rigorous model is used to get a deep insight into the process in order to identify the most crucial parameters in the production process. These variable then have to be considered in a simplified dynamic mathematical model.

First studies have already started using the simple model by Häfele et al. (2005). In this work the nonlinear behavior of the low-density polyethylene reactor-separator-recycle system is analyzed. Based on the detailed model presented here, with the simple model a numerical bifurcation and stability analysis is performed to predict the region of stable operation. As a result multiple steady states and oscillatory behavior were found with the simple model. Based on these findings, their implications for practical process operation are discussed there. As these studies predict a strong dependency of the process stability on the constant heat transfer coefficient, a variable heat transfer coefficient should be used to extend the stability analysis.

The model derived for the purpose of nonlinear analysis then should be used for model predictive control applications. With respect of the results of Sec. 4.2, the most important control variables for the optimization of the simple model. It is strongly recommended to use an objective function that reflects important product properties, as it has been shown in Sec. 4.3, that the optimization algorithm might use the wrong control variable to steer the process into the desired direction.

Chapter 6

Conclusions and Summary

I have had my results for a long time, but I do not yet know how I am to arrive at them.
– Karl Friedrich Gauss

In this work, both a rigorous and a simple dynamic model of the LDPE production process is derived. For the mathematical description of the tubular reactor, partial differential and algebraic equations are used. In order to solve the model equations numerically, the PDAE system is converted into a DAE description using different discretization methods, which are offered by the modeling tool SyPProT. In particular, an equidistant grid node distribution and an adaptive method for the variation of the grid node positions is used for a finite differences approximation.

A high resolution grid shows good agreement of the dynamic model compared to data given by our cooperation partner. However, the size of the model turns out to be one challenging factor throughout the whole project. Different techniques have been used in order to simplify the model, only a reduction of the number of grid nodes proves to be suitable. Yet, the error introduced by the low resolution schemes is very well visible in the output of the reactor.

The rigorous model includes an energy balance equation for the thick inner reactor wall. One of the findings is, that it is important to account not only for heat conduction in axial but also in radial direction. To keep the model as simple as possible, the thick reactor wall is divided into two layers, and the wall temperature then is represented as an average radial temperature. This procedure allows to account for

the radial heat conduction by means of heat transfer resistances without introducing a proper discretization in radial direction. Comparison of simulation results with this approximation for the inner wall to simulations without an additional energy balance for the wall (of course, also there the radial heat conduction is included) shows no significant difference in steady state, whereas the transient behavior is considerably affected. The time constant of the open loop system increases by a factor of ≈ 10.

The rigorous model of the tubular reactor proves to have good agreement with given data, which is resulting from a steady state simulator. Although simulation times are quite high, the mathematical model is robust with respect to arbitrary step changes in the input variables. However, closing the recycles introduces a feedback which renders the whole system unstable for some operating conditions. A further investigation on this thermal instability due to step changes in the monomer feed rate is carried out using a simple model representation of the process. Therefore some simplifying assumptions are introduced, e.g. constant heat transfer coefficient, constant coolant temperature, presence of only two initiators (in fact, only on initiator at a time), etc. Despite of such a simplification, the simple model initially agrees very well with the rigorous model. However, the more viscous the monomer-polymer mixture gets, the smaller the heat transfer coefficient becomes. Since this effect is not included in the simplified model, the difference in both outlet temperature and conversion becomes larger. Nevertheless, the temperature profile show a similar shape, hence the model is used for the non-linear analysis of the system.

The non-linear analysis of the simple model agrees with findings of other research groups, that for the LDPE production system which includes reaction and separation intricate non-linear behavior can be observed. A parameter continuation of the feed flow rate predicts up to 5 steady states and a Hopf bifurcation point. However, the region of operation at the Hopf bifurcation exceeds the nominal operating temperature by far. Different observations most likely could be made, if the matching between the two models in terms of heat transfer is improved. Moreover, the Hopf bifurcation point could be used for starting a two parameter continuation with the feed flow rate and the (constant part in a variable) heat transfer coefficient. This is left for further investigations. Moreover, better agreement between the rigorous and simple dynamic models could be achieved using an initiator mixture in all injector pumps for a better start of the chain growth reaction and/or a variable heat transfer coefficient, account-

ing for laminar flow regimes.

The sensitivity analysis as initial step for a dynamic optimization is done using the rigorous model of the LDPE production process. It is demonstrated, that the selection of a suitable objective function for the determination of the key input parameters has a large influence on the selection of those parameters. Hence, moments cannot be neglected for a dynamic optimization. However, even the restriction to only a few optimization parameters still results in an optimization problem, that cannot be solved within DIVA so far (not by means of algorithms, but by means of computation time and memory consumption).

Maybe, the selection of a different simulation tool could solve the problem of high simulation times, on the other hand, most commercially available simulation tools are not well suited for other tasks such as optimization or non-linear analysis. Though computers will be faster in the future, the simulation of a dynamic rigorous model for the LDPE production plant is still a challenging problem, which numerically is not very easy to handle. However, the detailed model is a thorough basis for deriving simpler models that can be used by various other applications, such as non-linear analysis, optimization or (non-)linear model predictive control.

Appendix A

Series Summation Correlations

The following equations have been used in the derivation of the moment equations for living primary and secondary as well as dead polymer, (Bronstein et al., 2006),

$$\sum_{n=2}^{\infty} n^k \sum_{m=1}^{n-1} w_{R,m} w_{R,n-m} = \sum_{n=1}^{\infty} w_{R,n} \sum_{m=1}^{\infty} (m+n)^k w_{R,m} \tag{A.1}$$

$$\sum_{n=1}^{\infty} n^k \sum_{m=n+1}^{\infty} w_{R,m} = \sum_{n=2}^{\infty} \Big(\sum_{m=1}^{n-1} m^k \Big) w_{R,n}. \tag{A.2}$$

Moreover, the finite series that occur in the summation of the moments can be simplified using

$$\sum_{j=1}^{n} j = \frac{1}{2} n(n+1) \tag{A.3}$$

$$\sum_{j=1}^{n} j^2 = \frac{1}{6} n(n+1)(2n+1) \tag{A.4}$$

$$\sum_{j=1}^{n} j^3 = \frac{1}{4} n^2 (n+1)^2. \tag{A.5}$$

Appendix B

Condensed Listing of the Model Equations

Here, the model equations used for the rigorous model are listed without any additional comments.

Initiators I_ν ($\nu = 1, 2, 3$)

$$\frac{\partial w_{I_\nu}}{\partial t} + v\frac{\partial w_{I_\nu}}{\partial z} = -k_{I_\nu} w_{I_\nu}, \qquad \text{with } \nu = 1, 2, 3 \tag{B.1}$$

$$IC : w_{I_\nu}(0, z) = w_{I_\nu, in}$$

$$BC : w_{I_\nu}(t, 0) = w_{I_\nu, in}$$

Initiator radicals

$$\frac{\partial w_{RI_\nu}}{\partial t} + v\frac{\partial w_{RI_\nu}}{\partial z} = 2 f_\nu k_{I_\nu} \frac{M_{RI_\nu}}{M_{I_\nu}} w_{I_\nu} - k_{p,I_\nu} \frac{\varrho}{M_M} w_M w_{RI_\nu} \tag{B.2}$$

$$IC : w_{RI_\nu}(0, z) = 0.0$$

$$BC : w_{RI_\nu}(t, 0) = w^*_{RI_\nu}$$

Modifier

$$\frac{\partial w_X}{\partial t} + v\frac{\partial w_X}{\partial z} = -k_{tr,X} \frac{\varrho}{M_R} w_R w_X \tag{B.3}$$

$$IC : w_X(0, z) = w_{X,in}$$

$$BC : w_X(t,0) = w_{X,in}$$

Modifier radicals

$$\frac{\partial w_{RX}}{\partial t} + v\frac{\partial w_{RX}}{\partial z} = k_{tr,X}\frac{\varrho\, M_{RX}}{M_X M_M} w_X \mu_0^R - k_{p,X}\frac{\varrho}{M_M} w_M w_{RX} \tag{B.4}$$

$$IC : w_{RX}(0,z) = 0.0$$

$$BC : w_{RX}(t,0) = w_{RX}^*$$

Monomer

$$\begin{aligned}\frac{\partial w_M}{\partial t} + v\frac{\partial w_M}{\partial z} =& -k_{p,X}\frac{\varrho}{M_{RX}} w_{RX} w_M - k_p \frac{\varrho}{M_R} w_M \mu_0^R \\ & - \sum_{\nu=1}^{3} k_{p,I_\nu}\frac{\varrho}{M_{RI_\nu}} w_M w_{RI_\nu} - 2\, k_{th}\frac{\varrho^2}{M_M^2} w_M^3 \\ & - k_{tr,M}\frac{\varrho}{M_R} w_M \mu_0^R - k_{p,sec}\frac{\varrho}{M_{R_{sec}}} w_M w_{R_{sec}}\end{aligned} \tag{B.5}$$

$$IC : w_M(0,z) = w_{M,in}$$

$$BC : w_M(t,0) = w_{M,in}$$

Polymer

$$0 = 1 - w_P - w_M - w_X - w_{RX} - \sum_{\nu=1}^{N_C}(w_{I,\nu} + w_{RI,\nu}) \tag{B.6}$$

Momentum balance tubular reactor

$$0 = -\frac{\partial p}{\partial z} - \frac{1}{2}\zeta\frac{\dot{m}_A^2}{\varrho\, d_1} \tag{B.7}$$

$$BC : p(t,0) = p_{in} \tag{B.8}$$

Zeroth moment living polymer

$$\frac{\partial \mu_0^R}{\partial t} + v\frac{\partial \mu_0^R}{\partial z} = \frac{\varrho}{M_M}\Bigg[2k_{th}\frac{\varrho}{M_M}w_M^3 + \sum_{\nu=1}^{3} k_{p,I_\nu}\frac{M_M}{M_{RI_\nu}}w_M w_{RI_\nu} - k_{tr,P}\mu_0^R\mu_1^P$$
$$- \left(k_{t,c}+k_{t,d}\right)(\mu_0^R)^2 + k_\beta\frac{M_M}{\varrho}\mu_0^{R,sec} + k_{p,sec}w_M\mu_0^{R,sec}$$
$$+ k_{p,X}\frac{M_M}{M_{RX}}w_M w_{RX} - k_{tr,X}\frac{M_M}{M_X}w_X\mu_0^R\Bigg] \tag{B.9}$$
$$IC : \mu_0^R(0,z) = 0.0$$
$$BC : \mu_0^R(t,0) = \mu_0^{R*}$$

First moment living polymer

$$\frac{\partial \mu_1^R}{\partial t} + v\frac{\partial \mu_1^R}{\partial z} = \frac{\varrho}{M_M}\Bigg[2k_{th}\frac{\varrho}{M_M}w_M^3 + \sum_{\nu=1}^{3} k_{p,I_\nu}\frac{M_M}{M_{RI_\nu}}w_M w_{RI_\nu}$$
$$+ k_{p,X}\frac{M_M}{M_X}w_M w_{RX} + k_{tr,M}w_M\left(\mu_0^R - \mu_1^R\right)$$
$$- k_{tr,X}\frac{M_M}{M_X}w_X\mu_1^R - \left(k_{tc}+k_{td}\right)\mu_0^R\mu_1^R$$
$$- k_{tr,P}\mu_1^P\mu_1^R + k_{p,sec}w_M\left(\mu_1^{R,sec} + \mu_0^{R,sec}\right)$$
$$+ k_p w_M\mu_0^R + \frac{1}{2}k_\beta\frac{M_M}{\varrho}\mu_1^{R,sec}\Bigg] \tag{B.10}$$
$$IC : \mu_1^R(0,z) = 0.0$$
$$BC : \mu_1^R(t,0) = \mu_1^{R*}$$

Second moment living polymer

$$\frac{\partial \mu_2^R}{\partial t} + v\frac{\partial \mu_2^R}{\partial z} = \frac{\varrho}{M_M}\Bigg[2k_{th}\frac{\varrho}{M_M}w_M^3 + \sum_{\nu=1}^{3} k_{p,I_\nu}\frac{M_M}{M_{RI_\nu}}w_M w_{RI_\nu}$$
$$+ k_{p,X}\frac{M_M}{M_X}w_M w_{RX} + k_{tr,M}w_M\left(\mu_0^R - \mu_2^R\right)$$
$$- k_{tr,X}\frac{M_M}{M_X}w_X\mu_2^R - \left(k_{tc}+k_{td}\right)\mu_0^R\mu_2^R$$

$$
\begin{aligned}
&- k_{tr,P}\mu_1^P\mu_2^R + k_p w_M\left(2\mu_1^R + \mu_0^R\right) \\
&+ k_{p,sec} w_M\left(\mu_2^{R,sec} + 2\mu_1^{R,sec} + \mu_0^{R,sec}\right) \\
&+ \frac{1}{6}k_\beta\frac{M_M}{\varrho}\left(2\mu_2^{R,sec} - \mu_1^{R,sec}\right)\Bigg] \qquad \text{(B.11)}
\end{aligned}
$$

$$
\begin{aligned}
IC &: \mu_2^R(0,z) = 0.0 \\
BC &: \mu_2^R(t,0) = \mu_2^{R*}
\end{aligned}
$$

Zeroth moment dead polymer

$$
\begin{aligned}
\frac{\partial\mu_0^P}{\partial t} + v\frac{\partial\mu_0^P}{\partial z} = \frac{\varrho}{M_M}\Bigg[&k_{tr,M} w_M \mu_0^R + k_{tr,X}\frac{M_M}{M_X} w_X \mu_0^R + \left(\frac{1}{2}k_{tc} + k_{td}\right)(\mu_0^R)^2 \\
&+ k_\beta\frac{M_M}{\varrho}\mu_0^{R,sec}\Bigg] \qquad \text{(B.12)}
\end{aligned}
$$

$$
\begin{aligned}
IC &: \mu_0^P(0,z) = 0.0 \\
BC &: \mu_0^P(t,0) = \mu_0^{P*}
\end{aligned}
$$

First moment dead polymer

$$
\begin{aligned}
\frac{\partial\mu_1^P}{\partial t} + v\frac{\partial\mu_1^P}{\partial z} = \frac{\varrho}{M_M}\Bigg[&\frac{1}{2}k_\beta\frac{M_M}{\varrho}\mu_1^{R,sec} + k_{tr,P}\left(\mu_1^P\mu_1^R - \mu_0^R\mu_2^P\right) \\
&+ k_{tr,M} w_M \mu_1^R + \left(k_{tc} + k_{td}\right)\mu_0^R\mu_1^R + k_{tr,X}\frac{M_M}{M_X} w_X \mu_1^R\Bigg] \qquad \text{(B.13)}
\end{aligned}
$$

$$
\begin{aligned}
IC &: \mu_1^P(0,z) = 0.0 \\
BC &: \mu_1^P(t,0) = \mu_1^{P*}
\end{aligned}
$$

Second moment dead polymer

$$
\begin{aligned}
\frac{\partial\mu_2^P}{\partial t} + v\frac{\partial\mu_2^R}{\partial z} = \frac{\varrho}{M_M}\Bigg[&k_{tr,M} w_M \mu_2^R + k_{tr,X}\frac{M_M}{M_X} w_X \mu_2^R + \left(k_{tc} + k_{td}\right)\mu_0^R\mu_2^R \\
&+ k_{tc}(\mu_1^R)^2 + k_{tr,P}\left(\mu_1^P\mu_2^R - \mu_0^R\mu_3^P\right)
\end{aligned}
$$

$$+\frac{1}{6}k_\beta\frac{M_M}{\varrho}\left(2\,\mu_2^{R,sec}-\mu_1^{R,sec}\right)\Big] \tag{B.14}$$

$$IC:\mu_2^P(0,z)=0.0$$

$$BC:\mu_2^P(t,0)=\mu_2^{P*}$$

Third moment dead polymer

$$0=\mu_3^P-\frac{\mu_2^P}{\mu_1^P\,\mu_0^P}(2\mu_0^P\mu_2^P-\mu_1^P) \tag{B.15}$$

n-th moment dead polymer ($n=0,1,2$)

$$\frac{\partial\mu_n^{R,sec}}{\partial t}+v\frac{\partial\mu_n^{R,sec}}{\partial z}=\frac{\varrho}{M_M}\Big[k_{tr,P}\mu_0^R\mu_{n+1}^P-\left(k_{p,sec}w_M+k_\beta\frac{M_M}{\varrho}\right)\mu_n^{R,sec}\Big] \tag{B.16}$$

$$IC:\mu_n^{R,sec}(0,z)=0.0$$

$$BC:\mu_n^{R,sec}(t,0)=\mu_n^{R,sec\,*}$$

Energy balance wall

$$\varrho_W c_v\frac{\partial T_W}{\partial t}-\lambda_W\frac{\partial^2 T_W}{\partial z^2}=\frac{k_{inner}}{A_W}(T-T_W)-\frac{k_{outer}}{A_W}(T_W-T_C) \tag{B.17}$$

$$IC:T_W(0,z)=T_{W,0}$$

$$BC:-\lambda A_W\frac{\partial T_W}{\partial z}\bigg|_{lb}=\dot{Q}_{lb}$$

$$-\lambda A_W\frac{\partial T_W}{\partial z}\bigg|_{rb}=\dot{Q}_{rb}$$

Energy balance reactor

$$\varrho c_p\frac{\partial T}{\partial t}+v\frac{\partial T}{\partial z}=-\frac{k_{inner}}{A_R}(T-T^*)+(\Delta h_{reac}^{init})\sum_{v=1}^{3}k_{p,I_v}\frac{\varrho^2}{M_M M_{RI_v}}w_M w_{RI_v}$$

$$+(\Delta h_{reac}^{prop})k_p\frac{\varrho^2}{M_M^2}w_M\mu_0^R$$

$$+(\Delta h_{reac}^{term})(k_{tc}+k_{td})\frac{\varrho^2}{M_M^2}(\mu_0^R)^2 \tag{B.18}$$

$$IC: T(0,z) = T_0$$

$$BC: T(t,0) = T_{in}$$

Energy balance coolant

$$\varrho_C c_{p,C}\frac{\partial T_C}{\partial t} - v\frac{\partial T_C}{\partial z} = -\frac{k_{outer}}{A_C}(T_* - T_C) + \frac{k_{amb}}{A_C}(T_C - T_{amb}) \tag{B.19}$$

$$IC: T_C(0,z) = T_{C,0}$$

$$BC: T_C(t,\frac{L}{16}) = T_{C,in}$$

Overall heat transfer coefficients *with* energy balance for the reactor wall ($T^* \equiv T_* \equiv T_W$)

$$k_{inner} = \frac{1}{R_i + R_{ll,i} + R_{rad,i}}$$

$$k_{outer} = \frac{1}{R_{sl,i} + R_{C,i} + R_{rad,o}}$$

Overall heat transfer coefficients *without* energy balance for the reactor wall ($T^* = T_C$ and $T_* = T$)

$$k_{inner} = \frac{1}{R_i + R_{ll,i} + R_{st,i} + R_{sl,i} + R_{C,i}}$$

$$k_{outer} = k_{inner}$$

Double bonds

$$\frac{\partial DB}{\partial t} + v\frac{\partial DB}{\partial z} = \frac{\varrho}{M_M}\left[k_{tr,M}\mu_0^R w_M + k_{td}(\mu_0^R)^2 + k_\beta \frac{M_M}{\varrho}\mu_0^{R,sec}\right] \tag{B.20}$$

$$IC: DB(0,z) = 0.0$$

$$BC: DB(t,0) = DB^*$$

Long chain branching

$$\frac{\partial LCB}{\partial t} + v\frac{\partial LCB}{\partial z} = k_{p,sec}\frac{\varrho}{M_M}\mu_0^{R,sec} w_M \tag{B.21}$$
$$IC : LCB(0,z) = 0.0$$
$$BC : LCB(t,0) = LCB^*$$

Short chain branching

$$\frac{\partial SCB}{\partial t} + v\frac{\partial SCB}{\partial z} = k_{bb}\mu_0^R \tag{B.22}$$
$$IC : SCB(0,z) = 0.0$$
$$BC : SCB(t,0) = SCB^*$$

Turbulent resistor number ζ_t for the Nusselt number

$$0 = \frac{1.0}{\sqrt{\zeta_t} + 2.0\log\left(0.1345\frac{\zeta_0}{r_1} + \frac{2.51}{Re\sqrt{\zeta_t}}\right)} \tag{B.23}$$

Number average P_n

$$0 = P_n - \begin{cases} 800.0 & \text{for } \mu_0^P \mu_1^P = 0.0 \\ \frac{\mu_1^P}{\mu_0^P} & \text{else} \end{cases} \tag{B.24}$$

Appendix C

Remarks on Method of Lines Approach

Using $\chi := \kappa(\kappa+1)$ for $\kappa \geq 0.0$, the discrete monitor function M and the grid point concentration ζ as defined in (2.76) and (2.77), the elements of the matrix $\mathbf{E}$ in the ordinary differential moving grid equation system (2.72) are

$$e_{1,1} = 1.0 \tag{C.1a}$$
$$e_{2,1} = -\left(\chi M_1 \zeta_1^2 + (1+\chi) M_2 \zeta_1^2\right) \tag{C.1b}$$
$$e_{2,2} = \chi M_1 \zeta_1^2 + (1+\chi) M_2 \zeta_1^2 + (1+2\chi) M_1 \zeta_2^2 + \chi M_2 \zeta_2^2 \tag{C.1c}$$
$$e_{2,3} = -\left((1+2\chi) M_1 \zeta_2^2 + \chi M_2 \zeta_2^2 + \chi M_1 \zeta_3^2\right) \tag{C.1d}$$
$$e_{2,4} = \chi M_1 \zeta_3^2 \tag{C.1e}$$
$$\vdots$$
$$e_{n,n-2} = \chi M_n \zeta_{n-2}^2 \tag{C.1f}$$
$$e_{n,n-1} = -\left(\chi M_n \zeta_{n-2}^2 + \chi M_{n-1} \zeta_{n-1}^2 + (1+2\chi) M_n \zeta_{n-1}^2\right) \tag{C.1g}$$
$$e_{n,n} = \chi M_{n-1} \zeta_{n-1}^2 + (1+2\chi) M_n \zeta_{n-1}^2 + (1+2\chi) M_{n-1} \zeta_n^2 + \chi M_n \zeta_n^2 \tag{C.1h}$$
$$e_{n,n+1} = -\left((1+2\chi) M_{n-1} \zeta_n^2 + \chi M_n \zeta_n^2 + \chi M_{n-1} \zeta_{n+1}^2\right) \tag{C.1i}$$
$$e_{n,n+2} = \chi M_{n-1} \zeta_{k+1}^2 \tag{C.1j}$$
$$\vdots$$
$$e_{N_z-1,N_z-3} = \chi M_{N_z-1} \zeta_{N_z-3}^2 \tag{C.1k}$$

$$e_{N_z-1,N_z-2} = -\big(\chi M_{N_z-1}\zeta^2_{N_z-3} + \chi M_{N_z-2}\zeta^2_{N_z-2} + (1+2\chi)M_{N_z-1}\zeta^2_{N_z-2}\big) \tag{C.1l}$$

$$e_{N_z-1,N_z-1} = \big(\chi M_{N_z-2} + (1+2\chi)M_{N_z-1}\big)\zeta^2_{N_z-2} + \big((1+\chi)M_{N_z-2} + \chi M_{N_z-1}\big)\zeta^2_{N_z-1} \tag{C.1m}$$

$$e_{N_z-1,N_z} = (1+\chi)M_{N_z-2}\zeta^2_{N_z-1} + \chi M_{N_z-1}\zeta^2_{N_z-1} \tag{C.1n}$$

$$e_{N_z,N_z} = 1.0 \tag{C.1o}$$

The elements of the right hand side vector $\mathbf{g}$ in Eq. (2.72) are

$$\mathbf{g} = \begin{bmatrix} z_1 \\ M_1\big(\zeta_2 - \chi(\zeta_3 - 2\zeta_2 + \zeta_1)\big) - M_2\big(\zeta_1 - \chi(\zeta_2 - \zeta_1)\big) \\ \vdots \\ M_{n-1}\big(\zeta_n - \chi(\zeta_{n+1} - 2\zeta_n + \zeta_{n-1})\big) - M_n\big(\zeta_{n-1} - \chi(\zeta_n - 2\zeta_{n-1} + \zeta_{n-2})\big) \\ \vdots \\ M_{N_z-2}\big(\zeta_{N_z-1} - \chi(\zeta_{N_z-1} - \zeta_{N_z-2})\big) - M_{N_z-1}\big(\zeta_{N_z-2} - \chi(\zeta_{N_z-3} - 2\zeta_{N_z-2} + \zeta_{N_z-1})\big) \\ L - z_{N_z} \end{bmatrix}. \tag{C.2}$$

Bibliography

M. Asteasuain, S. M. Tonelli, A. Brandolin, and J. A. Bandoni. Modelling and optimisation of polymerisation reactors in gPROMS. In S. Pierucci, editor, *Eurpoean Symp. on Comp. Aided Proc. Eng.*, volume 10. Elsevier Science B.V., 2000.

M. Asteasuain, S. M. Tonelli, A. Brandolin, and J. A. Bandoni. Dynamic simulation and optimization of tubular polymerization reactors in gPROMS. *Comp. Chem. Eng.*, 25(4):509–515, May 2001.

J. Auger and L. Nguyen. Using Polymer Characterization Techniques to Predict LDPE Resin Suitability for Extruded Foam Applications. *Journal of Cellular Plastics*, 37(6):485–499, 2001.

M. Bartke and K.-H. Reichert. Berechnung von Molmassenverteilungen bei Polyreaktionen mit Standard-Simulationsprogrammen. *Chem. Ing. Tech.*, 71:1310–1314, 1999.

S. Beuermann and M. Buback. Free-Radical Polymerization Processes at High Pressures. *High Press. Res.*, 15:333–367, 1997.

C. P. Bokis, S. Ramanathan, J. Franjione, A. Buchelli, M. L. Call, and A. L. Brown. Physical Properties, Reactor Modeling, and Polymerization Kinetics in the Low-Density Polyethylene Tubular Reactor Process. *Ind. Eng. Chem. Res.*, 41(5):1017–1030, 2002.

A. Brandolin, M. H. Lacunza, P. E. Ugrin, and N. J. Capiati. High Pressure Polymerization of Ethylene: An Improved Mathematical Model for Industrial Tubular Reactors. *Poly. Reac. Eng.*, 4(4):193–241, 1996.

I. N. Bronstein, K. A. Semendjajew, G. Musiol, and Heiner Mühlig. *Taschenbuch der Mathematik*. Verlag Harri Deutsch, Frankfurt am Main, 2006.

M. Buback. The high pressure polymerization of pure ethylene. *Makromol. Chemie*, 181(2):373–382, February 1980.

M. Buback, M. Busch, and C. Kowollik. Chain-length dependence of free-radical termination rate deduced from laser single-pulse experiments. *Macromol. Theory Simul.*, 9(8):442–452, 2000.

M. Busch. Simulations as a Tool for Feasibility Studies about PIP-SEC Experiments. *Macromol. Theory Simul.*, 10:262–274, 2001a.

M. Busch. Modeling Kinetics and Structural Properties in High-Pressure Fluid-Phase Polymerization. *Macromol. Theory Simul.*, 10:408–429, 2001b.

M. Busch and H. C. M. van Boxtel. Modeling of Kinetics and Polymer Properties in High-Pressure Free-Radical Polymerizations. *DECHEMA Monogr.*, 134:49–59, 1998.

M. Caracotsios and W. E. Stewart. Sensitivity Analysis of Initial Value Problems with Mixed ODE's and Algebraic Equations. *Comp. Chem. Eng.*, 9:359–365, 1985.

A. Cervantes, S. Tonelli, A. Brandolin, A. Bandoni, and L. Biegler. Large-scale dynamic optimization of a low density polyethylene plant. *Comp. Chem. Eng.*, 24(4): 983–989, 2000.

W.-M. Chan, P. E. Gloor, and A. E. Hamielec. A Kinetic Model for Olefin Polymerization in High-Pressure Autoclave Reactors. *AIChE Journal*, 39(1):111–126, January 1993.

J. P. Congalidis and J. R. Richards. Process Control Of Polymerization Reactors: An Industrial Perspective. *Polym. React. Eng.*, 6(2):71–111, 1998.

E. A. Dorfi and L. O'C. Drury. Simple Adaptive Grids for 1-D Initial Value Problems. *J. Comp. Phys.*, 69:175–195, 1987.

R. Ehrig, U. Nowak, L. Oeverdieck, and P. Deuflhard. Advanced extrapolation methods for large scale differential algebraic problems. In H.-J. Bungartz, F. Durst, and C. Zenger, editors, *High Performance Scientific and Engineering Computing*, volume 8 of *Lecture Notes in Computational Science and Engineering*, pages 233–244. Springer, 1999.

G. Eigenberger. Influence of the Wall on the Dynamic Behavior of Homogeneous Tubular Reactors with a Highly Exothermic Reaction. *Adv Chem Ser*, 133:477–488, 1974.

EPS Ethylen-Pipeline Süd GbR. *Ethylen-Pipeline Süd*. URL: http://www.eps-pipeline.de/, date: 2006-04-29, 2006.

E. D. Gilles and H. Schuchmann. Verhalten von Rohrreaktoren bei Polymerisationsreaktionen. *Chem.-Ing.-Tech.*, 38(12):1278–1286, 1966.

M. Häfele, I. Disli-Uslu, A. Kienle, V. M. Krishna, S. Pushpavanam, and C.-U. Schmidt. Nonlinear Behaviour of a Low-Density Polyethylene Tubular Reactor-Separator-Recycle System. In L. Puigjaner and A. Espuña, editors, *European Symposium on Computer Aided Process Engineering - ESCAPE 15*, volume 1, pages 1423–1428. Elsevier Science B.V., 2005.

P. Holl, W. Marquardt, and E.D. Gilles. DIVA- A Powerful Tool for Dynamic Process Simulation. *Comp. Chem. Eng.*, 12:421–425, 1988.

H. M. Hulburt and S. Katz. Some problems in particle technology: a statistical mechanical formulation. *Chem. Eng. Sci.*, 19:555–574, 1964.

R. A. Hutchinson and R. E. Fuller. Modeling and Measurement of High Pressure Ethylene Polymerization Long-Chain Branching and Molecular Weight Distributions. *DECHEMA Monogr.*, 134:35–47, 1998.

D.-M. Kim and P. D. Iedema. Molecular Weight Distribution in Low-Density Polyethylene Polymerization; Impact of Scission Mechanisms in the Case of a Tubular Reactor. *Chem. Eng. Sci.*, 59:2039–2052, 2004.

C. Kiparissides. Polymerization Reactor Modeling: A Review Of Recent Developments And Future Directions. *Chem. Eng. Sci.*, 51(10):1637–1659, 1996.

C. Kiparissides, G. Verros, and J. F. MacGregor. Mathematical Modelling, Optimization and Quality Control of High-Pressure Ethylene Polymerization Reactors. *J. Macromol. Sci.–Rev. Macromol. Chem. Phys.*, C33(4):437–527, 1993.

C. Kiparissides, G. Verros, A. Pertsinidis, and I. Goossens. On-Line Parameter Estimation in a High-Pressure Low-Density Polyethylene Tubular Reactor. *AIChE Journal*, 42(2):440–454, 1996.

A. A. Kiss, C. S. Bildea, A. C. Dimian, and P. D. Iedema. State multiplicity in PFR–separator-recycle polymerization systems. *Chem. Eng. Sci.*, 58(13):2973–2984, July 2003.

N. Koak, R. M. Visser, and T. W. de Loos. High-pressure phase behaviour of the systems polyethylene + ethylene and polybutene + 1-butene. *Fl. Phase Equil.*, pages 158–160, 1999.

R. Köhler. *Preprocessing Tool for Method-of-Lines Discretization of Process Models in the Simulation Environment DIVA.* PhD thesis, Universität Stuttgart, Fortschritt-Berichte VDI, Reihe 20 (Rechnerunterstützte Verfahren), Nr. 357, VDI-Verlag Düsseldorf, 2002.

R. Köhler, K. D. Mohl, H. Schramm, M. Zeitz, A. Kienle, M. Mangold, E. Stein, and E. D. Gilles. Method of Lines within the Simulation Environment DIVA for Chemical Processes. In A. Vande Wouwer, Ph. Saucez, and W. E. Schiesser, editors, *Adaptive Method of Lines*, pages 371–406. Chapman & Hall, 2001.

A. Kröner, P. Holl, W. Marquardt, and E.D. Gilles. DIVA– An Open Architecture for Dynamic Simulation. *Comp. Chem. Eng.*, 14:1289–1295, 1990.

M. H. Lacunza, P. E. Ugrin, A. Brandolin, and N. J. Capiati. Heat Transfer Coefficient in a High Pressure Tubular Reactor for Ethylene Polymerization. *Polym. Eng. Sci.*, 38(6):992–1013, June 1998.

K. H. Lee and J. P. Marano. Free-Radical Polymerization: Sensitivity of Conversion and Molecular Weights to Reactor Conditions. In *Polymerization Reactors and Processes*, number 104 in ACS Symp. Series, pages 221–251, Washington D.C., 1979.

H. Liu and Y. Hu. Equation of state for polymer systems. *Fluid Phase Equilibria*, 150–151:667–677, 1998.

P. Lorenzini, M. Pons, and J. Villermaux. Free-Radical Polyerization Engineering – III. Modelling Homogeneous Polymerization Of Ethylene: Mathematical Model And New Method For Obtaining Molecular Weight-Distribution. *Chem. Eng. Sci.*, 47(15/16):3969–3980, 1992a.

P. Lorenzini, M. Pons, and J. Villermaux. Free-Radical Polyerization Engineering – IV. Modelling Homogeneous Polymerization Of Ethylene: Determination Of Model Parameters And Final Adjustment Of Kinetic Coefficients. *Chem. Eng. Sci.*, 47(15/16):3981–3988, 1992b.

G. Luft. Hochdruck-Polyäthylen. *Chem.-Ing.-Tech.*, 51(10):960–969, 1979.

G. Luft. Hochdruckpolymerisation von Ethylen. *Chemie in unserer Zeit*, 34(3):190–199, 2000.

G. Luft, P. Mehrling, and H. Seidl. Decomposition of Polymerization Initiators under High Pressures. *D. Angew. Makromol. Chem.*, 73(1118):95–111, 1978.

G. Luft, R. Kämpf, and H. Seidl. Synthesis Conditions and Structure of Low Density Polyethylene – I. Short and Long Chain Branching. *Angew. Makromol. Chem.*, 108 (1708):203–217, 1982.

F.-O. Mähling, R. Klimesch, M. Schwibach, M. Buback, and M. Busch. Modellierung der Ethen-Polymerisation im Elenac-Hochdruck-Rohrreaktorverfahren. *Chem.-Ing.-Tech.*, 71(11):1301–1306, 1999.

M. Mangold, K.-D. Mohl, A. Kienle, and E. D. Gilles. Analyse nichtlinearer Phänomene bei verfahrenstechnischen Prozessen. *Chem. Ing. Tech.*, 70:371–381, 1998.

M. Mangold, A. Kienle, K. D. Mohl, and E. D. Gilles. Nonlinear computation using DIVA– Method and applications. *Chem. Eng. Sci.*, 55:441–454, 2000a.

M. Mangold, F. Klose, and E. D. Gilles. Dynamic Behavior of a Counter-Current Fixed-Bed Reactor with Sustained Oscillations. In *Proc. of ESCAPE-10*, Florence, Italy, May 2000b.

P. A. Melo, E. C. Biscaia Jr., and J. C. Pinto. The bifurcation behavior of continuous free-radical solution polymerization reactors. *Chem. Eng. Sci.*, 58:2805–2821, 2003.

Robert A. Meyers, editor. *Handbook of Petrochemicals Production Processes*. McGraw-Hill Professional, first edition, April 2004.

NAG Fortran Library Routine Documentation, Mark 19. NAG Ltd., Oxford, England, 1993.

H Orbey, C. P. Bokis, and C.-C. Chen. Equation of State Modeling of Phase Equilibrium in the Low-Density Polyethylene Process: The Sanches-Lacombe Statistical Associating Fluid Theory and Polymer-Soave-Redlich-Kwong Equations of State. *Ind. Eng. Chem. Res.*, 37:4481–4491, 1998.

The Plastics and Rubber Institute. *Golden Jubilee Conference, Polyethylenes 1933–1983*, 1983a.

The Plastics and Rubber Institute. *Golden Jubilee Conference, Polyethylenes 1933–1983*, 1983b.

S. Pushpavanam and A. Kienle. Nonlinear behavior of an ideal reactor separator network with mass recycle. *Chem. Eng. Sci.*, 56:2837–2849, 2001.

S. Räumschüssel, A. Gerstlauer, E. D. Gilles, and M. Zeitz. *Simulationstechnik, 9. ASIM-Symposium in Stuttgart*, chapter Ein Präprozessor für den verfahrenstechnischen Simulator DIVA, pages 177–182. Vieweg Verlag, Braunschweig, Wiesbaden, 1994.

W. H. Ray. On the Mathematical Modeling of Polymerization Reactors. In G. B. Butler, K. F. O'Driscoll, and M. Shen, editors, *J. Macromol. Sci.–Revs. Macromol. Chem.*, volume C8, pages 1–56, New York, 1972. Marcel Dekker, Inc.

W. H. Ray. Dynamic Behaviour of Polymerization Reactors. In K.H. Ebert, P. Deuflhard, and W. Jäger, editors, *Modelling of Chemical Reaction Systems*, pages 337–354, Berlin, 1981. Springer-Verlag.

W. H. Ray. Current Problens in Polymerization Reaction Engineering. *Chem. Reac. Eng.*, pages 101–133, 1983.

W. H. Ray and C. M. Villa. Nonlinear dynamics found in polymerization processes – a review. *Chem. Eng. Sci.*, 55:275–290, 1999.

N. K. Read, S. X. Zhang, and W. H. Ray. Simulations of a LDPE Reactor Using Computational Fluid Dynamics. *AIChE Journal*, 43(1):104–117, 1997.

M. Schlegel, W. Marquardt, R. Ehrig, and U. Nowak. Sensitivity analysis of linearly-implicitdifferential-algebraic systems by one-step extrapolation, ZIB-Report 02-38. Technical report, Konrad-Zuse-Zentrum für Informationstechnik, Takustrasse 7D-14195 Berlin-Dahlem, Germany, November 2002.

H. Schuler. *Polymerisations-Reaktoren*. DECHEMA-Kurs "Dynamik und Regelung chemischer Prozesse", März 1981.

R. B. Seymour and T. Cheng, editors. *History of Polyolefins*. Reidel Publ. Co., Dordrecht, 1986.

D. C. Sorensen. Implicit Application of Polynomial Filters in a k-Step Arnoldi Method. *SIAM J. Matr. Anal. Apps.*, 13:357–385, 1992.

P. Stephan, K. Schaber, K. Stephan, and F. Mayinger. *Thermodynamik. Grundlagen und technische Anwendungen 1: Einstoffsysteme*. Springer-Verlag, Berlin, 2006.

The American Society of Mechanical Engineers. *Performance Test Code on Compressors and Exhausters, ASME PTC10*. ASME Books, New York, 1997.

F. Tränkle. *Rechnerunterstützte Modellierung verfahrenstechnischer Prozesse für die Simulationsumgebung DIVA*. PhD thesis, Universität Stuttgart, Fortschritt-Berichte VDI, Reihe 20 (Rechnerunterstützte Verfahren), Nr. 309, VDI-Verlag Düsseldorf, 2000.

K. Tsai and R. Fox. PDF Modelling of Turbulent-Mixing Effects on Initiator Efficiency in a Tubular LDPE Reactor. *AIChE Journal*, 42(10):2926–2940, 1996.

A. Uppal, W. H. Ray, and A. B. Poore. On the dynamics behavior of continuous stirred tank reactors. *Chem. Eng. Sci.*, 29:967–985, 1974.

VDI-Wärmeatlas. *Berechnungsblätter für den Wärmeübergang*. VDI-Gesellschaft Verfahrenstechnik und Chemieingenieurwesen (GVC), 1991.

J. G. Verwer, J. G. Blom, R. M. Furzeland, and P. A. Zegeling. A Moving Grid Method for One-Dimensional PDEs Based on the Method of Lines. In J. E. Flaherty, P.J. Paslow, M. S. Shephard, and J. D. Vasilakis, editors, *Adaptive Methods for Partial Differential Equations*, pages 160–175, Philadelphia, PA, September 1989. SIAM.

C. M. Villa, J. O. Dihora, and W. H. Ray. Effects of Imperfect Mixing on Low-Density Polyethylene Reactor Dynamics. *AIChE Journal*, 44(7):1646–1656, 1998.

R. Waschler, O. Angeles-Palacios, M. Ginkel, and A. Kienle. Object-oriented modelling of large-scale chemical engineering processes with ProMoT. *Math. & Comp. Mod. Dyn. Syst.*, 12(1):5–18, Feb. 2006.

K. S. Whiteley, T. G. Heggs, H. Koch, R. L. Mawer, and W. Immel. *Ullmann's Encyclopedia of Industrial Chemistry*, chapter Polyolefins - Polyethylene. WILEY-VCH, D-69451 Weinheim, Germany, sixth edition, 1998.

A. Vande Wouwer, Ph. Saucez, and W. E. Schiesser, editors. *Adaptive Method of Lines*. Mathematics/Chemical Engineering. Chapman & Hall/CRC, 2001.

R. C. M. Zabisky, W. M. Chan, P. E. Gloor, and A. E. Hamielec. A kinetic model for olefin polymerization in high-pressure tubular reactors: a review and update. *Polymer*, 33(11):2243–2262, 1992.

J. J. Zacca, J. A. Debling, and W. H. Ray. Reactor residence-time distribution effects on the multistage polymerization of olefins – II. Polymer properties: bimodal polypropylene and linear low-density polyethylene. *Chem. Eng. Sci.*, 52(12):1941–1967, 1997.

W. Zhou, E. Marshall, and L. Oshinowo. Modeling LDPE Tubular And Autoclave Reactors. *Ind. Eng. Chem. Res.*, 40(28):5533–5542, 2001.